TRIBHUVAN UNIVERSITY

INSTITUTE OF ENGINEERING

PULCHOWK CAMPUS

THESIS NO. PUL080MSGtE009

FEM Based Stability Analysis of Micropile Supported Cantilever Retaining Wall: A Case Study of the Roshi Section of BP Highway

by

Madhusudan Ghimire

A THESIS

SUBMITTED TO THE DEPARTMENT OF CIVIL ENGINEERING

IN PARTIAL FULFILLMENT OF THE REQUIREMENTS FOR THE

DEGREE OF MASTER OF SCIENCE IN

GEOTECHNICAL ENGINEERING

DEPARTMENT OF CIVIL ENGINEERING

LALITPUR, NEPAL

APRIL, 2026

COPYRIGHT

TRIBHUVAN UNIVERSITY

INSTITUTE OF ENGINEERING

PULCHOWK CAMPUS

DEPARTMENT OF CIVIL ENGINEERING

The thesis titled "FEM-Based Stability Analysis of Micropile Supported Cantilever Retaining Wall: A Case Study of the Roshi Section of BP Highway " prepared and submitted by Madhusudan Ghimire in partial fulfilment of the requirements for the degree of Master of Science (M. Sc.) in Geotechnical Engineering has been examined by us and is accepted for the award of M. Sc. in Geotechnical Engineering by Tribhuvan University.

The undersigned certify that they have read, and recommended to the Institute of Engineering for acceptance, a thesis report entitled "FEM-Based Stability Analysis of Micropile Supported Cantilever Retaining Wall: A Case Study of the Roshi Section of BP Highway" submitted by Madhusudan Ghimire in partial fulfillment of the requirements for the degree of Master in Geotechnical Engineering.

Supervisor:
Asst. Prof. Dr. Ram Chandra Tiwari
Department of Civil Engineering
IOE, Pulchowk Campus

External Examiner:
Er. Prabhat Kumar Jha
Department of Road, Ministry of Physical Infrastructure and Transport
Government of Nepal

Program Coordinator:
Asst. Prof. Dr. Bhim Kumar Dahal
M.Sc. in Geotechnical Engineering
Department of Civil Engineering
IOE, Pulchowk Campus

Date: April 27, 2026

DECLARATION

I hereby declare that this study titled "**FEM-Based Stability Analysis of Micropile Supported Cantilever Retaining Wall: A Case Study of the Roshi Section of BP Highway**" is based on my original research work. Related works on the topic by other researchers have been duly acknowledged. I owe all the liabilities relating to the accuracy and authenticity of the data and any other information included hereunder.

Madhusudan Ghimire

080/MSGtE/009

MSc in Geotechnical Engineering

Date: April 27, 2026

ACKNOWLEDGEMENTS

I would like to express my sincere gratitude towards my supervisor, Assistant Professor Dr. Ram Chandra Tiwari, for his invaluable guidance, constant support, and encouragement throughout the project. The suggestions provided helped me to develop the research work to the next level. His expertise and encouragement were essential to this study.

I would wholeheartedly like to thank my external examiner, Er. Prabhat Kumar Jha for his valuable suggestions and guidance for the thesis work. I am also incredibly grateful to the program coordinator of M.Sc. in Geotechnical Engineering, Assistant Professor Dr. Bhim Kumar Dahal, Professor Dr. Indra Prasad Acharya, Assistant Professor Dr. Santosh Kumar Yadav, and Assistant Professor Dr. Basanta Raj Adhikari, as well as the entire Geotechnical Engineering Department at Pulchowk Campus. They have afforded me have played a pivotal role in expanding my perspectives and enhancing my academic journey. And also thankful towards the Road Division Bhaktpur Office, contractor, and entire team of the project office for their relentless support and the opportunities for field visit, data collection, and guidance in this study. This study would not have been complete without the tireless efforts of Mr. Surya Krishna Prajapati, who has been the backbone of the entire Geotechnical Engineering Department at Pulchwok Campus.

My thanks also go to the Department of Civil Engineering, Pulchowk Campus, Institute of Engineering, for providing resources and a conducive research environment.

Lastly, I am sincerely grateful to my family and friends for their unwavering inspiration and invaluable support throughout my studies. Additionally, I extend my thanks to all the individuals who directly or indirectly contributed to this endeavor.

Madhusudan Ghimire

080/MSGtE/009

ABSTRACT

This study presents a numerical evaluation of micropiles used to underpin and enhance the performance of cantilever retaining wall foundations in challenging geological conditions characterized by heterogeneous mixtures of sand, gravel, and boulders. A comprehensive finite element analysis approach is adopted to develop a numerical model of a cantilever retaining wall micropile soil system, incorporating non-linear soil behavior through a Mohr Coulomb constitutive model and explicitly defining soil-structure interaction mechanisms. The numerical model approach was validated using field test results of previous numerical research to demonstrate its effectiveness and reliability in modelling of underpinned foundations. The influence of micropile reinforcement is systematically investigated in terms of displacement, stability, bearing capacity, and load transfer mechanism under various conditions, including baseline static loading, water level rise, seismic excitation, and scouring effects, with comparative analyses conducted between micropile and non-micropiled configurations. Furthermore, a systematic parametric study was conducted to examine the effect of micropile parameters, including spacing, length, diameter, and on load-settlement behavior, bearing capacity, load transfer ratio, and deformation patterns of the micropile-supported cantilever retaining wall system under static loading.

Keywords: Micropiles; Cantilever Retaining Wall; Bearing Capacity; Bending Moment; Settlement; Finite Element Method

TABLE OF CONTENTS

LIST OF FIGURES

LIST OF TABLES

ABBREVIATIONS AND ACRONYMS

b, B	: Width of foundation
CL	: Lean clay
CH	: Thick, fat clay
D_f	: Depth of foundation
D	: Diameter of micropile
E	: Modulus of elasticity of soil
FE	: Finite Element
FEA	: Finite Element Analysis
FEM	: Finite Element Method
H	: Thickness of soil layer
L	: Length of micropile
L/D	: Length to diameter ratio of micropiles
PI	: Plastic Index
S/D	: Spacing to diameter ratio of micropiles
SP	: Poorly graded sand
W	: Width of soil domain
w	: Water content
2D	: Two Dimensional
3D	: Three Dimensional
φ, ϕ	: Angle of internal friction
ψ	: Dilatancy angle
q	:Load per unit area
V	: Load per unit length
N_c, N_q, N_γ	: Bearing capacity factors
σ_z	: Overburden stress
σ_u	: Ultimate Bearing Capacity

c, cu	: Cohesion
γ	: Unsaturated unit weight of soil
Υ_{sat}	: Saturated unit weight
e	: Void ratio
m_v	: Modulus of volume compressibility
μ	: Poisson's ratio
f_s	: Unit skin friction along the micropile shaft,
Δf_s	: Increase in unit skin friction due to grouting.

1 INTRODUCTION

1.1 Background

The foundation is one of the integral members of any engineering structure. Its function is to transmit the overall load of the above structure to the supporting ground. Foundations must be properly designed and constructed to perform satisfactory performance. In order for foundations to function as intended, they need to be protected from overall shear failure in the soil underneath them and must avoid experiencing excessive settlement. To design a foundation to perform in the desired way, the designer must possess sound knowledge of the type of soil beneath that will support the foundation and their stress related deformation(El Kamash & Han, 2017).

Retaining walls are fundamental geotechnical structures designed to stabilize soil masses and provide lateral support in civil engineering applications, including highways, railways, and building basements. Among different types of retaining structures, cantilever retaining wall structures were extensively constructed due to their structural efficiency, economic viability, and suitability for moderate-height applications (Konstandakopoulou et al., 2020).These walls, typically constructed from Rebar-reinforced concrete, include a vertical stem and a base slab that work together to withstand the lateral earth pressures given by backfill material. Performance and stability of cantilever retaining walls are determined by interactions of the wall, the soil of the foundation, and the backfill materials placed (Terzaghi, 1943).Traditional analytical methods for designing these walls were proposed by Rankine (1857) and Coulomb (1776), providing simplified approaches for estimating lateral earth pressures. They often fail to capture the complex soil-structure interaction that influences the actual performance of retaining wall systems (Konstandakopoulou et al., 2020).

The majority of foundations are well designed and built; some may experience problems with stability, settlement, or bearing capacity. Corrective action is necessary in these circumstances to guarantee the functionality of the existing foundation. Various technologies are available for this purpose, one of which is the underpinning of foundations. The process of a foundation's performance can be referred to as its underpinning, with micropiles being one of the most widely used techniques (Thorburn and Hutchison, 1985). Micropiles are drilled and grouted concrete piles with a diameter of typically less than 300 mm (FHWA, 2005). They are suitable for underpinning because they can be positioned vertically or at an inclined slope in low-headroom situations, offering significant advantages,

including the ability to be installed in restricted access areas with minimal vibration and noise (Kyung & Lee, 2018).

In the 1950s, the history of micropiles began in Italy, where they were originally developed by the renowned engineer Fernando Lizzi, widely recognized as "The Father of Micropiles." (Lizzi, 1982a) introduced the concept of "pali radice" or root piles, which were small-diameter, cast-in-place piles designed to be installed through existing foundations to reconstruct and strengthen historic buildings damaged during World War II (Lizzi, 1982). Since his contributions, micropile technology has evolved significantly, with various grouting methods and installation techniques developed to enhance load-carrying capacity. Recognizing the growing importance of micropiles, the Federal Highway Administration (FHWA) published the “Micropile Design and Construction Reference Manual” (FHWA NHI-05-039), which serves as an essential resource for geotechnical engineers and practitioners, providing detailed guidance on micropile classification, design methodologies, and construction techniques (FHWA, 2005).

Numerous projects have since strengthened existing foundations using micropiles. One of the earliest known uses was to support an existing shallow foundation to withstand the additional weight caused by a 50-year-old structure in China, adding two more levels (Han & Ye, 2006). (Lizzi, 1982a)documented the application of micropiles to enhance the functionality of the Arts and Science Museum's foundation, which was completely devastated by a hurricane in the United States. The effectiveness of micropiles for foundation rehabilitation has been further demonstrated through extensive field testing and numerical investigations. Kyung et al. (2017a) conducted comprehensive field load tests to investigate the vertical load carrying behavior of micropile under various configuration conditions, providing valuable insights into their performance. Kshatriya et al. (2022) analyzed the behavior of retaining walls resting on black cotton soil using PLAXIS 2D software, demonstrating that the provision of bearing piles below the retaining wall significantly reduces deformation and enhances stability. Furthermore, (Vijaykumar & Prasad, 2022) studied the pile-raft system using PLAXIS 3D and found that the addition of piles reduces total settlement by approximately 60% to 70%, with the load-carrying capacity increasing up to an optimum value.

Realistic modeling of boundary conditions, staged construction sequences, and non-linear soil behavior is made possible by Finite Element Method (FEM), which can be implemented using software PLAXIS 2D (Wulandari & Tjandra, 2015). Numerical modeling provides a powerful platform for investigating the behavior

of micropile-reinforced retaining wall systems, allowing for comprehensive parametric studies that would be impractical through physical testing alone. (El Kamash & Han, 2017)conducted a numerical investigation of existing foundations supported by micropiles using three-dimensional finite-difference software, performing parametric studies to examine the effects of micropile modulus, length, and diameter.

The specific application of micropiles for reinforcing cantilever retaining wall foundations, however, remains an area requiring systematic investigation. (Elsawwaf et al., 2023a; Kyung & Lee, 2018)While extensive research has been conducted on micropiled rafts and on retaining walls by (Kshatriya et al., 2022b).A combined micropile and foundation system of a cantilever retaining wall reinforced with micropiles beneath its base slab has received limited attention. The integration of micropiles beneath the base slab of existing cantilever walls presents a promising rehabilitation strategy for structures that have become inadequate due to increased loading demands and foundation settlement. This research study has addressed this gap by employing finite element method to comprehensively evaluated behavior of cantilever retaining wall foundations reinforced with micropiles under various loading conditions.

1.2 Research Gaps and Problem Statement

(Lamichhane et al., 2025) gives information that the 2024 flood event along the Roshi Khola transport corridor caused extensive damage, including 2.5 km of road completely washed away, 10 km of road damaged, 7 bridges destroyed, and nearly 1.4 km of retaining walls damaged. (Lamichhane et al., 2025)Further noted that unregulated mining activities and the confinement of rivers to narrow channels due to settlement expansion were primary factors that intensified the severity of the flood devastation.

Hazard mapping conducted for major settlement areas along the Roshi corridor, including Panauti, Chauki Dada, Mangaltar, and Nepalthok, revealed significant flood risks. For a 100-year return period rainfall event, inundation depths were projected to range from 0 to 3 m in Panauti, 0 to6m in Chauki Dada, 0 to 9 m in Mangaltar, and 0 to 15 m in Nepalthok, with velocities exceeding 20 m/s in the most affected areas (Karki et al., 2025). These extreme flow conditions pose severe threats to retaining walls, which are often inadequately designed to withstand such hydrodynamic forces.

In light of these circumstances, proactive measures are imperative to address and enhance the performance of cantilever retaining wall foundations. The micropiles

beneath the foundations emerge as a viable strategy, adopted to increase bearing capacity and minimize the settlement in the face of additional loads. However, the existing data on the performance of underpinned foundations under diverse loading conditions is limited. These limitations become critical when retaining walls are subjected to combined vertical and lateral loads from adjacent structures, surcharge loads, or seismic events, which can induce large destabilizing forces (Riyaz et al., 2020). The vulnerability of retaining walls is further exacerbated in regions with problematic soils, such as expansive clays or areas prone to flooding, where foundation stability is compromised (Kshatriya et al., 2022; Lamichhane et al., 2025)

In the Roshi section, the BP Highway cantilever retaining structures for the road section are proposed and under construction, reinforced with micropiles. (Shakeel et al., 2022)Numerical modeling tools such as PLAXIS 2D have been effectively utilized to analyze retaining wall stability yet validated models for micropile-reinforced cantilever retaining wall systems remain scarce.

To address this gap, a systematic investigation into the behavior of cantilever retaining wall foundations reinforced with micropiles was critically needed, particularly to prevent wall failure induced by soil erosion, increased water levels, and forces under pseudo-static loading conditions. Such investigations are essential to ensure that reinforced cantilever walls can withstand the combined effects of hydrostatic force, soil scour, and earthquake-induced lateral earth pressures, which are often the major causes of retaining wall distress and failure.

This study was conducted to fulfill this critical gap by performing a numerical study using FEM 2D software to investigate the performance of micropile-reinforced cantilever retaining walls under static conditions, pseudo-static load, water level rise conditions, and scouring conditions. Through parametric analysis, this study investigated the performance of micropile diameter, length, spacing, and its configuration on the stability of the micropile-supported cantilever retaining wall. The findings could contribute to evidence-based design recommendations for resilient and sustainable cantilever retaining wall foundations capable of withstanding soil erosion, flood events, and seismic forces.

1.3 Objectives

1.3.1 *General objective*

The general objective of this study is the FEM-Based Stability Analysis of Micropile-Supported Cantilever Retaining Wall: A Case Study of the Roshi Section of BP Highway.

1.3.2 *Specific objectives*

This study has the following specific objectives:

i. To develop a numerical model of actual field conditions and validate it with a previous study to assess the performance of cantilever wall foundations underpinned by micropiles.
ii. To examine how different loading conditions affect the stability of the foundation performance of micropile-supported cantilever retaining walls.
iii. To investigate the influence of the diameter, spacing, and length of micropiles on the behavior of micropile-supported cantilever wall foundations.

1.4 Scope

This study focuses on stability analysis of micropile supported cantilever retaining wall with reference to the case study site of the Roshi section of the BP highway. The scope includes the following aspects:

i. Preparation of the FEM numerical model: The analysis will consider the soil profile at the case study site, which includes gravelly sand layers. Prepared data for the input in the Plaxis 2D numerical model of a road section with a cantilever retaining wall. Prepared a numerical model as per actual field conditions.
ii. Static loading. Input: Static loading condition was considered in the prepared numerical model, and the applied vehicle load. Observed the displacement, bearing capacity, load carried ratio, and other results of the micropiles. Comparison of the cantilever wall with and without the micropile support was also analyzed.
iii. Water level rise condition: The study employed Plaxis 2D software to model water level rise and fall cases, and primarily observed the displacement and the failure criteria.

iv. Pseudo-static loading: The horizontal seismic coefficient value was applied to the prepared numerical model to evaluate the performance of the micropile and cantilever wall. The study also carried on comparision of the pseudo-static loading of the past earthquake data to the normal static loading. But not analyzed on the seismic loading conditions on the model.

v. Scouring condition: The study also analyzed the scoured depth and evaluated the performance of the scouring effects. Also, explore the stability of the wall on scoring.

1.5 Limitations

This study focused on the stability analysis of micropile-supported cantilever retaining wall, referring the case study site of the Roshi section of the BP highway. This study has the following limitations:

i. The research is limited to a soil sample from the Roshi section (Kavre District) of the BP Highway, and the findings may vary for other soil samples.

ii. The numerical model of raft and micropile used for this study is validated by using the field data obtained by (Kyung et al., 2017a) and later compared with the output of (Elsawwaf et al., 2023a) It does not have the field load test of the micropile.

iii. In addition to these, the study is constrained to a small set of parameters and a limited range of loading conditions, the various wall heights, and soil type, and the impact of flood on the cantilever wall, which may not fully capture all issues.

2 LITERATURE REVIEW

An overview of the prior research and published literature required to understand the study's basic premises is set out in this section. Developments in the area of micropiles, foundations, and retaining structures and their performance on heterogeneous soil are analyzed in this literature review section. This section begins with a discussion of some general principles and hypotheses of the study, followed by a review of past studies and research.

2.1 Introduction

The term "bearing capacity" denotes the ability of soil to withstand the load exerted by a structure, such as a building, bridge, or foundation, without undergoing significant deformation or failure. According to Terzaghi (1943), it is defined as "the maximum load per unit area which the soil or rock can carry without yielding or displacement."(Das & Sobhan, 2006).

In the context of a footing resting on the soil's surface, the relationship between foundation load and settlement was crucial. As load on the foundation increases, the foundation settles. When the load per unit area reaches the bearing capacity, the critical point is reached. At this juncture, soil experiences failure, and the failure surface may reach the ground surface, aligning with the specific failure mode of the soil. This failure is often accompanied by a significant increase in footing settlement, the limit of the soil's capacity to sustain the applied load without yielding or displacement (Das, 2019).

Major structures were constructed on deep foundation systems using driven or drilled piles, or they are supported directly on appropriate underlying soils. In bearing circumstances, the building's ability to withstand movement (settlement) usually determines the permissible capacity. Undoubtedly, bearing capacity forecasts could not always agree with measured values, necessitating corrective measures. In rare circumstances, substantial structures may outlive the deep foundation systems that were initially erected. Catastrophic occurrences that cause ground losses in other situations can undoubtedly jeopardize the stability of any structure, whether it is supported by pilings or soil. Put more simply, there are situations where a structure needs more foundation capacity to handle new loads (e.g., extra stories)(El Kamash & Han, 2017).

In these cases, it made sense to establish appropriate foundation support or do repairs. It has been demonstrated that pin piles, also known as micropiles, are a

dependable and adaptable geotechnical construction method for restoring support beneath existing structures.

Pin piles, often called minipiles or micropiles, are drilled and grouted small diameter piles whose diameter is less than 300mm. They are reliable for building and other foundations of structures on locations with unfavorable ground conditions, complex premises, low vertical clearance, or challenging spaces. Additionally, it works effectively for halting ground movements, strengthening already- existing foundations, and underpinning foundations. Either deep foundation techniques, like driven or drilled piles, or suitable soils in direct bearing are used to support large-scale projects. In bearing circumstances, the building's ability to withstand movement determines the permissible capacity. (Pearlman, 2001)

Significant constructions may occasionally outlive the deep foundation systems that were erected, and catastrophic events that cause ground losses may occasionally jeopardize the stability of any structure. (Pearlman, 2001) Micropiles are used to lessen settlements and reinforce preexisting foundations. Limited bearing capacity, high compressibility, uneven soil layers, and uneven loading conditions are all reasons for tilting, differential settlement, and excessive total settlement. Buildings with additional stories also contain more loads, which calls for stronger structures and better foundation soil bearing capacity. Both new and old structures with foundation issues can be treated using this approach. Micropiles shift construction loads to bearing layers in the majority of soil types. Drilling equipment improvements have made it feasible to design and build micro piles with diameters greater than 25 cm and load capacities greater than 300 tons (Bakr, 2016).

Pin Piles were sturdy, reasonably priced tools for drilling in confined areas that minimize ground loss while producing silent, vibration-free results. The drilling equipment can easily install tie-down anchors for secure anchoring, and they were also redirected to maintain clean environment. (Pearlman, 2001).

2.2 History of Micropile

In the early 1950s, Lizzi brought the micro-pile technology to Italy (Lizzi, 1980). Global adoption of this technology happened quite quickly. The United States, Canada, and the United Kingdom all adopted this technology in 1962, 1965, and 1973, respectively (Juran et al., n.d.).

(Gutierrez,2004) reported on the usage of micropiles to reinforce the Arts and Science Museum's foundation, which was completely wrecked by a hurricane in the

United States. In 1980, a laboratory model test was used in China to simulate the foundation of the Hu-Qiu structure, a leaning structure that was constructed more than a millennium earlier. This was the first test using micropiles. Micopiles were used in china to support footing of existing building. Increasing the number of floors in an existing structure is thought to be a viable way to expand the working area of an organization. Nevertheless, pile-soil-structure interactions are complicated when micropiles are installed on preexisting footings. Human experience or judgment serves as the primary source of inspiration when designing micropiles to sustain stories added to an existing building. In 1996, (Makarchian & Poulos) created a simplified process for creating underpinning piles. Nevertheless, there wasn't much field evidence available to support this theory. The findings of field testing utilizing micropiles and an already-existing micropile-supported foundation were released by (Han and Ye, 2006).

Subsequent research has significantly advanced the understanding of micropile behavior.Kyung et al. (2017b) conducted comprehensive model load tests and field load tests to investigate the vertical load-carrying behavior of micropiles under various configuration conditions, including different installation angles and pile spacings. Their work provided valuable insights into the performance of micropiles as both single piles and group piles, contributing for development of design models for micropile foundations.

Elsawwaf et al. (2023b)performed a comprehensive numerical analysis using finite element modeling to study the behavior of micropiled raft foundations under combined vertical and lateral loading, evaluated that micropiles significantly enhance the lateral load capacity of foundation systems, and provided significant guidelines for choosing suitable micropile raft configurations.

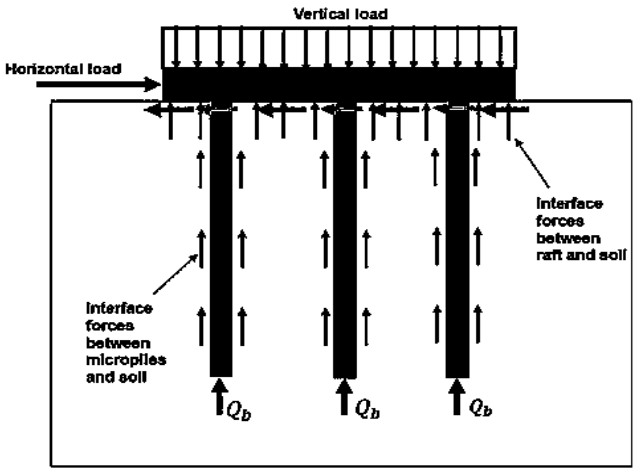

Figure 2.1: Load transfer in micropiles (Elsawwaf et al., 2023)

2.3 Development of Micropile Classification

2.3.1 *Classification based on design application*

Micropiles have been used in many kinds of new foundation constructions as well as slope stability enhancement. Certain low capacity micropile have no structural steel reinforcement and are made entirely of grout. Nonetheless, steel parts and steel casing are typically used in micropile design. Steel pipe sections, H-beams, hollow bars, and steel rods made up the micropile structural components. The strength of grout used in micropile was mostly determined by the water to cement ratio, pressure of grout, which can be mixed on site (Ebadi-Jamkhaneh & Kontoni, 2023) .

FHWA (2005), first breaks down the classification of micropiles based on the fundamental theory of how the load is transferred to the soil.

Case 1 micropiles are stated as directly loaded piles. Loaded in the axial and/or lateral direction, case 1 micropiles transfer the load directly into the competent stratum of soil or rock and are mainly supported by the soil directly surrounding the micropile. Almost all micropiles constructed in North America and 90 percent of international micropiles, are identified as Case 1 (FHWA, 2005).

Case 2 micropiles, developed by Dr. Lizzi, focuses on constructing a three-dimensional network of root piles fully bonded over the entire length(Lizzi, 1982).

2.3.2 *Classification based on construction type*

FHWA (2005) micropiles are mainly categorized according to the kind and grouting pressure. There are four established categories, as shown in Figure 2.2.

Type A (gravity-grout micropile): A gravity head is used to introduce grout into the pile.

Type B (low-pressure grout micropile): the auger or temporary steel drill casing is removed, and cement grouting is injected in the drilled hole at pressures between 0.3 and 1 MPa (FHWA, 2005).

Type C (high-pressure grouted micropiles): Grout is injected once at a pressure of at least 1 MPa through an installed sleeved grout pipe, but before setting of primary grout, plain cement grout is placed in the borehole as described for type A(FHWA, 2005).

Type D (post-grouted micropiles): The hole is filled with neat cement grout, same like in Type A. Similar grout is used in a preplaced, sleeved post grout pipe after

the grout has set. If necessary, specific horizons can be treated more than once at pressures between 2 and 8 MPa by utilizing an inside packer.

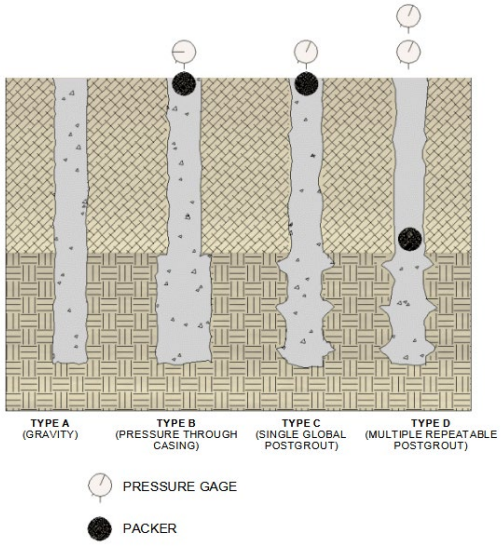

Figure 2.2: Types of micropiles based on grouting type(FHWA, 2005).

2.4 Installation Methods

One of the main benefits of using Pin Piles for underpinning and building foundations is their capacity to be installed in the most challenging and troublesome geotechnical settings. The best drilling and grouting methods are primarily responsible for this capability. The specialist contractor is frequently the most skilled in selecting the optimal installation method to achieve the desired outcome while honoring the owner's and his engineer's concerns, especially with regard to allowable ground disturbance during drilling. Similar to what's done in the oil and gas sector, rotary drilling techniques are employed to place pin piles. Through grout, the piles strengthen their geotechnical ability to ground adhesion in the bond zone. Tremie grouting is used in rock, and pressure grouting is usually used in soils to create this bond. The following is a description of the main kinds of drilling and grouting procedures employed(El Kamash & Han, 2017).

2.5 Drilling Method

2.5.1 *External flush drilling*

With this technique, a vertical load or downward pressure is applied as a drill casing or pipe is rotated into the earth. Drilling fluid is used to flush out the soil inside the casing. At the drill head, drilling mud is pushed into the casing of drill, exits drill casing, and rises back up. Drilling mud and compressed air are also utilized occasionally, but water is the most widely employed fluid. The easiest and

most affordable way to drill pin piles in soil is to use external flush drilling, provided that there are no obstructions and that a small amount of temporary ground loss is acceptable(Das & Sobhan, 2006).

2.5.2 *Duplex drilling:*

An inner drill rod with a roller bit tip is advanced simultaneously with the outer drill casing in a process known as duplex drilling, which is used to clean up and advance the drill casing. Drill fluid moves through the center of the inner drill rod. It exits through the annular gap between the drill rod and drill casing to return to the surface. Once again, water is the most widely used drilling fluid for this method. Maintaining close contact between the soil layers and drill casing when drilling is one of the main benefits of duplex drilling. This is crucial in cases when there is a risk of ground loss or when external flushing is unable to return fluid to the soil due to its extreme openness. In fractured rock formations, duplex drilling is frequently utilized to maintain an open hole or to break through impediments. This method's drawbacks include the fact that it requires more manpower and is slower than external flush drilling, making it more expensive(Das & Sobhan, 2006).

2.5.3 *Rotary eccentric percussive duplex drilling:*

This method of drilling is similar to the duplex drilling method, but uses a down-the-hole hammer rather than a roller bit on the inner drill rod. The pilot and the reamer are the two parts that make up the hammer bit. During drilling, the reamer bit mechanically expands to a diameter that is marginally greater than the drill casing's outer diameter. This bit makes a somewhat bigger hole through rocks or other barriers, which enables the casing to follow it down at the same time. In addition to being the drilling fluid that raises the cuttings, compressed air is utilized to power the hammer. This type of drilling method greatly eases drilling through zones of heavily fractured (e.g., karstic limestone) or irregularly weathered formations (e.g., the mica schist formations in the New York metropolitan area). It is also utilized in soils that have a lot of impediments, such as debris from demolition projects or cobbles and stones. In many situations, the technique works very effectively, even if the required equipment of drill is more expensive than for external flush or ordinary duplex drilling(Das & Sobhan, 2006).

2.6 Grouting Method

2.6.1 *Tremie grouting:*

In this type of grouting method, place the grout in the hole that is still damp. A grout tube is run to the bottom of the drill casing, open hole, or the rock socket. Grout is gradually extracted from the hole by pumping it via the tube. Drilling fluid is displaced by the grout as it fills the drill casing or hole. Tremie grouting is mostly utilized in granular soils under optimal conditions or if the bond zone of the Pin Pile is based on rock. Grout loss is likely while working in extremely fractured or shattered rock, or in voided, karstic settings. This may call for testing to determine whether a sealed bond zone exists. Before installing the last piece of pile reinforcement, it is customary to carry out a few tests to confirm the integrity of the grout. Occasionally, it makes sense to grout a pile once, then re-rill it and grout it one more time before finishing it (Elarabi & Soorkty, 2015).

Pressure Grouting:

One technique to increase dirt pile capacity is pressure grouting. In order to accomplish this, pressure is applied through the drill head to the top of the fluid grout column as the drill casing is removed from the bond zone. A "grout bulb" is formed when the grout is forced into the surrounding soil by the pressure. The friction and adhesion that form between the grout bulb and the surrounding soil determine the pile capacity.(Elarabi & Soorkty, 2015).

2.6.2 *Post grouting:*

Using a tube with drilled holes and rubber sleeves (one-way valves) covering it, post grouting is a technology that permits the controlled addition of more grout at pressures that may surpass the lateral strains that occur naturally. When steel-sleeved pipes are utilized, the sleeved port pipe is occasionally a component of the reinforcing and is typically dropped into the hole with the core reinforcement. Once the first grout has partially set, certain sleeve ports are used to introduce regulated volumes of grout at high pressure using a packer. This method causes greater in-situ lateral pressure on the surrounding bond zone. When expanding it, breaking the original grout, and enabling the application of more grout(Elarabi & Soorkty, 2015).

2.7 Loads on Retaining Walls

2.7.1 *Rankine's theory of active earth pressure*

The equation mentioned below (*1*) determines the effective horizontal soil pressure at a depth H, where the amount of lateral stress the soil imposes is calculated by the active earth pressure coefficient (Ka) and unit weight (γ) of soil (Das & Sobhan, 2006).

$$\sigma_{h'} = \gamma H K_a \qquad (1)$$

where $\sigma_{h'}$ is vertical effective stress,

H is height from the ground surface,

K_a is the active earth pressure coefficient,

ϕ is the internal friction angle of the soil.

$$K_a = tan^2(45 - \frac{\phi}{2}) \qquad (2)$$

2.7.2 *Rankine passive earth pressure*

At depth z, the effective vertical pressure on a soil element is σv' = γH. Initially, if the wall does not yield at all, the lateral stress at that depth will be σh' = KHσv'. if the wall is displaced by an amount Δx, the vertical stress at depth H becomes the same. The horizontal stress increases with depth. Thus, σh will be greater than $KH\sigma_o$' (Das and Sobhan, 2017).

$$K_p = tan^2(45 + \frac{\phi}{2}) + 2c\ tan(45 + \frac{\phi}{2}) \qquad (3)$$

where c is cohesion of the soil; for cohesionless soil, c = 0.

2.7.3 *Rankine active and passive earth pressure in inclined backfill*

Rankine gives the Rankine active and passive earth pressure in the case of a frictionless wall with a vertical back and a horizontal backfill of granular soil(Das & Sobhan, 2006a).

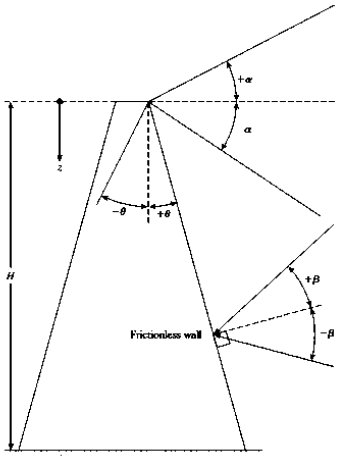

σh' active or passive earth pressure

Figure 2.3: Rankine active and passive pressures (Das, 2019)

Rankine active earth pressure

$$\sigma_{h'}\ (active) = \frac{\gamma H cos_{\alpha}\sqrt{1 + sin\,2\phi\ - 2sin\phi cos\varphi a}}{cos\alpha + \sqrt{sin2\phi' - sin2\alpha}} \tag{4}$$

where α is the inclination of the bakfill with the horizontal.

$$\varphi_a = sin^{-1}\left(\frac{sin\alpha}{sin\phi}\right) - \alpha + 2\theta \tag{5}$$

Rankine Passive Case

$$\sigma_{h'}\ (passive) = \frac{\gamma H cos\alpha\sqrt{1 + sin\,2\phi + 2sin\phi cos\varphi_p}}{cos\alpha - \sqrt{sin2\phi' - sin2\alpha}} \tag{6}$$

$$\varphi_p = sin^{-1}\left(\frac{sin\alpha}{sin\phi}\right) + \alpha - 2\theta \tag{7}$$

2.8 DESIGN EQUATIONS FOR THE MICROPILES

End bearing and skin friction resistance work in the micropiles' load transfer mechanism. Micropile design processes were discussed, although only the axial structural capacity of the micropile, with the bond stress approach, was used specifically for the micropile (BRIDGES, n.d.) .

2.8.1 *Axial capacity of the micropile*

The capacity of the micropile:

$$Q = Q_b + Q_s \tag{8}$$

where:

Q = Ultimate capacity

Q_b = End bearing resistance

Q_s = Skin friction resistance

2.8.2 *End bearing resistance*

The end bearing capacity of a micropile is mainly determined by the load-bearing capacity of the rock or soil layer at the base of the pile. This resistance is a result of the soil or rock's ability to withstand compressive stresses.

The end-bearing of (Q_b) can be calculated using the Terzaghi and Meyerhof bearing capacity equations (Liew & Fong, 2003). These equations are widely used in geotechnical engineering:

$$Q_b = A_b \times c \times N_c + A_b \times \gamma \times N_q \times D_f \quad (9)$$

where:

A_b is the pile tip's foundation region for the micropile.

c is the cohesion of the soil bearing stratum.

γ is the unit weight of the soil.

N_c and N_q are bearing capacity factors related to the soil or rock properties.

D_f is the depth of the pile tip beneath the ground surface

2.8.3 *Skin friction resistance*

The interaction of the pile and the surrounding soil develops skin friction resistance along the micropile shaft. It is affected by several factors, including the soil properties, pile dimensions, and the roughness of the pile shaft.

The ultimate skin friction (Qs) of a micropile can also be be calculated using the following formula provided by (AASHTO, 1993):

$$Q_s = \pi D \sum_{i=1}^{n} f_{si}\, d_{li}\, f_s \quad (10)$$

where:

D, diameter of pile.

D_{li}, the micropile's length when it is in interaction with the ground in each layer

f_{si} =ultimate unit friction for each soil layer i

n = no of soil layers considered

The ultimate unit skin friction fsi in cohesionless soils is calculated by using the β method(Abdul Karim Elsalfiti, 2011).

$$f_{si} = \beta \sigma_{v'} \quad (11)$$

where:

$\sigma_{v'}$ is the vertical effective stress at depth H

β is the coefficient of proportionality

B = K *tanδ

K = coefficient of earth pressure on the surface of the wall of the drilled shaft during side shear failure.

δ = angle of effective stress and friction for the soil-pile interface.

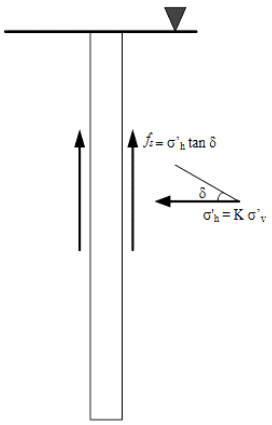

Figure 2.4: Skin friction of drilled shafts in cohesionless soil

Rollins et al. (2005) studied on the results of 28 axial tension (uplift) load tests of drilled shafts' soil profiles, which ranged from uniform medium sand to well-graded sandy gravel layers. Using measured skin friction and the angle of shearing resistance, the coefficient of lateral earth pressure K for the load tests. Back calculation of K values against depth gives the equation(Elsalfiti, 2011).

$$k = 4.62e^{-0.137H} \quad (12)$$

where:

H is the depth below the ground surface.

δ is equal to φ

2.8.4 *Geotechnical compression or tension load by bond stress method*

(FHWA, 2005) The geotechnical capability of the micropile was described in the Micropile Design and Construction Manual in terms of bond strength. The bond

strength is the bond relation between the soil and grout. To resist the tension and/or compression load expected. Grouting enhances the load transfer mechanism of micropiles beneath the foundation. Soil or rock layers attached to the pile increase the skin friction along the pile stem(FHWA, 2005).

$$P_{G-allowable} = \frac{\alpha_{bond}\,(\pi D H_i)}{FS} \quad (13)$$

where:

$P_{G\text{-allowable}}$ = compression or tension loading in (kN)

α_{bond} = grout to ground ultimate bond strength (kPa). It was taken from (FHWA, 2005)

FS = factor of safety (recommended 2-2.5)

D = diameter of micropile drilled hole

H = bond length designated for micropile in height of soil layers (m)

2.8.5 *Axial compression-tension capacity with structural consideration*

The axial capacity of the micropile's structural parts is determined by the combination of steel and grout in terms of allowable stress design. The following equation to figure out the compression design as per (FHWA, 2005)

Compression capacities

$$P_c = 0.4\,P_g + 0.47\,P_{ft} \quad (14)$$

Tension capacities

$$Pt = 0.55\,P_{ft} \quad (15)$$

where:

P_{ft} = f_y_rebar A rebar + f_y casing A casing,

$P_g = f_c\,A_g$

f_c is the unconfined compressive strength (UCS) of the grout,

A_g is the cross-sectional area of the grout in the pile,

f_y rebar and $f_y\,casing$ are the yield strengths of the steel rebar and casing, respectively, and

Arebar and $Acasing$ are the cross-sectional areas of reinforcement and casing pipe, respectively.

2.8.6 *Elastic modulus of the micropiles*

$$E_m = (A_g \times E_g + A_{sl} \times E_s)/A_m \quad (16)$$

(FHWA, 2005)

where:

E_m is the elastic modulus of the micropile,

A_g, area of grout,

E_g is the elastic modulus of grout,

A_s is the area of reinforcement used,

E_s is the elastic modulus of the reinforcement,

A_m is the cross-sectional area of the micropiles.

2.8.7 *Scour depth estimation*

Scour depth is the vertical distance below the high flood level (HFL) of the natural channels' flow over a scour bed level. Mean scour depth beneath the high flood level can theoretically be predicted by the equation given (Indian Roads Congress, 2014)

$$d_s = 1.34(\frac{Q_b^2}{K_{sf}})^{\frac{1}{3}} \quad (17)$$

where:

d_s = scour depth,

Q_s = design discharge per meter width,

K_{sf} = Silt factor, and a representative sample of bed material obtained at the level of the anticipated deepest scour.

K_{sf} is given by the expression of Lacey's silt factor

$K_{sf} = \sqrt{1.76\ d_m}$

Where, d_m =weighted mean diameter in millimeters.

2.8.8 *Scouring geometry characterization*

Method 1: Slope of scour

Through laboratory experiments, the geometry of local scour holes, including upstream and downstream slope ratios, has been thoroughly investigated.

Hong et al. (2020) research on physical model investigations on scour holes downstream of release structures was carried out by, who reported gentler downstream slopes near 1:10 due to silt deposition and upstream slope ratios of 1:3 to 1:5 (H:V) driven by significant outflow velocities. The greatest lateral scour extent can be estimated empirically using the formula

$$x_0 = y_s \times H{:}V \quad (18)$$

where, y_s = scour depth, x_o= lateral extent of scour

Method 2: Lateral extent of scour

The lateral extent of abutment scours as per (FHWA, 2005) is discussed in relation to flow depth and scour depth at vertical wall abutments.

$$x_0 = 2.0 \times d_s \quad (19)$$

where, D_s = scour depth

Method 3: Critical Velocity and Scour Initiation

Modern scour-initiation criteria are based on the fundamental incipient-motion concept developed by Shields (1936)., which links dimensionless shear stress to particle mobility. (Laursen, 1963) used field and laboratory regression to establish the critical velocity formula.

$$V_n = K_u \times y^{1/6} \times {D_{50}}^{1/3} \quad (20)$$

where:

Vc is critical velocity

K_u= shield parameters,

y_1 depth of flow,

D_{50} is particle size.

Richardson and Davis (2001) formalized in HEC-18 with Ku = 6.19 in SI units. Equation becomes:

$$V_c = 6.19 \times {y_1}^{1/6} \times {D_{50}}^{1/3}$$

Velocity Decay and Lateral Scour Extent:

As momentum is transferred throughout the channel, flow velocities decrease with distance from a structure. Melville and Coleman (2000) reported decay coefficients compatible with k = 0.32 for abutment and bank structures, which are further supported by velocity distribution profiles in USACE (1994). Raudkivi (1998) uses a negative exponential function to express this lateral decay.

$$V(x) = V_0 \times e^{-kx} \quad (21)$$

Profile Representation of Scour Holes:

It is easier to define stable protection extents and estimate volume when the scour hole cross-section is described by a smooth, continuous function. (Adduce & Sciortino, 2006) (Hong et al., 2020)

The shape of scour holes is an irregular or semi-ellipse that is well approximated by a parabolic (quadratic) function in cross-section.

$$y = D_s \times [1 - (\frac{x}{x_o})^2] \quad (22)$$

where D_s is the scouring depth from the ground surface and X_o is the extent of the scouring.

3 STUDY AREA

The study area was located along B.P. Highway (Araniko–Sindhuli Highway), which traverses the Roshi Khola transport corridor spanning two districts, Kavrepalanchowk and Sindhuli, in the central-eastern hill region of Nepal. The corridor follows the Roshi River for approximately 66 km, from Fulchoki Hill in Kavrepalanchowk to Nepalthok in Dumja, Sindhuli, covering a catchment area of 565.4 km^2.

The B.P. Highway is one of Nepal's strategically important national road corridors, connecting the Kathmandu Valley to the hilly and Terai regions of eastern Nepal. However, the catastrophic flood event of September 2024, triggered by extreme rainfall exceeding 200 mm in 24 hours during 27–29 September, caused widespread and severe damage along this corridor. Numerous cantilevers retaining walls, road embankments, and bridge structures along the Roshi section of the B.P. Highway were either partially or completely destroyed by the flood, leaving the corridor critically disrupted.

In the aftermath of the 2024 Roshi flood, reconstruction and new construction works have been initiated along the damaged sections of the highway. As part of these reconstruction efforts, the design and retrofitting of retaining wall structures has become a priority concern for engineers and planners, given the demonstrated vulnerability of existing infrastructure to flood-induced and seismic loading. It is within this post-disaster reconstruction context that the present study investigates the use of micropiles beneath cantilever retaining walls as a resilience-enhancing measure for the Roshi corridor.

The case study site lies within the Sub-Himalayan (Siwaliks) Zone along the BP Highway, Nepalthok to Bhakundebesi Road Section. Geologically, the Siwalik Zone was bounded by the Main Boundary Thrust (MBT) to the north, separating it from the Lesser Himalayan Zone, and the Main Frontal Thrust to the south, separating it from the Terai. The Siwalik rocks are predominantly sedimentary in nature, consisting of mudstone, sandstone, and conglomerate, while the terrain exhibits rugged topography with deeply eroded gullies and steep slopes. The highway corridor was drilled to a total depth of 10.5 meters. The subsurface profile at this location is predominantly characterized by a dense to very dense heterogeneous mixture of Sand with Gravel and Boulders (classified as SP under USCS) throughout the entire depth of exploration.

SPT N-values obtained from field testing range from 21 at 1.5 m depth to refusal (N = 50) at 9.0 m and 10.5 m depth, confirming the dense to very dense compactness classification of the granular material across the borehole profile. The borehole log of the soil test at the site is mentioned in the annex.

Figure 3.1: Study area of Roshi section of BP Highway

4 METHODOLOGY

A summary of the methods applied to complete the analysis, together with a report on results, is included in this section. A short summary of the entire procedure may be provided by using a flow chart, as shown in Figure 4.1 below.

The research was conducted in different stages.

i. Literature review and data acquisition: The objective of this part of the study was to collect the required data needed to enter into the FE program including the parameters of sandy soil and a literature analysis to identify the correlation that would be useful for the processing of the data collected to prepare the input. A brief review of the literature on earlier studies compared with these is also included in this section.
ii. Processing of data for input: In this phase, taking into account both the mathematical and empirical relationships found in many books and literature, all the data were processed from step a, and the data were prepared for modelling.
iii. Input data collection: Field data taken from the case study site of the BP highway Roshi Section. Soil test results are collected, and field observation of the site is conducted with the client and contractor's permission. From field observation, all required dimensions of structural components and nearby site conditions were considered for the analysis.
iv. The empirical values taken from the publications and literature reviewed at step b, and further relevant collected data from step c, are ready to model FE software's problem, i.e., Plaxis 2D.
v. Value taken from a similar type of model from steps a and b. Prepare the model in the FE software's problem, i.e., Plaxis 2D. And validate the model results with the literature.
vi. Prepare the model in the FE software as per the data collected from steps c, d. Validate the model by an analytical method.
vii. Run the model: Take out the output result in different scenarios for the case study site. Scenarios are static conditions, pseudo-static conditions, water level rise and fall conditions and seismic conditions.
viii. A parametric study was carried out using several numerical models built taking in account various variables.
ix. Output data: The output data, including the soil's ultimate capacity, load transfer capacity of structures, settlement, and deformation, have been obtained after successful use of this model in the FE program.

x. Processing of the output data: In this phase, all outputs from steps (g), (h), and (i) were arranged and processed to ensure they are presentable and include the necessary verifications to validate the results. After that, the outcomes were aggregated and compared across various scenarios.

xi. Comparison of parametric study data with scenario data: Additionally, comparisons were made between the data obtained from different parametric studies and the data from various scenarios' overall analysis.

xii. Result analysis: Conduct the various result analyses based on step a, with the results taken from j and k, and conclude the results. And Recommendations further with limitations of the research study.

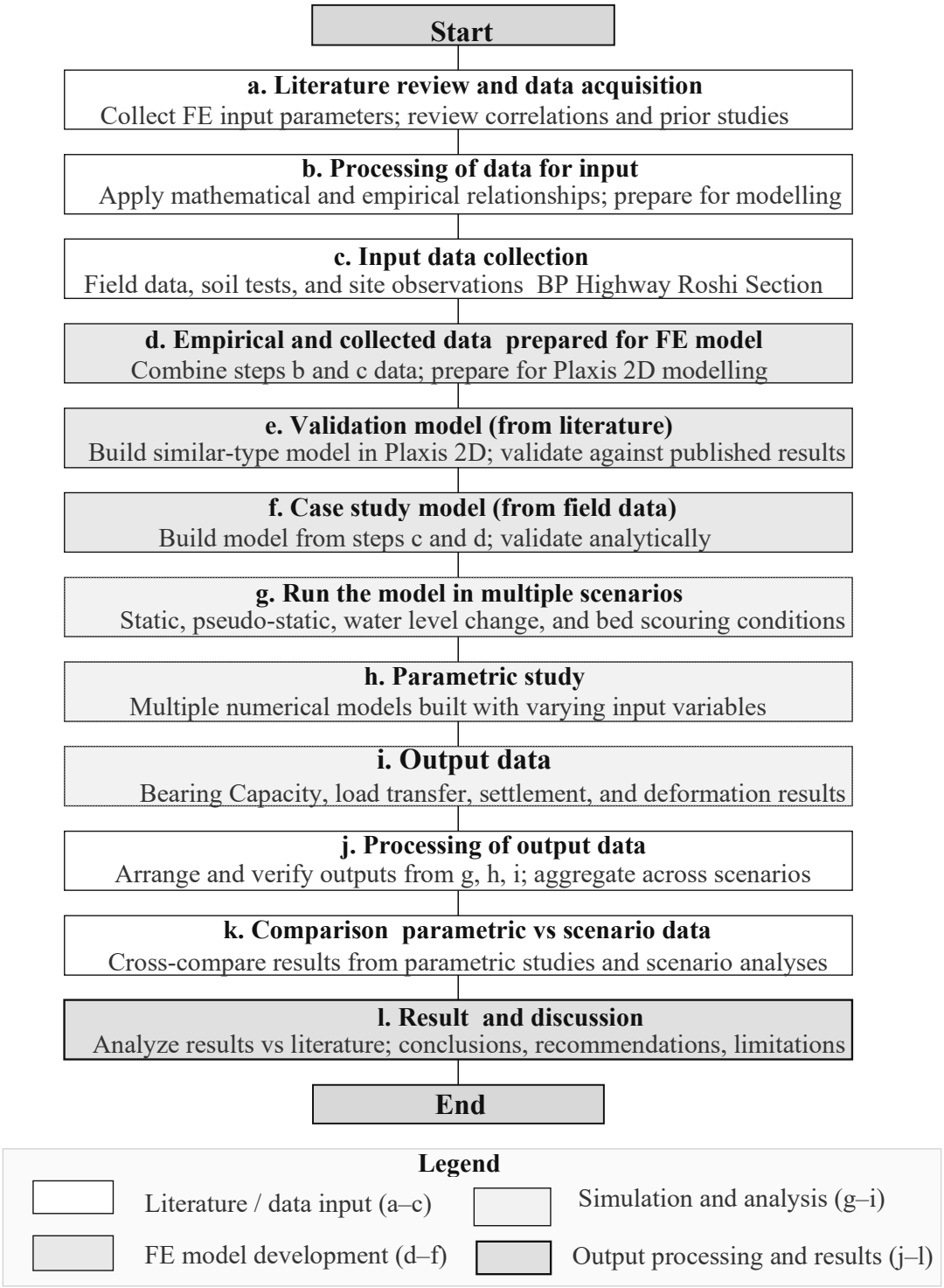

Figure 4.1: Flowchart of the methodology of the study

4.1 Material Model and Property

4.1.1 *Material model*

A soil constitutive model is a mathematical representation or mathematical equation used to describe the mechanical behavior of soil under various loading and deformation conditions. These models are used in geotechnical engineering and soil mechanics to predict how soils will respond to different types of loads, such as those from building foundations, retaining walls, embankments, and other civil engineering structures. Understanding the behavior of soil is crucial for designing safe and stable structures.

There are several types of soil constitutive models, each tailored to specific soil types and loading conditions. Some common soil constitutive models include:

i. Linear Elastic Model: This assumes that soil behaves elastically; it returns to its original shape after removal of load. It's suitable for small strains and short-term loading conditions.
ii. Elastic-Plastic Model: This model accounts for both elastic and plastic deformation. When the soil undergoes excessive loading, it deforms plastically and retains some of that deformation after the load is removed. This model is often used for predicting soil settlement and stress redistribution in long-term loading situations.
iii. Mohr Coulomb Model: For granular soils like sand and gravel, the Mohr Coulomb model was frequently utilized. Cohesion (c) and internal friction angle (φ) were used to explain soil behavior. It is very helpful in analyzing failure circumstances and shear strength.
iv. Hardening Soil Model: This model accounts for soil hardening (increasing stiffness) with increased loading.
v. Softening Soil Model: Conversely, this model accounts for soil softening (decreasing stiffness) with increased loading, which is common in some types of soils.
vi. Viscoelastic and Viscoplastic Models: These models is about time dependent behavior, which is used for analyzing soil behavior under dynamic loading

The choice of a specific soil constitutive model relies on the type of soil and the loading conditions. Engineers use these models in numerical simulations and analyses to predict soil behavior and ensure the safety and stability of civil engineering projects.

Soil failure in two-dimensional conditions of stress is incredibly difficult, in addition to the behavior of the soil. In recent years, many models have been suggested to depict the stress-strain and failure behavior of soils. All these models have drawbacks and limits that are mostly dependent on their use. To study this research, the Mohr Coulomb soil model was employed.

4.1.2 *Mohr Coulomb soil model*

Mohr-Coulomb is a constitutive soil model used in soil mechanics, generally used to describe the shear strength and failure behaviour of soils such as clays and granular soils like sands and gravels. This model was developed based on the principles of soil mechanics and is particularly useful for analyzing soil behaviour analysis and slope stability.

According to the Mohr Coulomb cohesion (c) and the angle of friction (φ), the soil's shear strength is determined. The parameters, which are usually determined by laboratory testing, describe the strength characteristics of soil. The model works as follows:

i. Cohesion (c): Cohesion represents the strength of the soil due to cohesive forces between particles. Cohesion is more important for cohesive soils (like clays) and usually nil for non-cohesive soils (like sands).
ii. Internal Friction Angle (φ): The angle of internal friction determines how resistant the soil is to shear deformation. It is the angle created by the normal stress that lies on the failure plane, also known as the shear plane. The shear strength of soil increases with the angle of internal friction.

The Mohr Coulomb soil model relates shear stress (τ) to the normal stress (σ_n) on the plane of failure by the equation:

$$\tau = c + \sigma_n * tan(\varphi) \qquad (23)$$

where:

τ is the failure plane's shear stress.

φ is the angle of internal friction.

c is the cohesion of the soil.

σ_n represents the typical stress applied to the failure plane.

According to the Mohr-Coulomb model, soil collapse happens when a plane's shear stress is more than its shear strength, which is determined by internal friction and cohesiveness. It is anticipated that high pore water pressures will gradually drop when shear deformation occurs because the model is often

employed in a drained condition. The Mohr Coulomb soil model offers straight forward yet efficient method for evaluating soil stability and forecasting the likelihood of slope failures occurring, bearing capacity of the foundation, and other geotechnical engineering issues. For effective use of this model, accurate values for cohesion and the internal friction angle are required, which can be determined by laboratory testing for particular soil types. The Mohr Coulomb model is mostly used in geotechnical engineering practice in conjunction with safety considerations for the analysis of stability of retaining walls, slopes, and foundations to ensure the safety of engineering structures.

4.1.3 *In undrained conditions*

The Mohr-Coulomb model can also be adapted for undrained conditions, which occur when there is little or no time for pore water pressures to dissipate during shear deformation. Undrained conditions are commonly associated with quick loading events, such as rapid excavation or seismic loading. In undrained conditions, the soil's effective stress remains nearly constant during shearing. To account for this behavior, the Mohr Coulomb model is modified by incorporating the effective stress concept.

The effective stress becomes critical under undrained conditions. It is difference between total stress and pore water pressure. That affects soil strength and deformation. This is considered by the modified Mohr Coulomb soil constitutive model in undrained conditions, which accurately predicts the behaviour and shear strength of soil.

In situations where undrained conditions are anticipated to arise, engineers utilize this updated model to assess the stability of slopes, foundations, and other geotechnical structures subjected to rapid loading. Effective cohesion (c'), effective angle of internal friction (φ'), and the effective stress coefficient (α) must all be precisely determined in the lab to apply this model.

4.2 Field Data Collection

The B.P. Highway is one of Nepal's strategically important national road corridors, connecting the Kathmandu Valley to the hilly and Terai regions of eastern Nepal. However, the catastrophic flood event of September 2024, triggered by extreme rainfall exceeding 200 mm in 24 hours during 27–29 September, caused widespread and severe damage along this corridor. Numerous cantilevers retaining walls, road embankments, and bridge structures along the Roshi section

of the B.P. Highway were either partially or destroyed by the flood, leaving the corridor critically disrupted.

In the aftermath of the 2024 Roshi flood, reconstruction and new construction works have been initiated along the damaged sections of the highway. As part of these reconstruction efforts, the design and retrofitting of retaining wall structures has become a priority concern for engineers and planners, given the demonstrated vulnerability of existing infrastructure to flood-induced and seismic loading. It is within this post-disaster reconstruction context that the present study investigates the use of micropiles beneath cantilever retaining walls as a resilience-enhancing measure for the Roshi corridor. Road Section of the proposed is a 7 m 2-lane road. And the section of the riverside is raised by the support of the cantilever retaining wall of 7m in height from the base of the foundations. The base of the wall is reinforced by the micropiles as shown in the figure below.

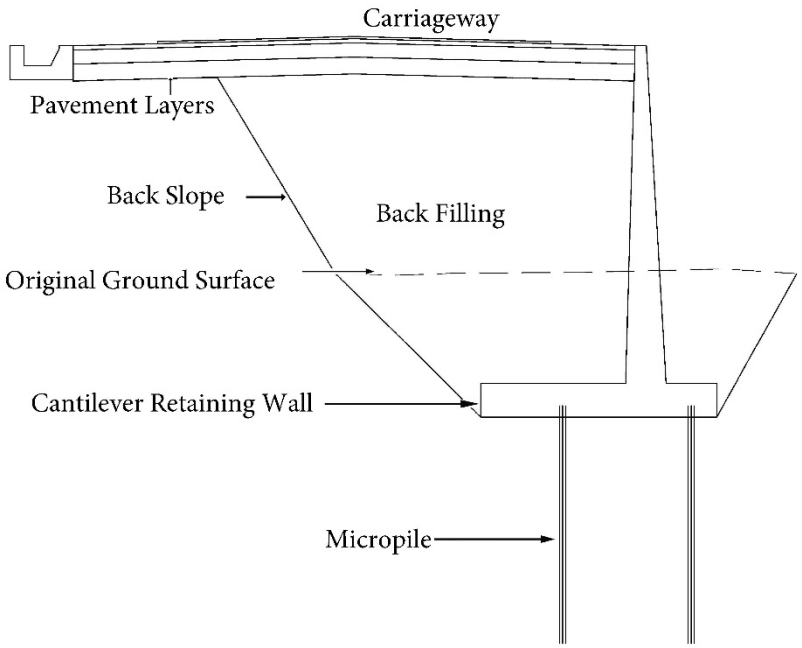

Figure 4.2: Road section of the case study site

The base of the cantilever wall is 4.2 m, and height is 7m from foundation of the wall. Micropile was placed below the foundation at 1.5 from the heel part of the foundation and 0.5 m from the toe part of the cantilever wall foundations. Center-to-center spacing of micropile in a row is 1.5m. Total Height of the micropile is 5.5m, where o.3m is above the ground surface of the foundation level.

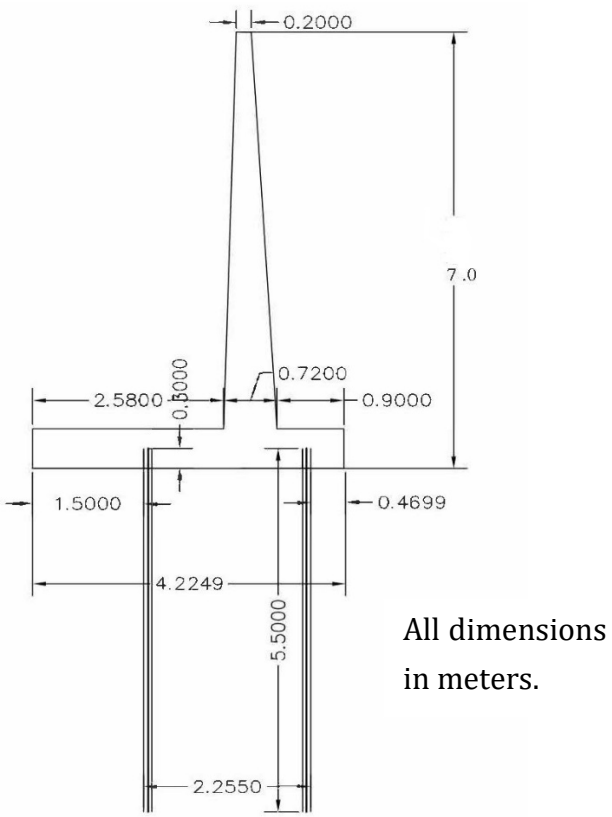

Figure 4.3: Cantilever retaining wall and micropile section

Cantilever retaining wall is M20 grade, and the grout used in the micropile also has M20 grout strength. Rebar is used of 25mm. Micropile having an inside diameter of 100mm, and a thickness of the steel casing is 5mm. Total diameter was 110mm.

The highway corridor was drilled to a total depth of 10.5 meters. The subsurface profile at this location is predominantly characterized by a dense to very dense heterogeneous mixture of Sand with Gravel and Boulders (classified as SP under USCS) throughout the entire depth of exploration.

SPT N-values obtained from field testing range from 21 at 1.5 m depth to refusal (N = 50) at 9.0 m and 10.5 m depth, confirming the dense to very dense compactness classification of the granular material across the borehole profile. The borehole log of the soil test at the site is mentioned in the annex.

4.2.1 *Material property*

Soil profile and properties

In situ soil test by Standard Penetration Test (SPT), the test site was made out of granular material.

Table 4.1: Soil parameters adopted in this study of the model

Layer	Height (m)	Υ_{sat} kN/m3	Υ_{unsat} kN/m3	Void ratio e	E'$_{ref}$ kN/m3	Poission's ratio μ (nu)	Anfle of internal friction φ (°)
Topsoil layer	0-3	18.98	17	0.81	29300	0.3	30.8
Middle soil layer	3-6	18.86	17	0.8	37920	0.35	31.5
Bottom soil layer	>10.5	19.45	18	0.73	67160	0.35	32.55
Backfill soil	0-3	18.98	17	0.81	29300	0.3	30.8
Subgrade of the road section		19	16	0.5	50000	0.35	30.5
Subbase of road section		22	21.52	0.3	157800	0.35	38
Base of road section		23	22.54	0.5	279100	0.35	36
Asphalt Layer			22.30	0.5	2x106	0.35	

4.2.2 *Footing plate parameters*

Table 4.2: Parameters of cantilever wall foundation

Parameter	Values
Material	Concrete
Materials type	Elastic
Young's modulus (E) kN/m^2	22.36 x 10^6
Unit weight (Υ) kN/m^3	25
Poisson's ratio μ	0.15
Dimensions (LxBxH) m	12 x 4.2 x 0.6

Table 4.3: Parameter of cantilever wall stem

Parameter	Values
Material	Concrete
Materials type	Elastic
Young's Modulus (E) kN/m^2	22.36×10^6
Unit Weight (Y) kN/m^3	25
Poisson's ratio μ	0.15
Thickness	Avg(0.72+0.2)=0.46 m
Dimensions (LxBxH) m	12 x 0.46 x 7

4.2.3 *Micropile parameters:*

Elastic Modulus of micropile using Equation (16) and other parameters are as:

E_{steel} rebar = 200,000 MPa

E_{steel} casing = 210 GPa

f_{ck} concrete =20 MPa

$E_{grout} = 22.36 * 10^6$ kPa

Table 4.4: Parameters of micropile

Parameter	Values
Material	Concrete, rebar, and steel casing
Young's Modulus (E) kN/m^2	64.1×10^6
Unit Weight (Y) kN/m^3	24
Poisson's Ratio μ	0.15
Shape	Cylindrical
Length (m)	5.5
Outer diameter (m)	0.11
Inner diameter (m)	0.1
Rebar Diameter (mm)	25

4.3 Development of Finite Element Model

A software based on finite elements was employed to examine the behavior of the foundations of cantilever retaining wall supported by micropiles. As seen in Figure 7. The numerical model was conducted under an undrained and drained condition as per the soil types. The top 2.5m of soil was removed and a water table was created at that level. The cantilever wall was modelled as a plate element. Micropile was modelled as an embedded beam element of length and diameter 5.5m and 0.11m, respectively.

The Finite Element Method (FEM) is a numerical method applied in engineering and scientific domains to solve partial differential equations describing physical events. FEM breaks down complex problems into smaller, simpler elements, allowing for the approximation of solutions. Here's a detailed description of FEM:

i. Problem Discretization: FEM starts by dividing the continuous domain of the problem into smaller, discrete elements or subdomains. These elements can be simple geometric shapes like triangles or quadrilaterals in 2D or tetrahedra and hexahedra in 3D.
ii. Approximation of Solution: Within each element, an approximation of the solution is made using piecewise functions called shape functions. These shape functions are chosen to represent the behavior of the solution within each element.
iii. Assembly of Global System: To create a global system of equations, the discrete elements are joined at their common borders or nodes. The equations are put together from the element-level equations and are usually based on physical concepts.
iv. Boundary Conditions: Boundary conditions, which define the behavior of the numerical model on the problem boundaries, were applied to the global system of numerical model. These conditions can be essential for specifying constraints, forces, or prescribed values.
v. Solution of Linear System: Numerical methods such as Gaussian elimination or the direct solver are employed to solve the resulting system of linear or nonlinear equations. Iterative approaches are also an option (e.g., conjugate gradient method or Newton-Raphson method for nonlinear problems).
vi. Post-Processing: Once the system is solved, the computed solution values (e.g., displacements, temperatures, stresses) can be extracted at specific points of interest within the domain or along the boundaries.

vii. Error Estimation and Refinement: FEM allows for the assessment of the solution's accuracy. Error estimators can identify areas where the solution is less accurate, which can guide mesh refinement for improved results.

Applications:

- FEM is widely used in various engineering fields, including geotechnical, structural analysis, fluid dynamics, electromagnetics, earthquake load analysis, and more.

Advantages:

- FEM is highly versatile and capable of handling complex geometries and material properties.
- It provides accurate solutions for a wide range of problems.
- It allows engineers to explore different design variations and perform sensitivity analyses.

Challenges:

- Proper meshing is crucial, and a poorly designed mesh can lead to inaccurate results.
- Solving large-scale problems may require significant computational resources.
- Nonlinear problems can be challenging and require iterative solvers.

FEM is a powerful numerical method that has revolutionized the way engineers and scientists approach complex problems. It is a fundamental tool in modern engineering analysis and design, allowing for the simulation of physical systems and the optimization of designs with a high degree of accuracy and efficiency.

4.3.1 *Model geometry*

The model's dimensions were selected to ensure that there would be very little strain near the boundary. The computation time will increase with the size of the model's geometry. Thus, the total dimension of the model is selected for three situations in order to maximize both the computational time and the geometry of the model. In order to save computation time in the event of an underpinning foundation, a quarter of the plate was modelled due to the symmetry of the problem.

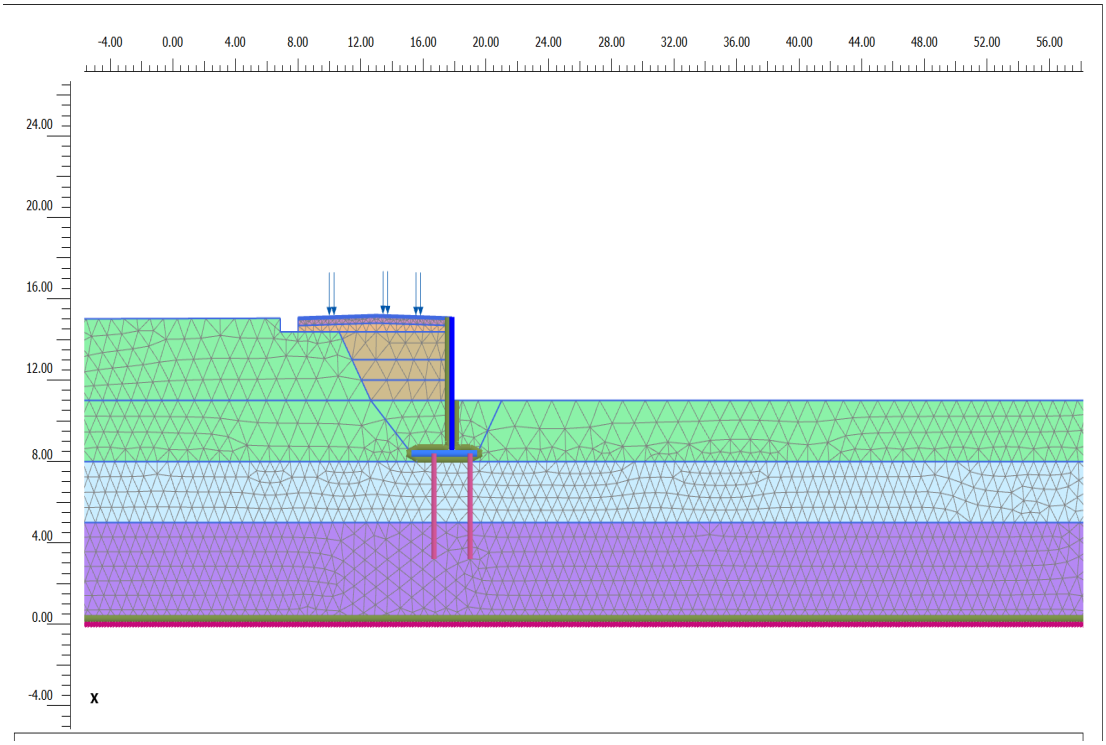

Figure 4.4: Geometric model of the road section

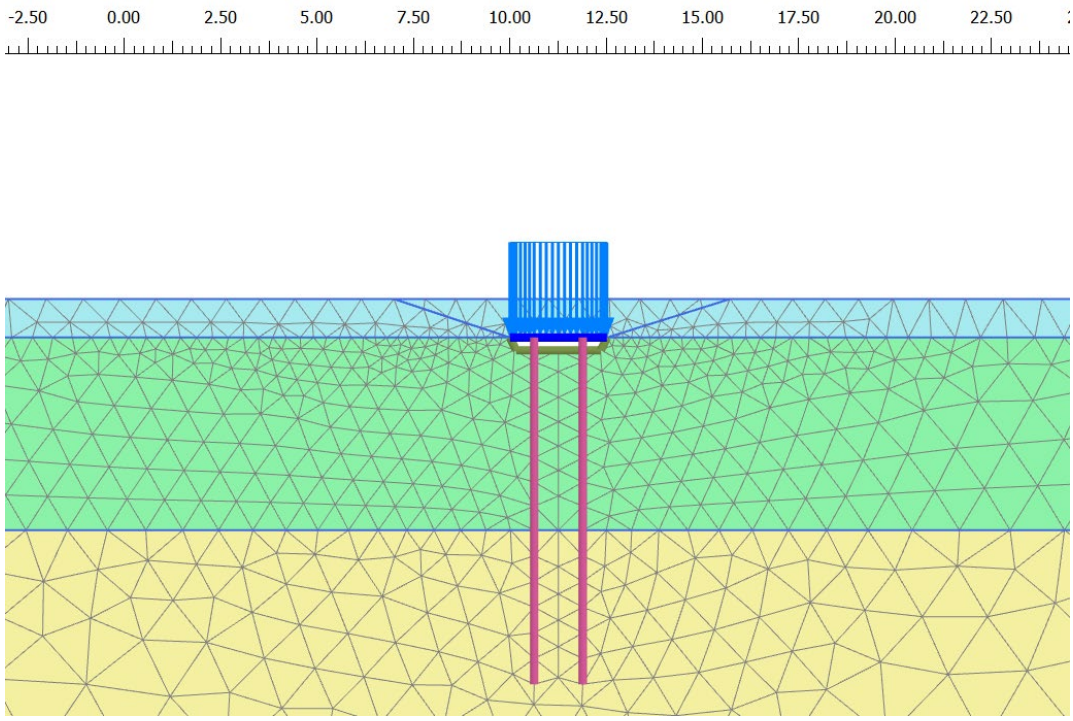

Figure 4.5: Validation model with Kyung et al., 2017

4.3.2 *Boundary condition*

Every FEM-based program executes an iterative analysis during the computation of stresses and strains induced in the model, which converges to a solution that fulfills the boundary conditions. Therefore, it is important to select boundary conditions such that the displacement or strain at the model boundaries reflects the actual site conditions in all three dimensions. To accurately represent the actual site state for this study, the displacement or strain at any location more than a few meters from the point of load application was set to zero.

In Plaxis 2D, the deformation boundary conditions are defined as follows: "Normally fixed" indicates that displacement in the direction normal to the plane under consideration is constrained, while displacement in the remaining direction is permitted. "Fully fixed" means that displacement in all directions is constrained to zero. Conversely, "free" allows displacement in both directions of the considered plane.

4.3.3 *Finite element meshing*

With the formation of the geometric model, meshing has been done. In order to have a smooth, accurate, and numerically stable calculation, thousands of soil elements were generated, which were regular, i.e., without being excessively long and thin. The mesh should be of good quality, meaning the elements should be regular without being very lengthy and thin, for the numerical stability of the calculation. The elements should be small enough to ensure computation accuracy, especially in locations where considerable variations in stress or strain might be anticipated during the study. However, this does not imply that one should just build a full mesh of tiny elements because doing so will result in a very long calculation time. So, while keeping an eye on the mesh quality, adequate care should be taken to strike the ideal balance between accuracy and calculation time. Fifteen-noded tetrahedral elements were generated for soil material as shown in fig 10, For the accuracy of the calculation, the meshing has been done assigning the element distribution to be “fine” with enhanced mesh refinement. The geometry model after the mesh generation can be visualized.

Forces and displacements of soils and structures are described by a coupled system of (partial) differential equations. In PLAXIS 2D, the model can either be plane strain or axisymmetric. Various material models are used to describe the soil behavior. Structures can be made by multiple point-, -line-, and plate elements. For modelling foundations in PLAXIS in 2D a plate element, node-to-node anchor or embedded beam (row) can be used.

4.3.4 *PLAXIS embedded beam (rows)*

In PLAXIS 2D, the Embedded Beam (row) is a function that models a beam crossing soil volume element at any arbitrary location and orientation. It connects to the surrounding soil through special interfaces that simulate skin and foot resistance.

Although the beam itself occupies no volume, the formulation assumes a surrounding elastic zone, the size of which is based on an input equivalent pile diameter. Due to this zone, the embedded beam behaves almost like a volume pile (T.P.T. Dao, 2011). However, unlike a volume pile, it does not influence the finite element mesh generated from the geometry model, resulting in lower mesh refinement requirements and reduced calculation time.

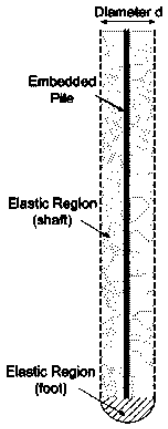

Figure 4.6: Embedded beam element in Plaxis 2D (Plaxis Manual 2025)

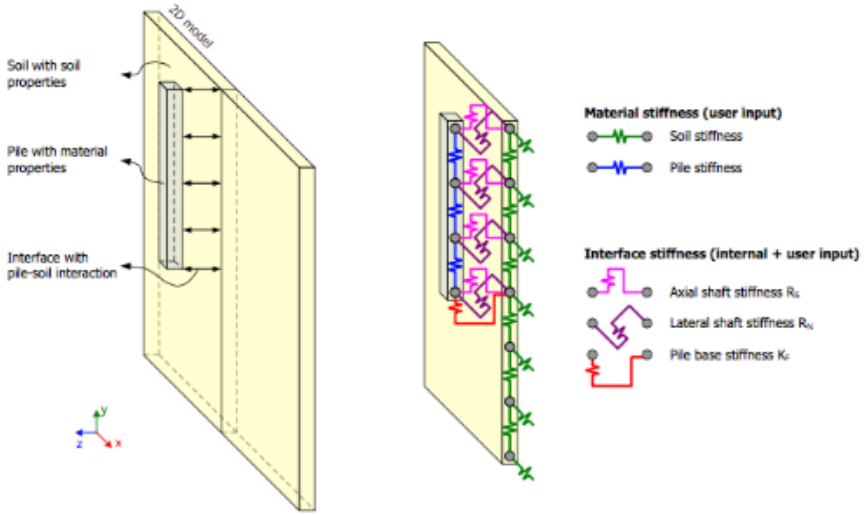

Figure 4.7: 2D pile modelling as embedded beam row (Plaxis Manual 2025)

In PLAXIS 2D, the embedded beam (row) was recently enhanced with new features, including limiting lateral skin resistance and elastic-plastic beam behavior. The implementation in 2D differs from the 3D version because a plane strain model represents a repetitive 1-meter slice, meaning the beam row models a row of piles with 1-meter out-of-plane spacing. Soil-structure interaction is handled via line-to-area interfaces along the pile shaft and a point-to-area interface at the base, utilizing spring stiffnesses and limiting forces for skin resistance, lateral resistance, and end bearing.

4.3.5 *Analytical calculation*

Determination of axial compression- tension in aspects of structural consideration:

Compression capacities P_c and Tension capacities P_t was calculated as 495.71 kN and 135 kN using Equation (14) and Equation (15), respectively, with the following parameter values.

Outer Dia of Micropile = 110mm

A_g = 7363.11 mm^2

A_{rebar} dia 25mm = 490.87 mm^2

A_{casing} = 2408.64 mm^2

Finally, P_c = 495.71 kN and P_t = 135 kN

Determination of Geotechnical Capacity of Micropile in Compression or Tension by Load Bond Stress Method:

The geotechnical capacity of micropile was obtained using Equation (13) with the following parameter values.

H_i = 5.5-0.3 m = 5.2m (0.3 m inserted into pile cap)

α_{bond} = 95 (as per FHWA 2005)

FS = 2

Finally, $P_{G-allowable}$ = 88.46 kN

Determination of Ultimate Capacity of Micropile:

Single axial capacity of the micropile was calculated using Equation (8) where, end bearing capacity and skin friction resistance was obtained using Equation (9) and Equation (10) respectively with the following parameter's values.

$Q_b = A_b * N_t * \sigma_v$,

c=0

$Q_b = A_b * \gamma * N_q * D_f$

A_b= 0.0129 m^2

N_t= 100 (Canadian Foundation Engineering Manual, 3rd Edition,1992)

D_f = 5.2 m

Γ =18 kN/m3

$\sigma_{v'} = 74$ kN/m2

Q_b =-70.32 kN

Table 4.5: Calculation of the skin friction

Depth (H) m	Γ (kN/m3)	ΣV (kN/m2)	K	Tan δ	f_{si}	Q_s (kN)
0.4	17	3.4	4.37	0.612	9.09	1.31
3	17	32.3	2.89	0.639	59.648	64.24
1.8	18	74	2.265	0.642	107.60	69.51
					Total	135.6 kN

Ultimate capacity of micropile (Q) = 205.92 kN

Calculation of scour depth:

Mean scour depth below the high flood level was theoretically calculated by using the formula given in Equation (17) (Indian Roads Congress, 2014) with the parameter's values shown in Table 4.6.

Table 4.6: Calculation of scour depth

Parameter	Value	Unit
Design Discharge (100-yr return period) Q cumec	1,021	m^3/s
Flow Velocity vs	4.17	m/s
Weighted Mean Diameter (D_{50})	0.545	mm
Silt Factor (K_{sf}) IRC coarse sand	1.50	
Channel Width (W)	58	m
Specific Discharge (Discharge per width (q)	17.60	m^2/s
RL of Ground Surface	844.00	m
RL of River at HFL	852.00	m
Depth of Flow at 100-yr Flood	8.00	m
Lacey Normal Scour Depth (D_s)	7.92	m
Design Scour Depth (Ds) Straight Reach (1.27 × D_s)	10.06	m
Depth of Scour Below Ground Surface (Ds)	2.058	m

Determination of Scouring Geometry:

Scouring geometry for scour hole lateral extent was evaluated by different methods.

Method 1: Slope Ratio Method

In this method, the lateral extent of scour was calculated as follows using Equation (18)

$x_{max} = y_s \times$ H:V ratio

For upstream steep slope (1:3): $x = 2.05 \times 3 = 6.15$ m

For upstream gentle slope (1:5): $x = 2.05 \times 5 = 10.25$ m

Method 2: Critical Velocity Method

In this method, critical velocity V_n was calculated as follows using Equation (20)

$$V_n = 6.19 \times (8)^{1/6} \times (0.000545)^{1/3}$$

$V_n = 0.715$ m/s

Velocity decay: As per Equation (21)

$V_{(x)} = V_0 \times e^{-kx}$, *where k = 0.32* Raudkivi (1998)

Zero scour point where V(x) = V_n:

$0.715 = 4.17 \times e^{-0.32x}$

$x = ln_{(4.17 / 0.575)} / 0.32 = 5.51\ m$

∴ x = 5.51 m = 6.0 m (adopted)

Method 3: Hydraulic Engineering Circular Number (HEC-18) Geometry Method:

As per Equation (19)

$x = 2.0 \times d_s$ (FHWA, 2005)

$x = 2.0 \times 2.05$

x = 4.10 m

Adopted the average of three methods, lateral extent of scouring x =6.5m

Scouring Profile Calculation: As per Equation (22)

$y = D_s \times [1 - (x / x_o)^2]$

$y = 2.05 \times [1 - (x / 6.5)^2]$

Parabolic equation used for the FEM analysis of the scoured profile near the wall foundations.

4.3.6 *Numerical calculations*

In the FEM 2D building stage tab, the geometric model is separated into multiple project phases following meshing. The soil and buildings were activated in each phase in accordance with the needs. The initial stress field for the initial geometry configuration is always calculated using the K0 method during the first calculation phase, which was defined automatically. Following the first phase, the corresponding geometry and structure were manually activated to specify the remaining computation stages. Other phases are as the calculation type is Plastic and the loading type is stage construction.

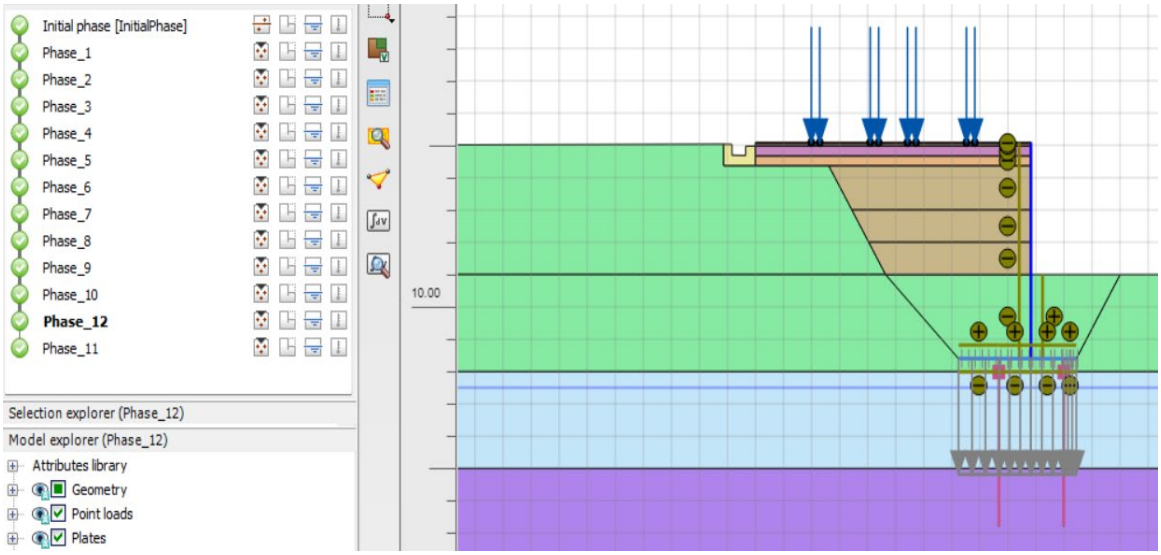

Figure 4.8: Stages of the model in FEM software

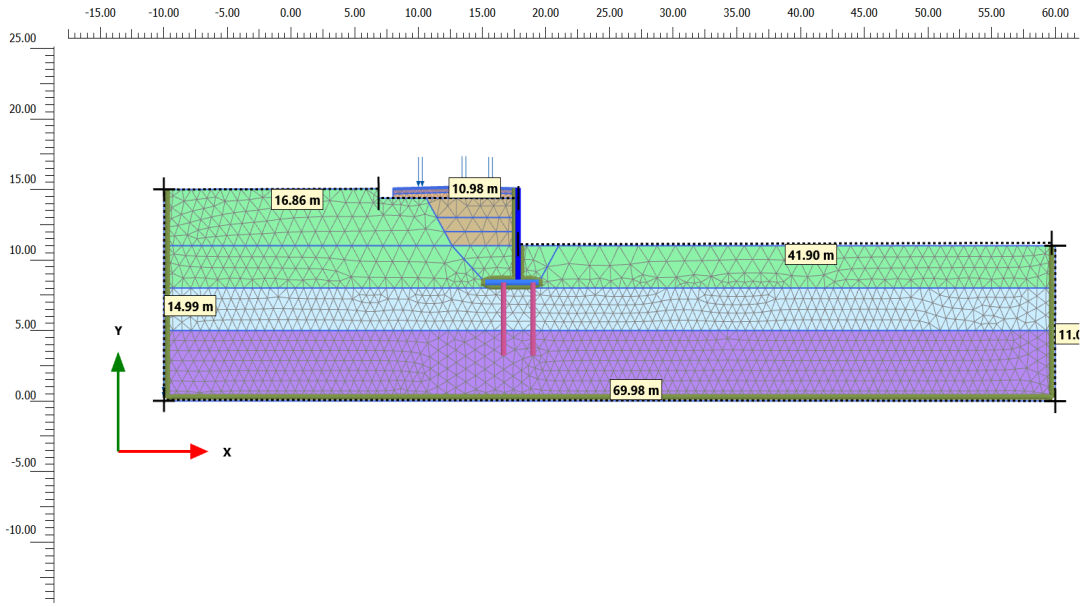

Figure 4.9: Boundary of the FEM model

5 RESULTS AND DISCUSSION

The stability of a micropile-supported cantilever retaining wall was evaluated with reference to the case study, examining displacement, bearing capacity, bending moment, skin friction, load-carrying ratio by micropile, and lateral displacement of the micropiles. Both micropile-supported cantilever wall and unsupported wall were assessed under static conditions, pseudo-static seismic loading, water level rise and fall, and scour depth scenarios. Additionally, a parametric study was conducted on the spacing-to-diameter ratio and the length-to-diameter ratio on the behaviour of the wall.

5.1 Model Validation

5.1.1 *Introduction:*

The numerical model used was validated for the reliability of the Finite Element (FE) analysis. The test results of the numerical analysis are presented, compared, and described in this section. Initially, the results obtained are compared with the experimental data provided by and the numerical result provided by (Elsawwaf et al., 2023a; Kyung et al., 2017c) .

5.1.2 *Numerical model validation:*

i) Validation of the Micropile and Foundation in terms of the vertical load

A. Soil parameters used for the validation of the field test done by Kyung et al. 2017.

Table 5.1: Soil parameters used for validation by Kyung et al., (2017)

Parameter	Upper silty sand	Middle clay	Lower silty sand
Depth (m)	0–1	1–6	6–10
Unit weight (kN/m3), γ_i	17.58	18.77	17.83
Angle of internal friction (°), Ø	28.64	-	33.52
Cohesion (kN/m^2), C	17.4	22.4	32.6

B. Parameters of raft and micropile are as follows:

Table 5.2: Parameters of micropiled raft for validations, (Kyung et al., 2017)

Parameter	Raft	Micropile
Constitutive modeling	Linear elastic	Linear elastic
Unit weight (kN/m^3), γ_i	24	24
Modulus of elasticity	22×10^6 kPa	52×10^6 kPa
Poisson's ratio, ν	0.15	0.15

Micropiles with a diameter of 0.165 m and a length of 9.00 m were used in the study. For the micropile group, a raft measuring 2.52 m × 2.52 m × 1.00 m was employed, supported on four micropiles arranged with a spacing of 1.26 m. The numerical model incorporated three distinct soil layers. The average elastic modulus (E) values for the upper silty sand, middle clay, and lower silty sand were 5000 kN/m^2, 14,000 kN/m^2, and 14,000 kN/m^2, respectively.(Elsawwaf et al., 2023a; Kyung et al., 2017c)The numerical model is shown in the figure below.

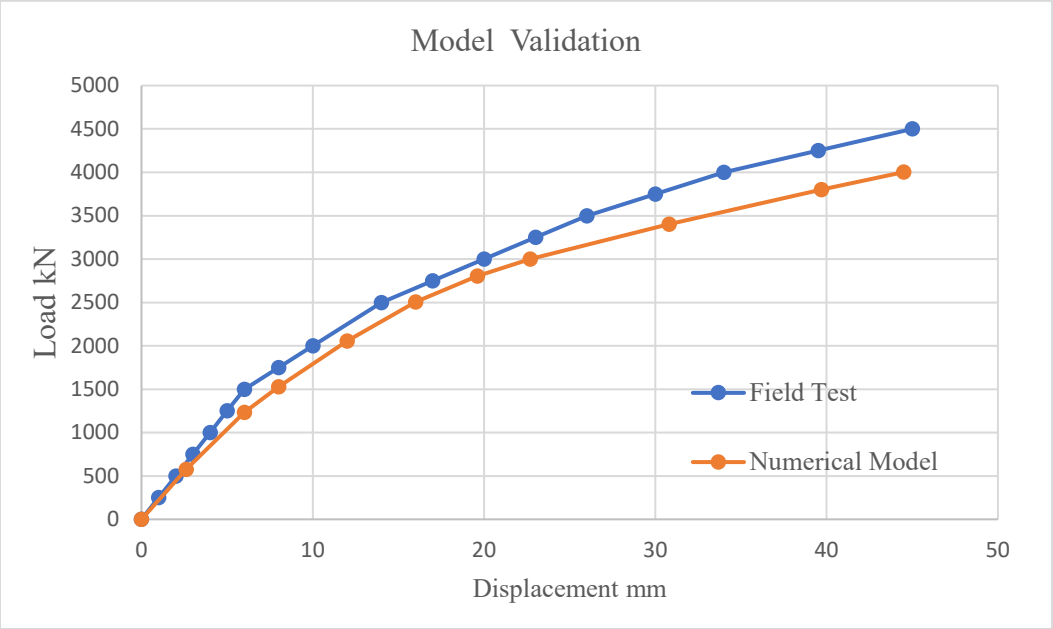

Figure 5.1: Validation of numerical model with Kyung & Lee (2018)

The result of the study was compared with Kyung & Lee (2018). The above fig 16 is how these test results were utilized to validate the numerical models.

ii) Validation of the Micropile and Foundation in terms of the lateral load

The numerical model used was validated for the reliability of the Finite Element (FE) analysis. The FEM as per the similar method used in this research, was compared with the result of the full-scale lateral load test carried out byKyung & Lee (2018). Furthermore, for reliability, it was also compared with the Numerical validation done by Elsawwaf et al. (2023). A field test was done by Kyung & Lee (2018) in Gochang city, where soil was found to be silty sand, and a group of micropiles of length 8m and 0.165m in diameter. Soil layers' parameters of Gochang city are presented in Table 8. A gravity grouting method was used in micropiles. Raft of 2.52 x 2.52x 1 m supported by micropile at a spacing of 1.26m. The interface assumed was 0.95 m in the lower layer of sand. An upper steel casing and a 65mm rebar were also used in the micropile. Material parameters of the raft and the micropiles used were presented in a table.

This validation in the figure below confirmed the reliability of FE analysis in the use of the micropile-supported foundations. Figure 16 shows that the FE result gives good agreement with the field load test and FE analysis. This fig the more or less overestimated load displacement curve. This comparison result gave reasonable agreement with the field test done by Kyung & Lee (2018), and the FE analysis done by Elsawwaf et al. (2023). (Roh et al., 2019) gives a similar note for the validation of the model.

The validation of the FE model of the cantilever retaining wall was done by calculation of the force exerted on the wall using the analytical method given by Rankine and Coulomb's method.

Table 5.3: Soil properties of Gochang City(Kyung & Lee, 2018)

Parameter	Upper Silty Sand	Middle clay	Lower silty sand
Depth (m)	0–1	1–6	6–10
Unit weight (kN/m^3), γ_i	17.6	18.8	17.8
Angle of internal friction (°), Ø	28.64	-	33.5
Cohesion 'c' (kN/m^2)	17.4	24.2	-
Modulus of Elasticity (kN/m^2)	5000	8000	8000

Table 5.4: Micropiled raft parameters used in validation (Kyung & Lee, 2018)

Parameter	Raft	Micropile
Constitutive modeling	Linear elastic	Linear elastic
Unit weight (kN/m^3), γi	24	24
Modulus of elasticity	22×10^6 kPa	52×10^6 kPa
Poisson's ratio, ν	0.15	0.15

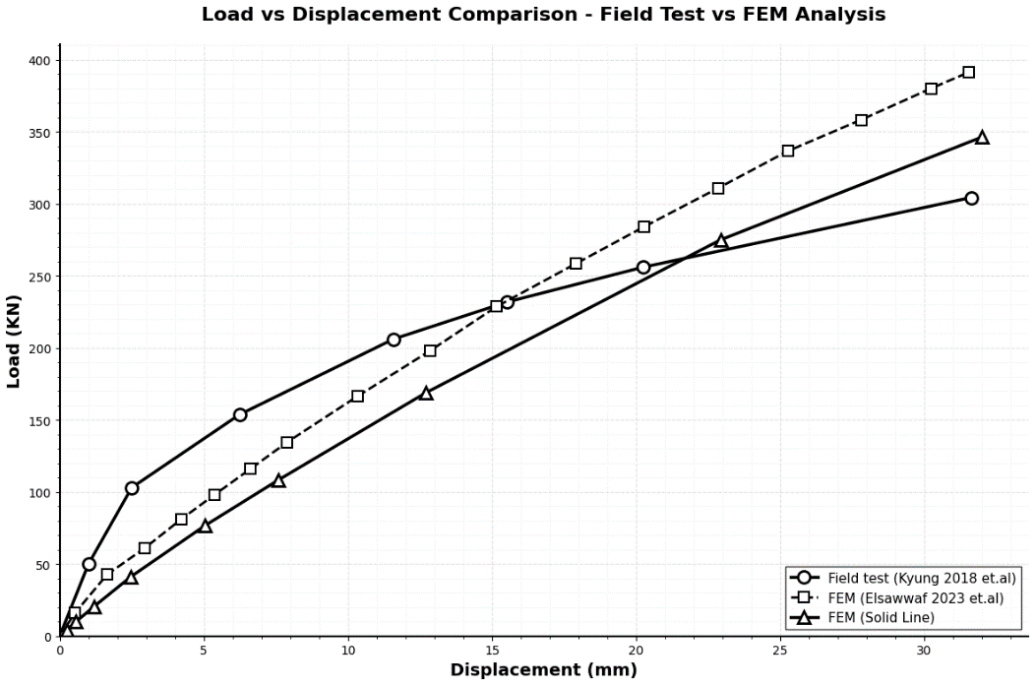

Figure 5.2: Numerical validation of the model.

iii) Validation of the model of the Cantilever Retaining wall.

For validation of the lateral earth pressure given by the soil backfill on the cantilever retaining wall is calculated manually by the analytical method. Compared with the lateral earth pressure given by the finite element modelling. This also gives a similar value. This concludes that validation of the cantilever retaining wall is done.

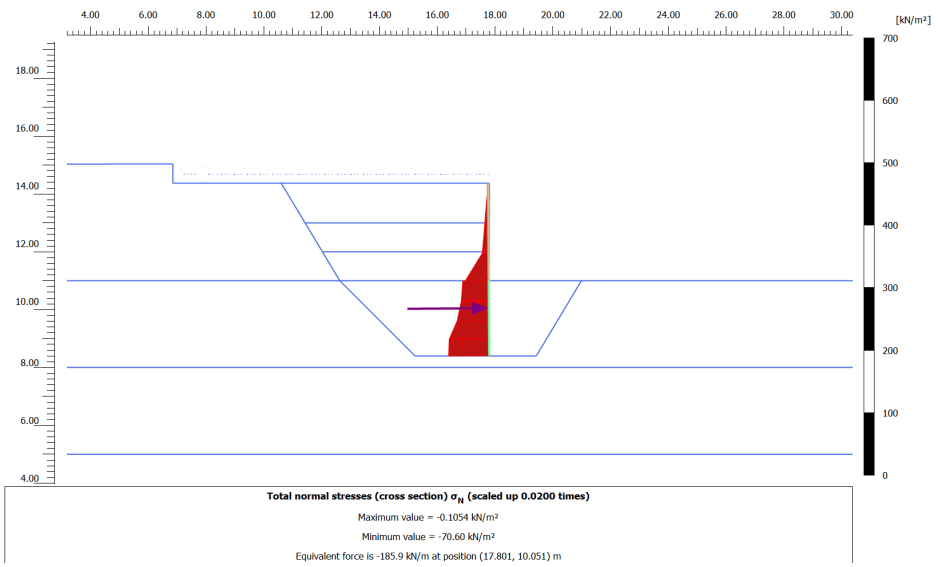

Figure 5.3: Validation of the lateral earth pressure of the wall

5.2 Displacement Analysis

Displacement analysis of the model was analyzed in the various scenarios was observed by use of the numerical modelling software. Observed the displacement of the lateral, vertical, and total in multiple scenarios. Multiple scenarios as follows:

Major scenarios:

i) Without a micropile-supported cantilever wall

ii) With micropile-supported cantilever wall

Sub scenarios:

i) Static conditions

Displacement at different layers of the structures: At top of the road, top of the wall, base of the wall, toe and heel portion of the wall

ii) Flow conditions

Flow at base (normal level), flow rise 3.5m, flow rise 7.5m, flow rapid drawdown -4m in 2 days.

iii) Seismic conditions

Pseudo static conditions: Analyzed by applying horizontal seismic coefficient Kx from +-0.15g to +- 0.2g, Earthquake loading conditions: Pseudo-static coefficient of Past Earthquake conditions.

PGA value of nearby station of the earthquake load, we used the Gorkha Earthquake loading conditions in the model.

i) Without a micropile-supported cantilever wall

The cantilever retaining wall in the road section, as per the case study site, is modeled in the finite element software. And deformation is observed in the static conditions. This is shown in the figure below.

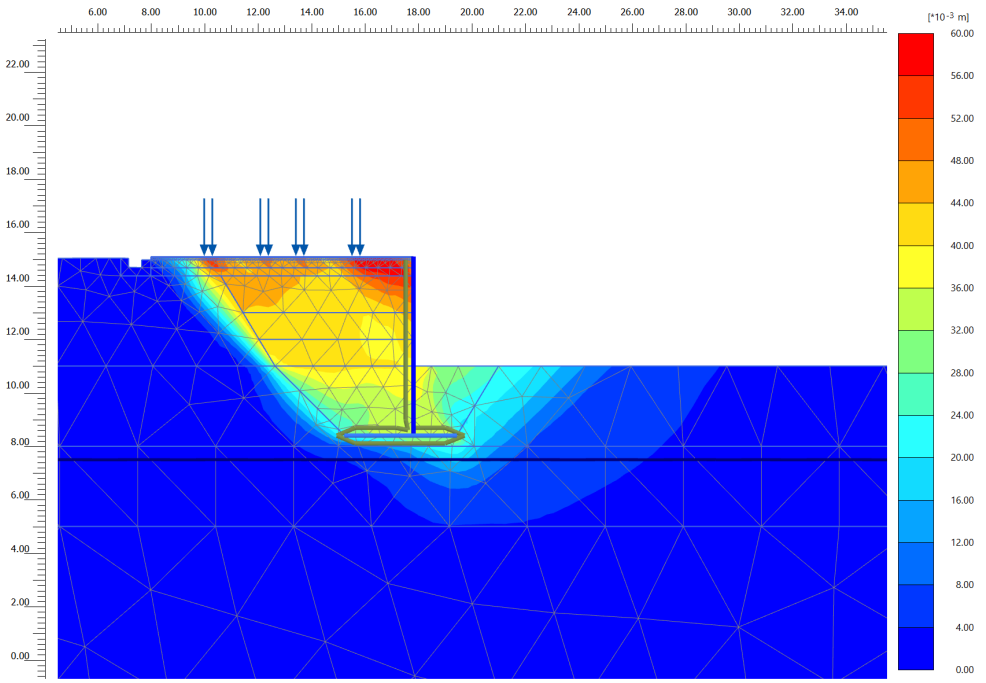

Figure 5.4: Cantilever retaining wall without micropile support.

Deformation was observed in the static conditions when the cantilever wall without micropile support was used. This was shown in Figure 5.4 . In these cases, I have modeled as per the field data and prepared the modeled and analyzed vertical, lateral, and total displacement.

ii) With a micropile-supported cantilever wall:

The cantilever retaining wall in the road section was supported as per the case study site, which was modeled in the finite element software, i.e., PLAXIS 2D. And deformation is observed in the scenarios, which is shown in the figure below.

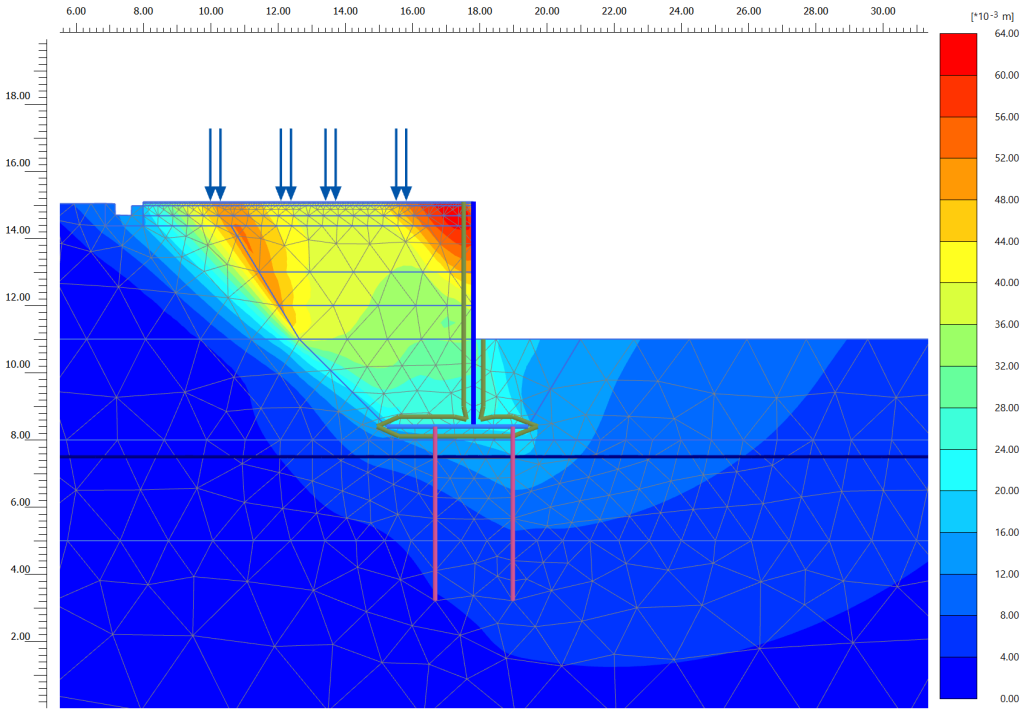

Figure 5.5: Deformation in micropile supported wall at static condition

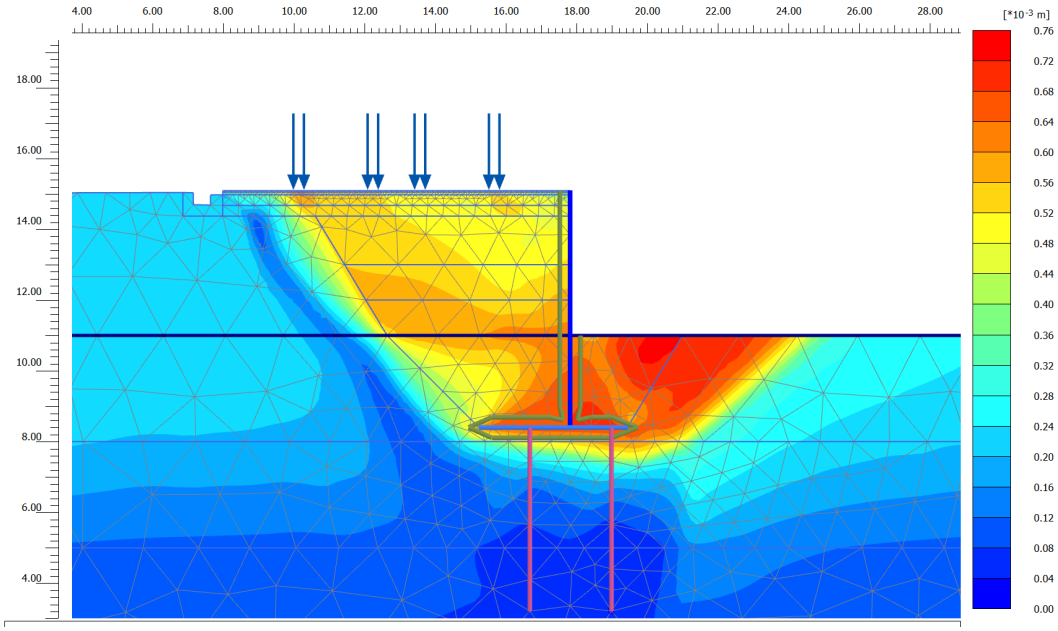

Figure 5.6: Deformation in micropile supported wall at flow rise of 3.5m

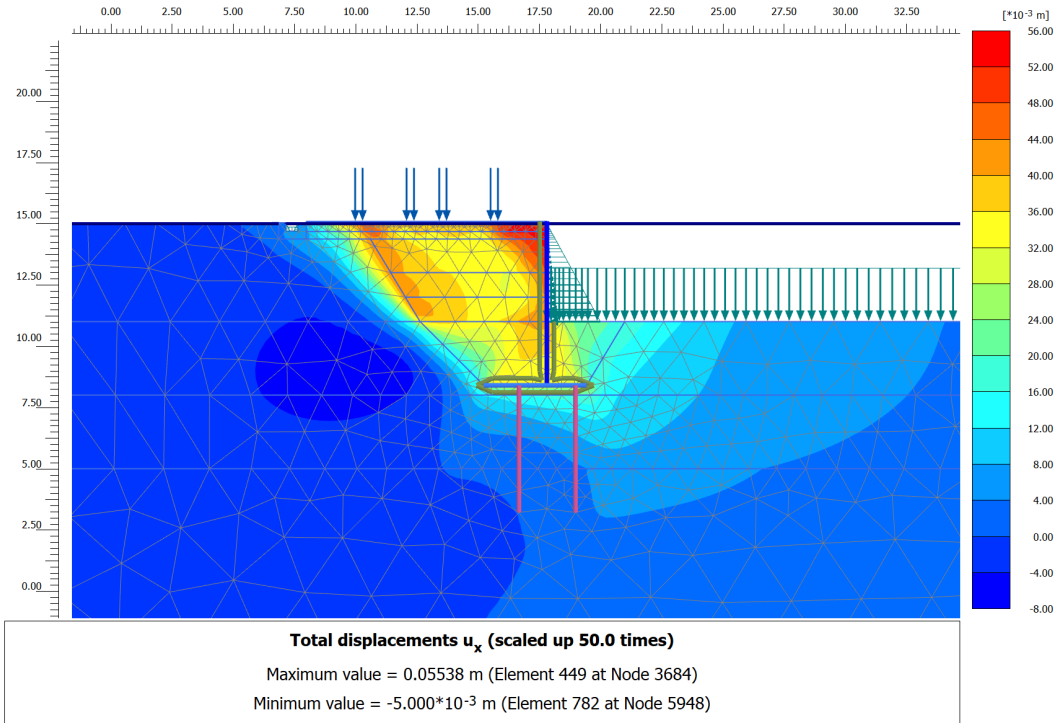

Figure 5.7: Deformation in micropile-supported wall at flow rise of 7.5m

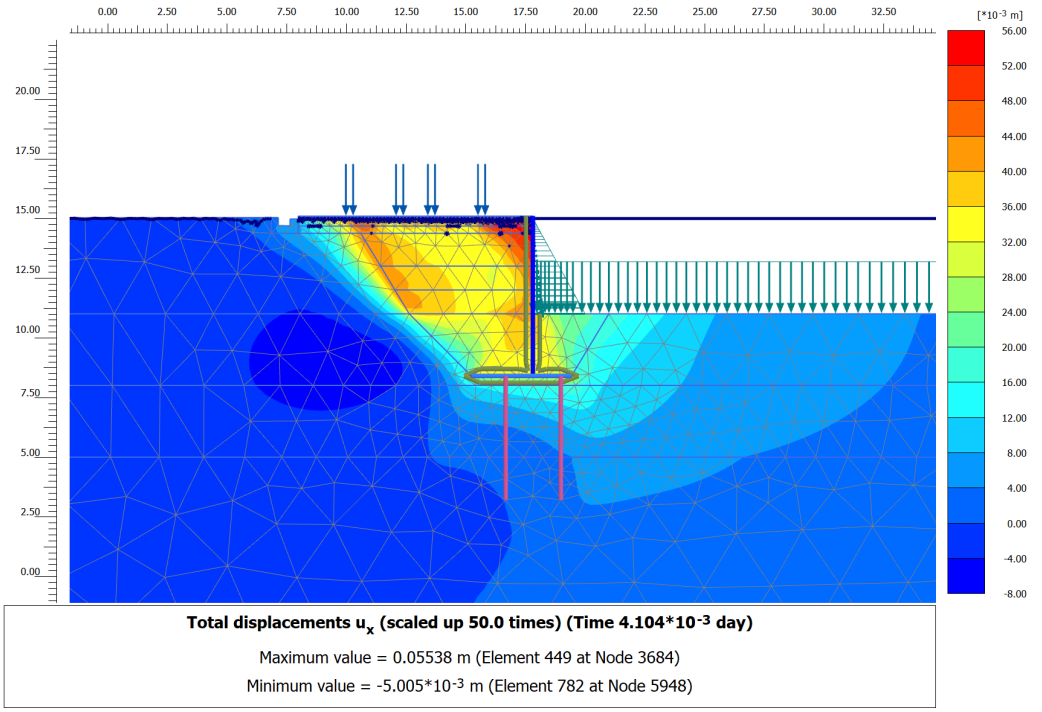

Figure 5.8 Deformation in micropile-supported wall at rapid drawdown

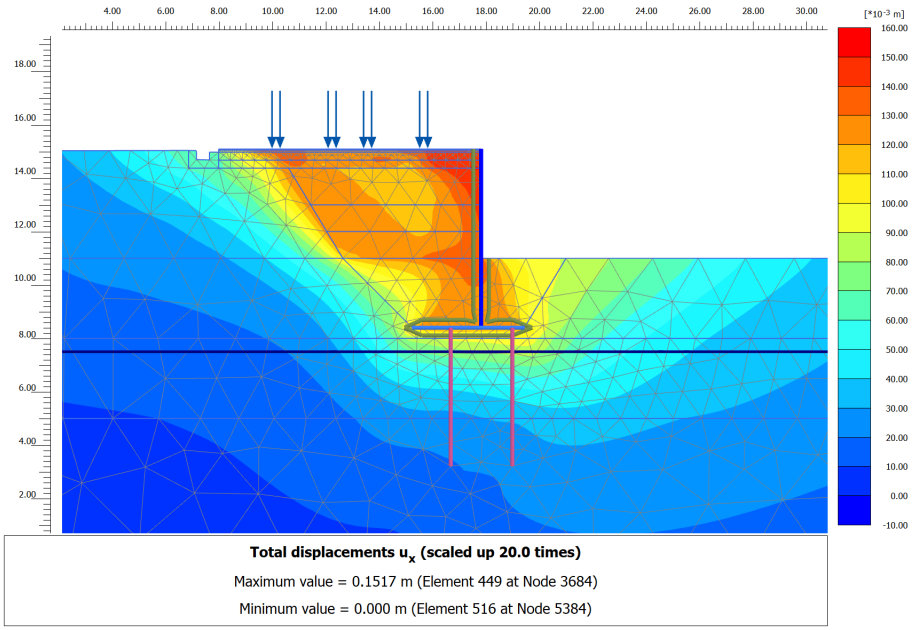

Figure 5.9: Deformation in micropile-supported wall at a load of -0.2g.

5.2.1 *Displacement of the wall supported with and without micropiles*

Displacement comparison between the micropile-supported and unsupported cantilever wall is mentioned below.

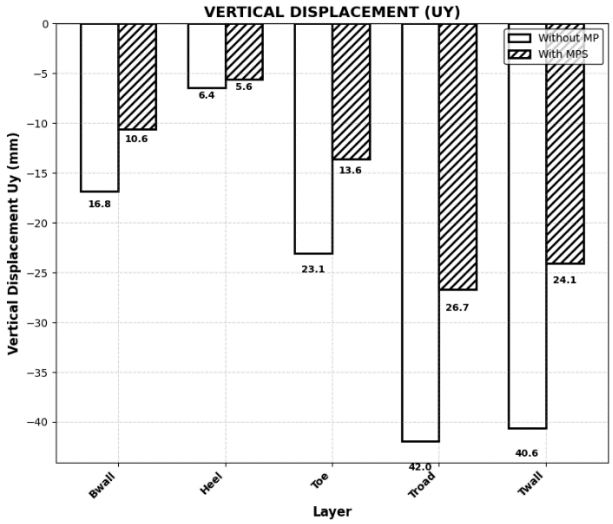

Figure 5.10: Displacement comparison with and without MPs support wall.

The cantilever wall without the micropile pinned was under stable conditions as per the stability criteria. The vertical displacement of the cantilever wall was reduced as compared to the displacement of the cantilever retaining wall without micropile support on the foundation.

5.2.2 *Deformation in water level rise and fall conditions*

The model was prepared for FE analysis of the displacement in the flow conditions of the cantilever wall with micropile reinforced foundation in base normal flow, flow rise by 3.5m, 7.5 m, and rapid drawdown by -4m from the 7.5m rise level as present in the figure above. It indicates that lateral displacement is more significant and dominant than vertical settlement. Water level at 3.5m from the normal water level, which doesn't affect the displacement in both directions, while rising to the top of the wall decreases by 5-6% as compared to the normal water level, which is not more significant. This shows that the wall is stable under the horizontal displacement criteria of < 0.02H (140mm) and in the failure limit of 0.1H (700mm) (Wu & Prakash, 1999), and the settlement under the 5-7cm (Das, 2019) in the water level rise cases in the field. So, Which indicate that the rise in water level does not affect the lateral displacement of the wall, which is stable in water level rise and rapid drawdown in both the case of the micropile-supported and unsupported cantilever wall.

5.2.3 *Displacement in pseudo-static loading conditions*

FE analysis under the seismic conditions by applying the pseudo-static loading to the wall was evaluated at different horizontal seismic coefficients (Kx). Kx + (Positive direction). The seismic force acts towards the backfill, pushing the wall into the soil wedge, increasing the passive earth pressure. Kx – (negative) seismic force acts away from the backfill, increasing the active earth pressure. Coeff. Kx – (negative) critically affecting the overturning and sliding stability of the wall.

(Terzaghi, 1943) The horizontal seismic coefficients are Kx 0.1 for a severe earthquake, 0.2 for a violent, destructive type, and 0.5 for a catastrophic earthquake. FE analysis was done in (Kx, Ky): (+- 0.15g,0), (+- 0.18g, 0), and (+- 0.2g,0) as modeled as present in Figure 14. Under Kx – (negative) seismic force gives more displacement in the lateral and vertical direction than the Kx + (Positive direction), as indicated by the fig. Where Ux is the lateral displacement, and Uy is the vertical displacement in the chart. Lateral displacement of the micropile-supported wall in seismic loading at (- 0.15g,0) to (- 0.2g,0) is almost twice that of normal static loading conditions. This concludes that the micropile-supported cantilever wall is stable under the lateral displacement criteria under the seismic load (- 0.15g,0) to (- 0.2g,0), with limit deformation criteria given by maximum earthquake acceleration, of 250 amax mm and 300 amax mm as per the AASHTO and Euro code, respectively.

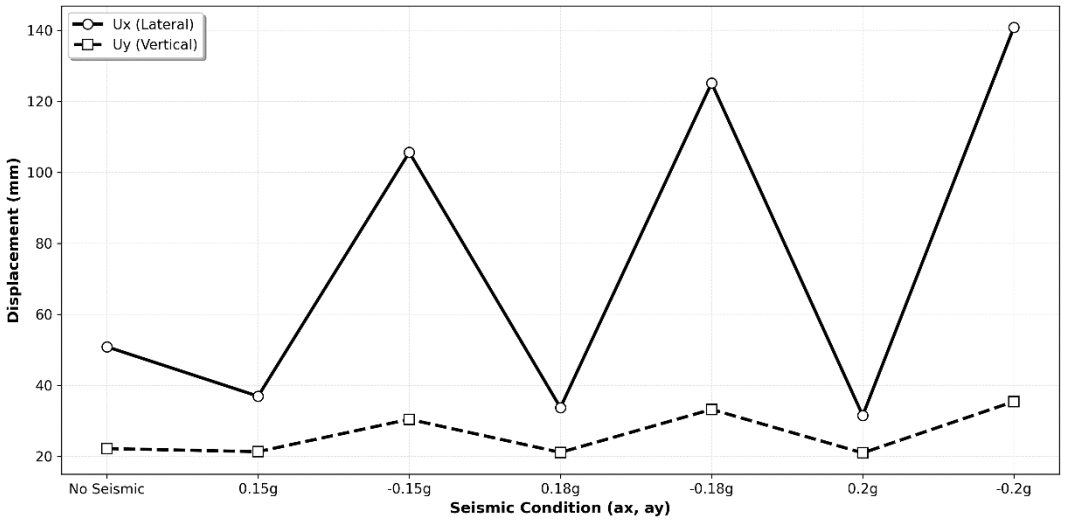

Figure 5.11: Displacement in different pseudo-static conditions

Based on the data, as the pseudo static loading (horizontal seismic acceleration) increases from 0g to +-0.15g and then to +-0.2g, the total displacement shows a clear upward trend. In this pseudo-static analysis, the negative pseudo-static coefficient gives more lateral displacement than the vertical displacement, which was observed from the above chart. The total lateral displacement rises from 49 mm under no seismic loading to 135 mm at 0.2g pseudo-static loading, which is almost 1.7 times(almost twice) more than under no seismic loading. This indicates that higher pseudo-static acceleration directly results in a significant increase in lateral displacements. And the vertical displacement at 0.2g is more than 1.5 times the normal conditions, but it was lower than the lateral displacement, which was also present in the figure above.

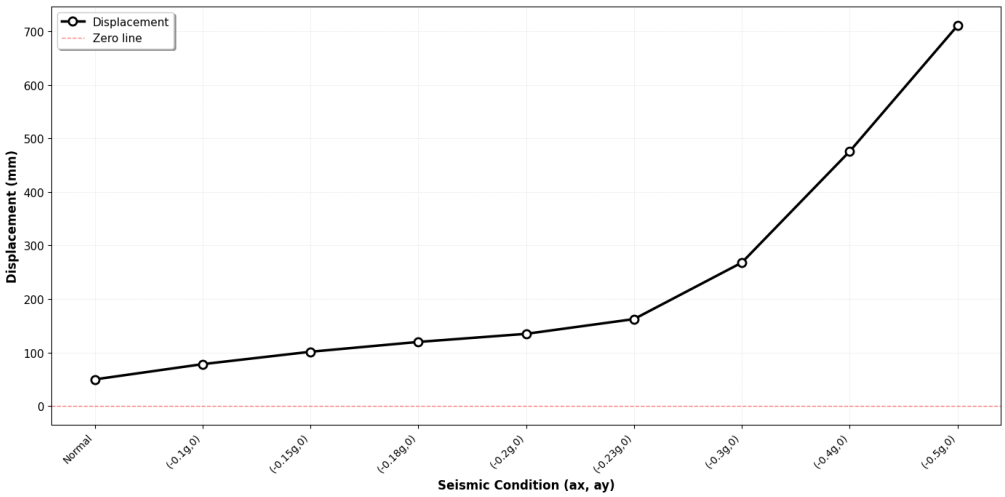

Figure 5.12: Lateral displacement at different pseudo-static coefficients.

Pseudo-static loading of the Gorkha earthquake was also evaluated. The PGA value recorded during the Gorkha Earthquake 2015, at different locations near the case study sites, is mentioned in the table below as taken from (Takai et al., 2016).

Table 5.5: PGA values recorded during the Gorkha Earthquake 2015

Station Code	Full Name	Location	Site Type	EW PGA cm/s^2	EW PGA (g)
KTP	Kirtipur Municipality Office	Kirtipur	Rock	241	0.246g
TVU	Central Department of Geology, Tribhuvan University	Kirtipur	Sediment	238	0.243g
PTN	Pulchowk Campus, Institute of Engineering, Tribhuvan University	Patan	Sediment	133	0.136g
THM	University Grants Commission Office	Sanothimi, Bhaktapur	Sediment	122	0.124g
KATNP	Kanti Path (USGS Station)	Kathmandu	Sediment	155	0.158g

For the case study site of the Roshi Section of the BP highway nearer station is the THM. So, the PGA value 0.124 g was taken as a pseudo-static coefficient for the seismic analysis of the micropile-supported cantilever wall.

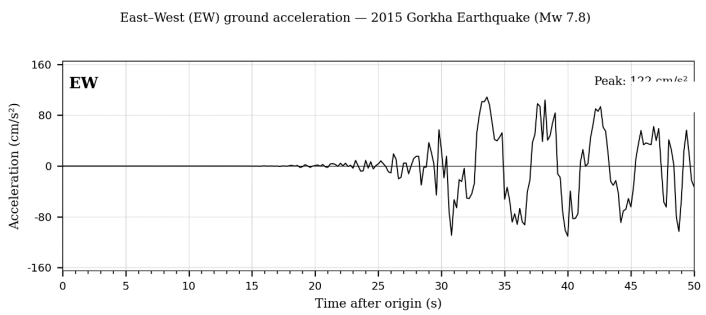

Figure 5.13: Acceleration vs time graph of the Gorkha Earthquake 2015

The lateral displacement at the top of the wall was observed to be 88 mm, which is under the stable conditions as per the horizontal displacement criteria of < 0.02H (140mm) and in the failure limit of 0.1H (700mm) (Wu & Prakash, 1999), and the settlement under the 5-7cm(Das, 2019)

5.3 Bearing Capacity

The bearing capacity of the cantilever wall foundation with and without micropiles was calculated by plotting load versus deformation charts to determine the effectiveness of micropiles.

Table 5.6: Bearing capacity of types of cantilever wall

Cantilever Wall Foundation Type	Ultimate Bearing Capacity (kPa)	Allowable Bearing Capacity (kPa)	FOS Against Bearing
Without Mps Supported	666.5	222.2	3.7
With Mps Supported (S/D =13)	779.1	259.7	4.4
Maximum pressure at the toe of the wall	178.2		

i) In a cantilever wall without micropile support.

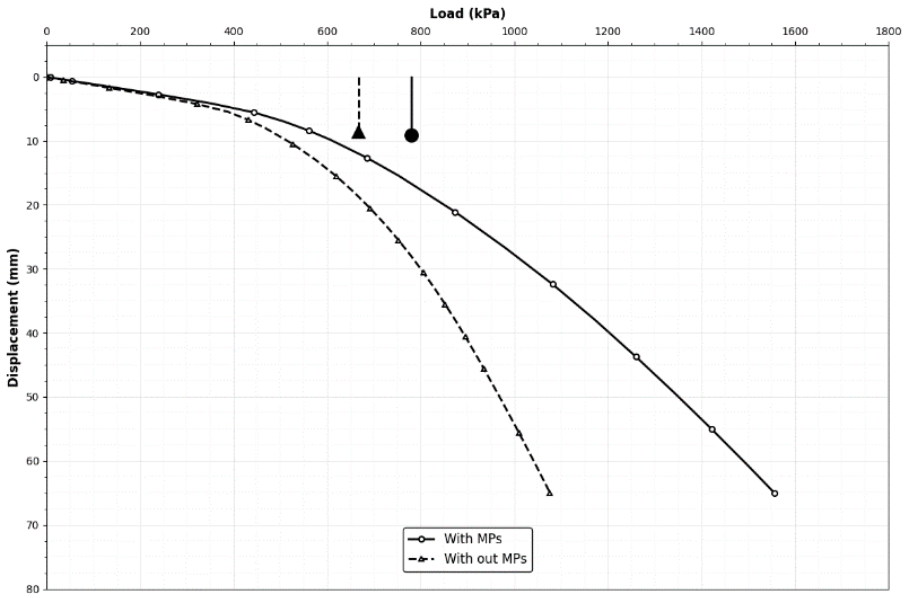

Figure 5.14: Bearing capacity without micropile supported wall.

The ultimate bearing capacity of the cantilever wall foundations without a micropile-supported cantilever wall is 666.48 kPa. And the allowable bearing capacity is 222.16 by taking FOS 3 as per Meyerhof's, as present in the figure above. Ultimate bearing capacity is more than the maximum bearing pressure at the toe of the wall, which is 178.23 kPa. FOS in terms of the bearing is FOS > 3. It showed that the wall without micropiles is safe against bearing failure and performed effectively under bearing capacity criteria.

ii) In a micropile-supported cantilever retaining wall

Based on the analysis, the ultimate bearing capacity of the cantilever wall foundation is 779.11 kPa with micropiles, and the allowable bearing capacity is 259.7 kPa, as shown in Figure 30. The ultimate bearing capacity at the micropile-supported wall is increased by more than 16.8%, and also increases the FOS against bearing failure by 4.37. This improvement demonstrates that the use of micropiles effectively enhances the foundation's bearing capacity. Therefore, micropiles serve as a reliable reinforcement solution for improving the stability and performance of cantilever wall foundations. This showed a decrease in the settlement of the wall with a micropile.

5.4 Bending Moment of the Micropiles Under Various Conditions

FE evaluation of the bending moment of the micropile rows for the toe side and the heel side micropile separately. The bending moment developed in micropiles is significantly influenced by key geometric parameters such as diameter and length, which directly affect the load distribution and structural response of the foundation system.

i) Bending Moment of micropile in normal static conditions

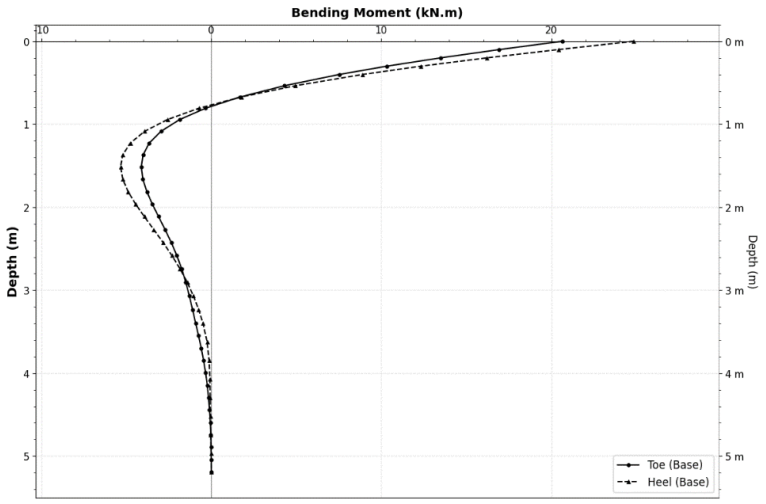

Figure 5.15: Bending of the micropiles of the toe and heel side.

Figure 5.15 shows the bending moment distribution of micropiles located at the toe and heel of the cantilever wall. Both positive and negative bending moments are observed in the micropile positioned at the heel and toe side of the wall foundation.

The bending moment was consistently maximum at the micropile head, at the connection point with the pile cap, and decreased with depth, indicating that the uppermost position of the pile is the most structurally critical zone regardless of inclination angle. The heel micropile experiences a greater bending moment compared to the toe micropile, as shown in Figure 5.15: Bending of the micropiles of the toe and heel side.in normal static conditions, indicating that the heel micropile carries higher flexural demand under the applied loading. The heel side micropile rows dominate in flexural (bending) demand.

i. Bending Moment of micropiles in water level rise conditions

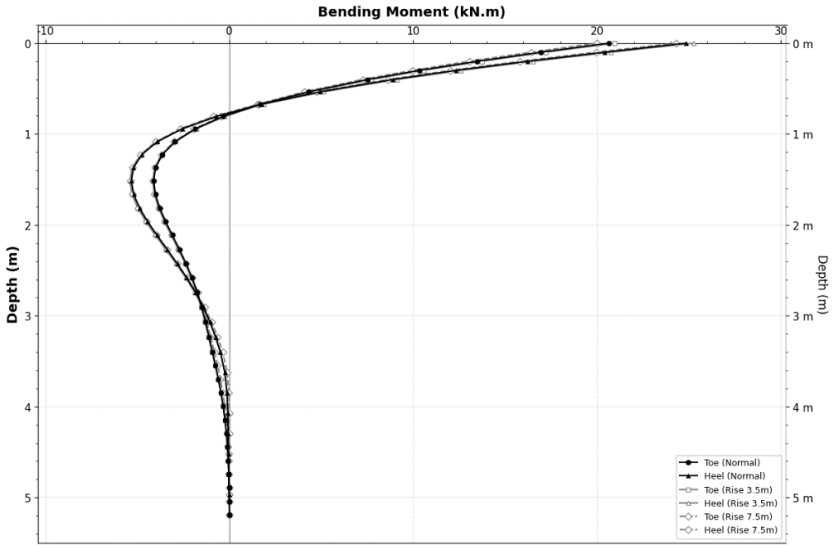

Figure 5.16: Bending moment of micropile at water level rise

FE analysis under the water level increases from 3.5m to 7.5m from the normal water level, which does not largely impact the bending moment developed in the micropiles as present in Figure 5.16.

ii. Bending moment of micropiles in pseudo-static loading conditions

Figure 5.17 illustrates the bending moment response of the micropile rows under different seismic conditions. The results demonstrate that seismic loading considerably amplifies the bending moment in the micropiles compared to the static case, with higher seismic intensity (pseudo-static coefficient) levels producing larger peak bending moments. The micropiles at the heel of the wall

were found to be more critically loaded under seismic excitation, consistent with the observations from the static loading scenario.

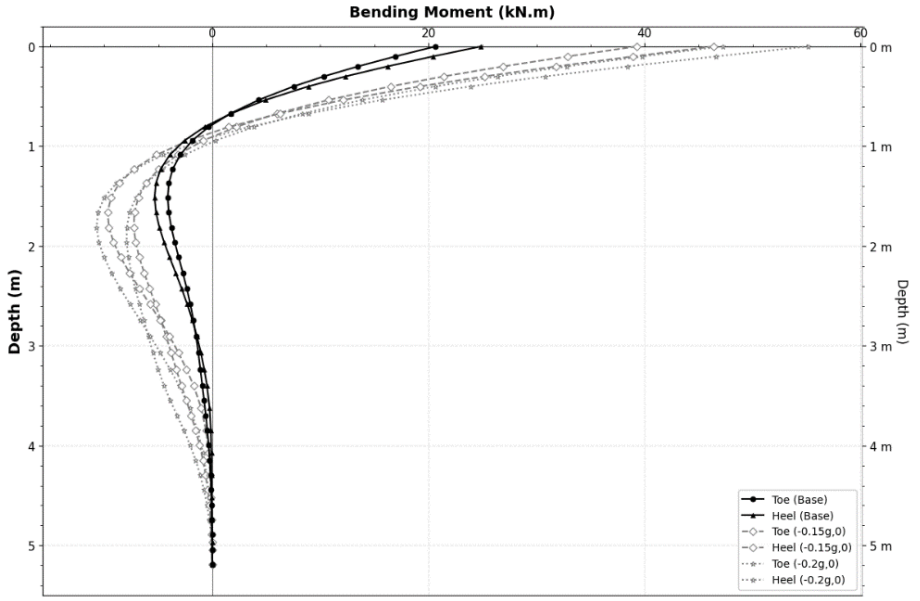

Figure 5.17 Bending moment of the micropile at Kx 0.15g to 0.2g

5.5 Lateral Displacement of Micropiles at Different Scenarios

The lateral displacement that occurred at the micropile locations at the heel and toe of the wall foundation was analyzed and is presented below.

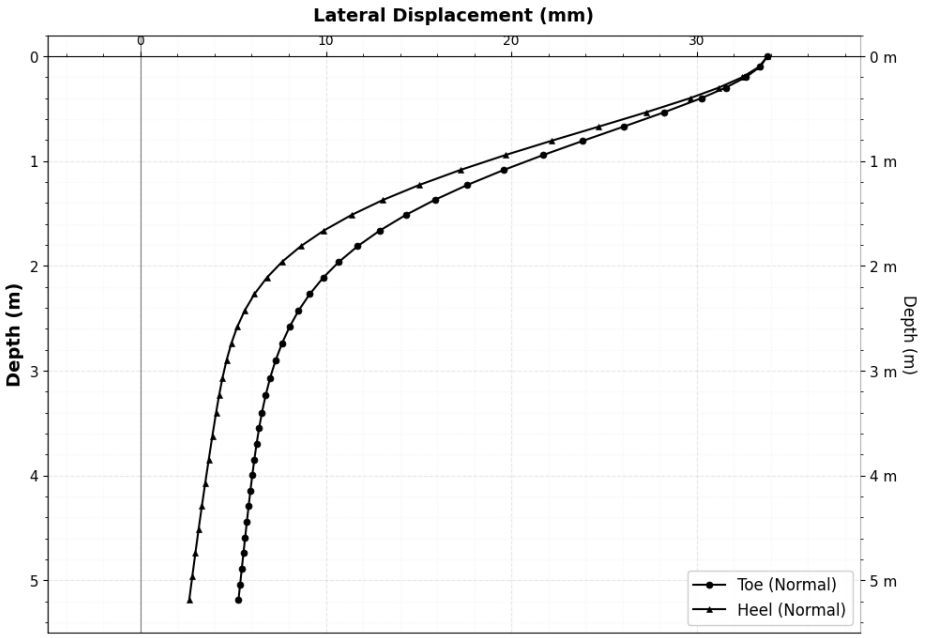

Figure 5.18: Lateral deformation of the micropiles

Figure 5.18 presents the lateral displacement profiles of the micropiles at the heel and toe of the cantilever wall under normal static conditions. Both micropiles

reach a maximum lateral displacement of approximately 33 mm at the surface; however, the toe micropile consistently exhibits greater lateral displacement than the heel micropile throughout the mid to lower depth range of approximately 1 m to 5.3 m, with a difference of around 3–5 mm observed between the two profiles.

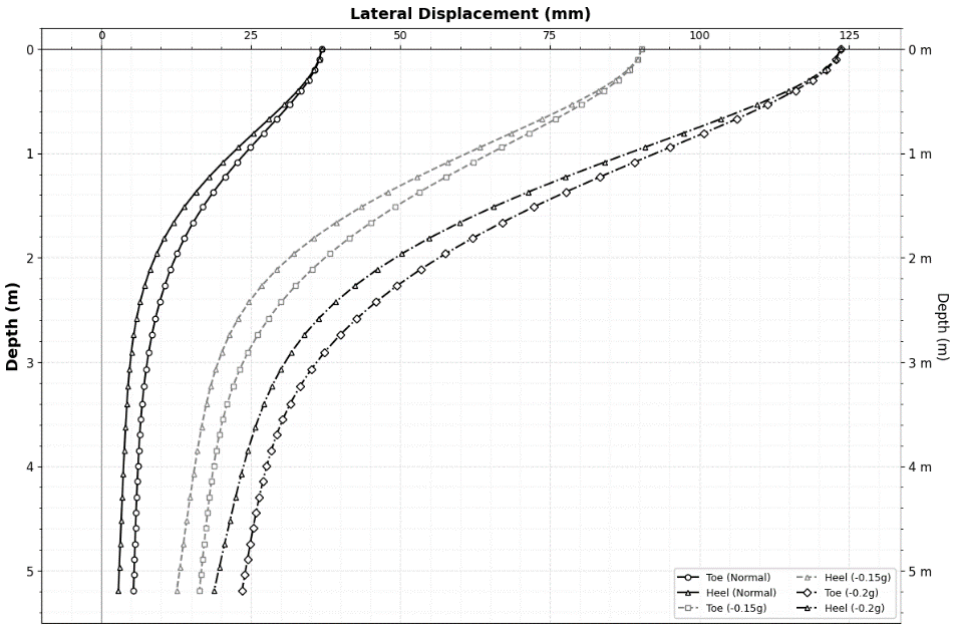

Figure 5.19: Lateral deformation of micropiles in pseudo-static coeff.

The increasing seismic coefficient significantly amplifies the lateral displacement, where the micropile at the toe side consistently displaces slightly more than the heel side. This indicates that the toe micropile is subjected to higher lateral deformation demands, suggesting that the lateral earth pressure and wall rotation effects are more critically transferred to the toe side. Both profiles show a gradual reduction in displacement with increasing depth, confirming that lateral deformation is concentrated in the upper portion of the pile where soil confinement is weakest.

5.6 Load Transfer Mechanism

The load transfer mechanism in micropiles refers to the process by which axial and lateral loads applied to the micropile are distributed to the surrounding soil and rock through interface shear stresses along the cased and bond zones. According to (Theinat & Luna, 2019), the weathered rock in the cased zone can transfer a significant portion of the load (>70%) despite low friction at the interface, highlighting that ground stiffness plays a major role alongside interface friction. (Elsawwaf et al., 2023a)Describe that in micropiled raft systems, loads are shared between the micropiles and the raft through interface friction, with the

load-sharing ratio being influenced by factors such as micropile spacing, length, and the magnitude of applied loading. The load transfer mechanism of this cantilever wall and the micropile is analyzed by the FEM software.

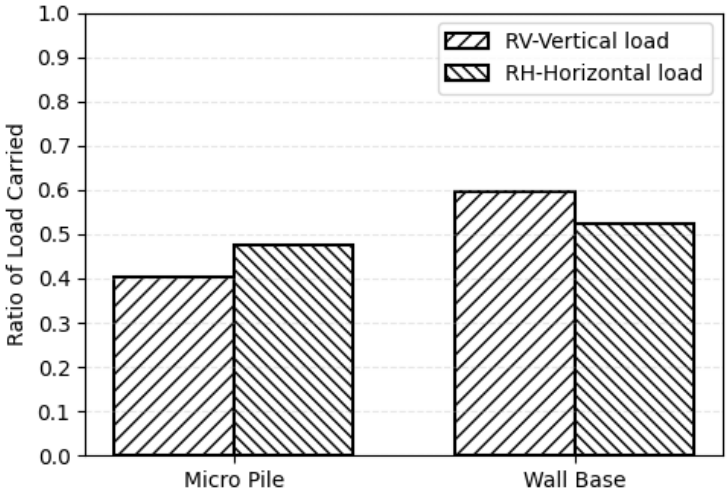

Figure 5.20: Load transfer of micropile and wall foundation.

Figure 5.20 presents the load transfer distribution between the micropile and wall base under vertical and horizontal loads. The wall base carries a higher proportion of vertical load, 52.53%. While the micropile carries a higher proportion of lateral load of 47.46%, indicating that micropiles play a more prominent role in resisting horizontal forces than vertical loads.

5.7 Mobilization of Skin Friction

The mobilization of skin friction in the micropiles was analyzed using embedded beam elements in the FEM software. Skin friction was evaluated in each micropile, specifically at the heel and toe micropile positions.

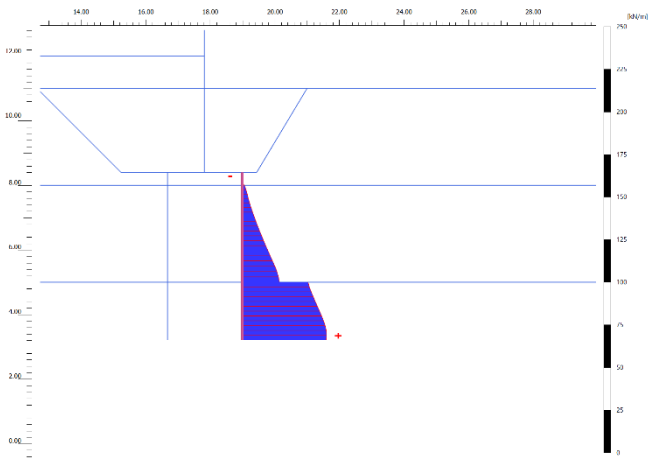

Figure 5.21: Skin friction of toe side micropiles

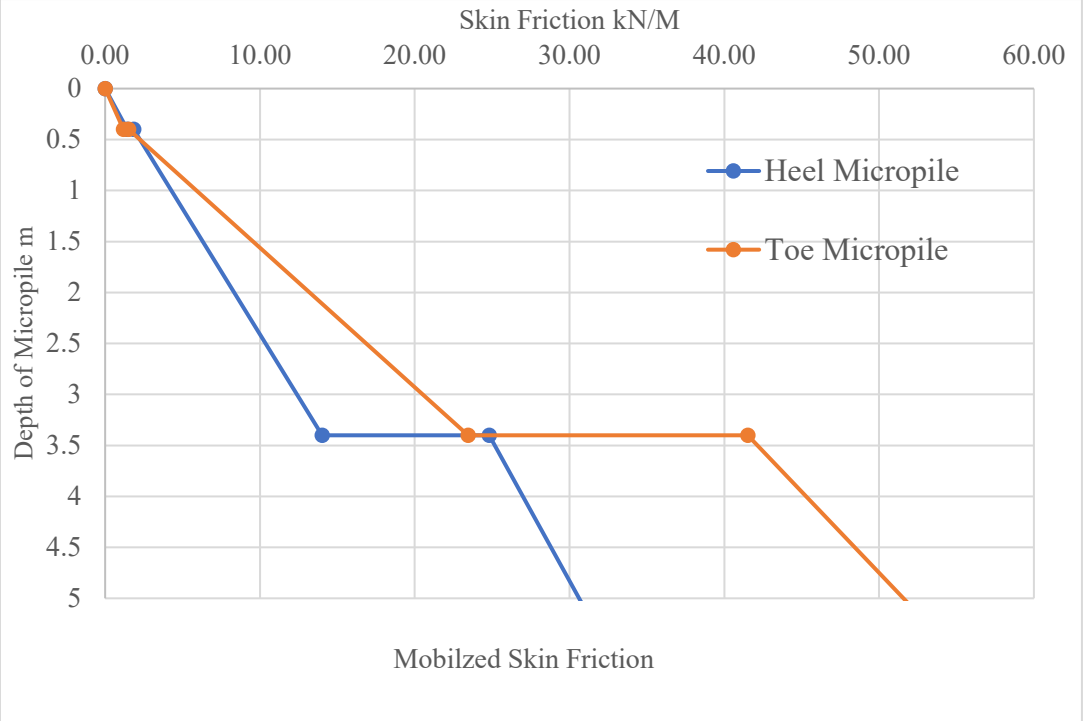

Figure 5.22: Mobilized skin friction of micropiles.

The mobilized skin friction distribution along the depth of the heel and toe micropiles. The results clearly show that the toe micropile mobilizes significantly greater skin friction than the heel micropile throughout its entire depth, reaching a maximum value of 52.83 kN/m at the pile tip, which is 68% more than the heel micropile at the same depth. Both micropiles exhibit near-zero skin friction at the surface at top with friction increasing progressively with depth, which is consistent with the increase in effective vertical stress with depth as reported by (Elsalfiti, 2011). The substantially higher skin friction mobilized in the toe micropile indicates that it carries a greater share of the load through interface friction with the surrounding soil.

5.8 Evaluation of Scouring

Scour depth refers to the vertical distance by which the riverbed is lowered due to erosion action by flowing water. This removes the sediments around the structures. Scour depth was evaluated based on the available data source by taking reference from the case study site. The 100-year return discharge at the for the case study site was taken as 1021 cumec (Duwal et al., 2023). The following parameters are adopted based on hydrological analysis and site investigation data. Using IRC guidelines, calculate the scour depth as mentioned in the literature review.

Table 5.7: Parameters used for scour depth calculation

Parameter	Value	Unit
Design Discharge (100-yr return period) Q cumec	1,021	m^3/s
Flow Velocity vs	4.17	m/s
Weighted Mean Diameter (D_{50})	0.545	mm
Silt Factor (K_{sf}) IRC coarse sand	1.50	
Channel Width (W)	58	m
Specific Discharge(Discharge per width (q)	17.60	m^2/s
RL of Ground Surface	844.00	m
RL of River at HFL	852.00	m
Depth of Flow at 100_{year} Flood	8.00	m
Lacey Normal Scour Depth (D_s)	7.92	m
Design Scour Depth (Ds) Straight Reach ($1.27 \times D_s$)	10.06	m
Depth of Scour Below Ground Surface	2.058	m

5.8.1 *Evaluation of with and without micropile-supported wall*

FEM modeling was done to evaluate the displacement at the scour depth. The model was presented below:

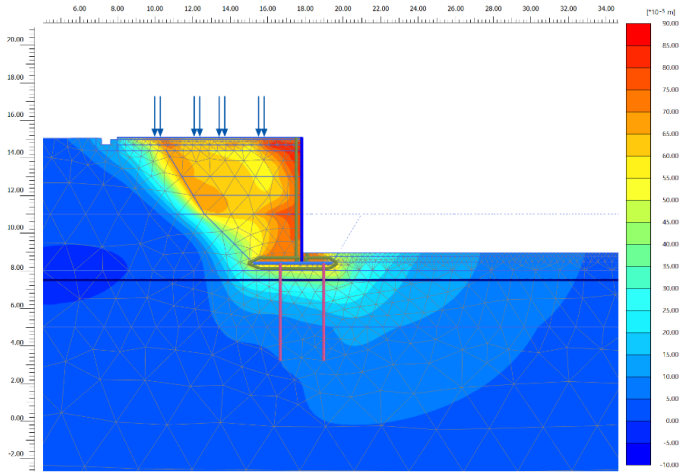

Figure 5.23: FEM of the MPs-supported wall module at scour depth

In the scour depth, lateral displacement is more critical than the vertical displacement, which causes the instability of the wall. Maximum lateral displacement in the micropiles (MPs) supported cantilever 90mm was observed, which is under the permissible limit. Also, vertical displacement is within the permissible limit.

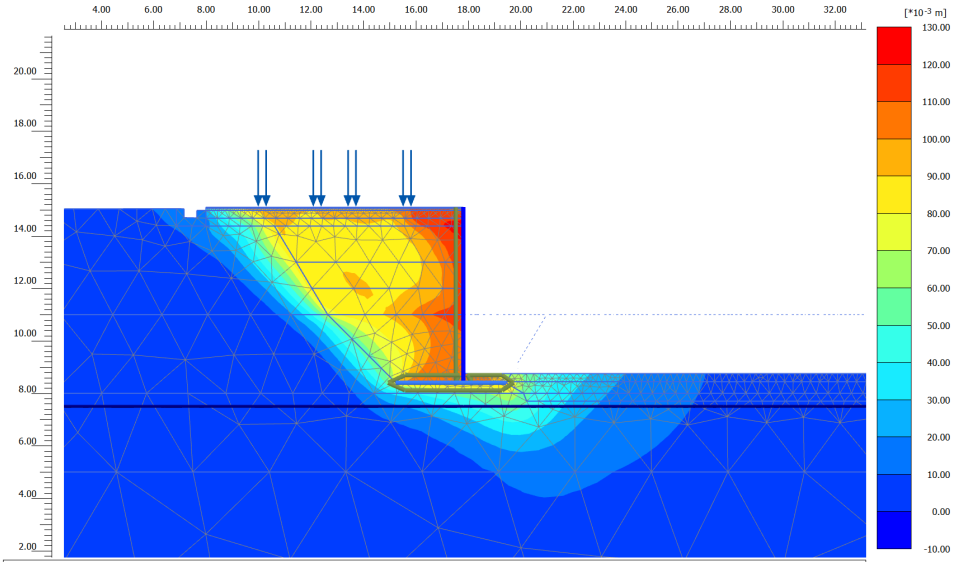

Figure 5.24: Displacement without micropile supported wall at scour.

FEM analysis of the wall with scoured depth has a lateral displacement of 130mm, which was more than that of the wall with a micropile support. Compared to the micropile-supported cantilever wall, the unsupported wall is more likely to topple and move laterally at the projected scour depth.

5.8.2 *Evaluation in increased scoured depth*

In order to assess foundation stability, FEM study was carried out by increasing the scour depth from 2.05 m to 3.30 m (about 50%), with scouring starting from the wall's toe. The unsupported wall's lateral displacement approaches 170 mm, as seen in the figures below, suggesting a risk of failure. The micropile-supported wall, on the other hand, shows a maximum lateral displacement of 110 mm, which was still within the allowable range of lateral displacement. This indicates that micropiles are effective for decreasing lateral displacement and enhancing overall wall stability during scouring within the proposed limit.

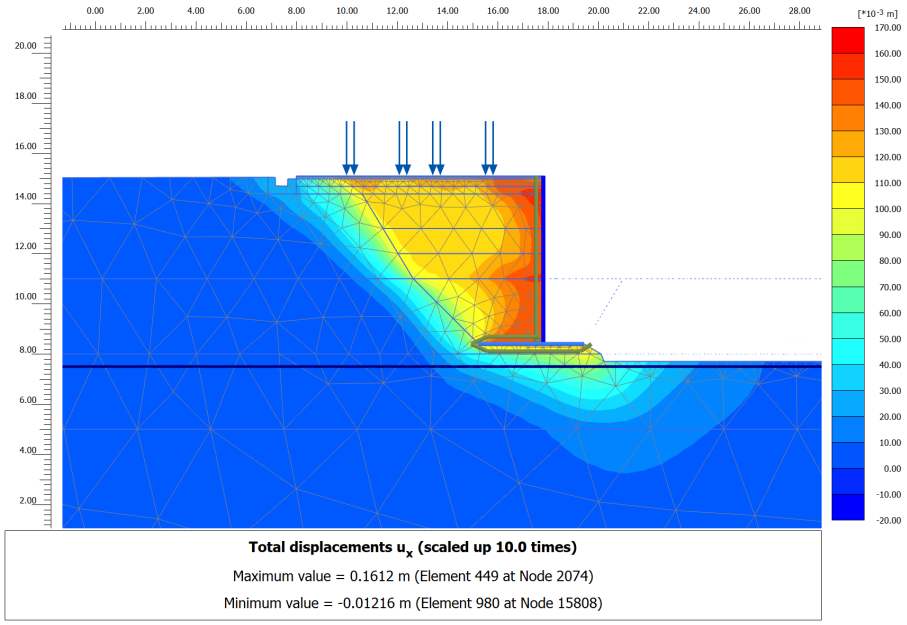

Figure 5.25: Displacement of the wall without micropile in scour 3.3m.

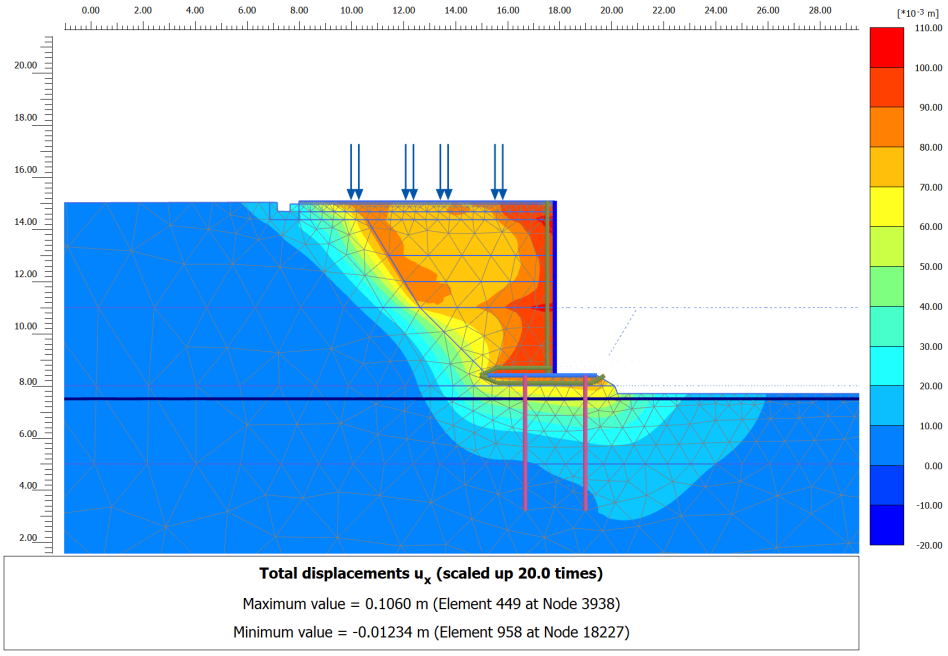

Figure 5.26: Displacement in micropile supported wall at scour 3.3m

5.8.3 *Evaluation of scouring geometry.*

Scouring geometry was calculated by using the parameters from Table 5.7. The calculated scouring parabolic equation and scour profile were mentioned below and the parabolic scouring profile was adopted in the FEM analysis:

$$y = 2.05 \times [1 - (x / 6.5)^2]$$

Figure 5.27: Cross-section of scouring

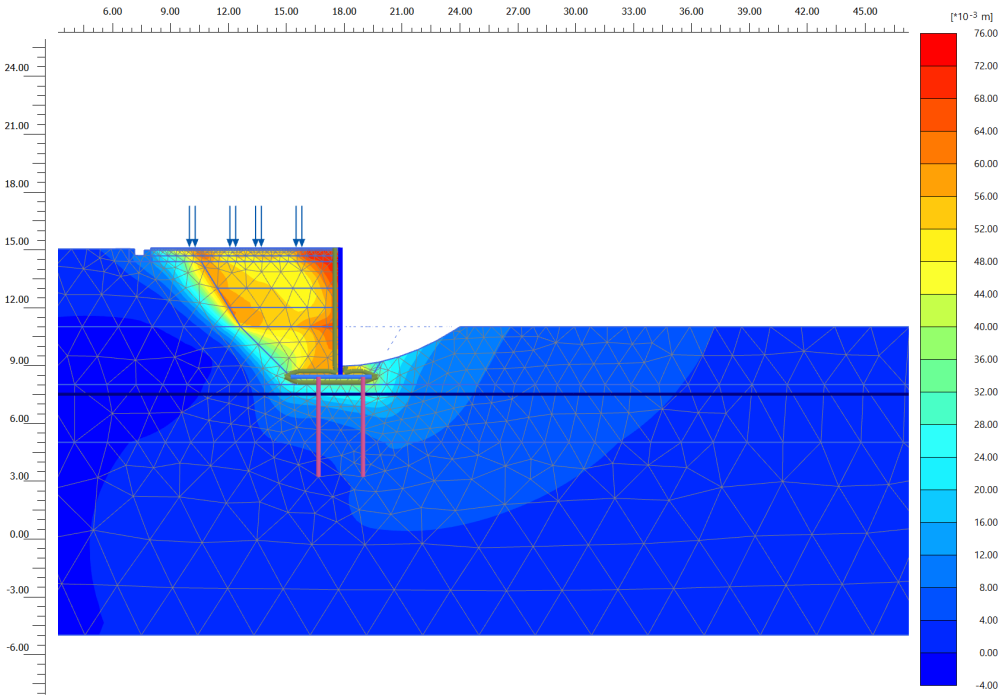

Figure 5.28: FEM analysis by using parabolic scouring

FEM analysis using the parabolic scouring pattern in foundations shows that the maximum lateral displacement of 76mm was observed, which is under the permissible lateral displacement. The micropile-supported cantilever wall is stable under the projected scouring depth of 2.05m. Thus, micropiles enhance the performance of the retaining wall in terms of stability from the scouring effect.

5.8.4 *Evaluation of stability at different increasing depth patterns*

The lateral stability of a cantilever retaining wall exposed to progressive scour at the foundation level was evaluated using FEM analysis. Two scour patterns were

examined: (i) vertical scour, where scour depth grows downward from the wall toe, and (ii) lateral scour, where scour depth grows downward from the wall toe below the cantilever wall foundation. All scouring was started from the wall toe for both walls with and without micropile support (Spacing = 1.5 m, s/d = 13). 2.058 meters below the ground's surface is the design scour depth. To determine how sensitive wall stability is to scour above the design limit, an extended scour scenario of 3.30 m (50% increase over design) was also assessed. FEM analysis figures are presented in Appendix 1 and 2.

Vertical scour:

The lateral displacement (u_x) at the wall face gradually increases from 90 mm to 110 mm as the scour depth increases vertically from 2.05 m to 3.00 m, as presented in Annex 1. By restricting the high-displacement zone to the wall stem, the micropiles serve as an effective anchor for the wall foundation. The micropile group offers sufficient lateral restraint under vertical scour conditions within the design range, as evidenced by the displacement contours being localized to the wall face with limited propagation into the adjacent soil mass.

Lateral Scour:

Four lateral scour extents were examined at an extended scour depth of 3.30 m in order to assess stability as scouring gradually erodes the foundation base. As the scoured zone grows wider beneath the foundation, this scenario, which depicts a post-design difficult situation, shows a notable rise in lateral displacement, which was mentioned in the figure in Annex 2. The displacement increases by 58% compared to the toe-only example, from 120 mm when scour reaches the micropile toe to 190 mm when it reaches the complete foundation. The lateral extent of scour is a critical factor in wall stability. Micropiles by themselves were unable to stop critical displacement levels after scour completely erodes the foundation. Lateral scour beneath the foundation is more critical than vertical scour of equivalent depth. Full foundation undermined at 3.30 m produces lateral displacement of 190 mm, exceeding the unsupported wall at the same depth by 20 mm, indicating loss of effectiveness of micropile anchorage below the foundation.

5.9 Parametric Study

A parametric study was conducted to investigate the effect of micropile spacing and length on the structural and geotechnical performance of the cantilever retaining wall foundation. The micropiles were arranged in rows beneath the retaining wall foundation, and their spacing and length were systematically varied

to evaluate the corresponding changes. The performance of the micropiled retaining wall was assessed in terms of lateral displacement, settlement, bearing capacity, and load-carrying ratio.

5.9.1 *Bearing capacity in varying micropile spacing to diameter ratio*

A parametric study was conducted to investigate the influence of micropile spacing on the bearing capacity of the cantilever retaining wall foundation system. The micropile spacing was varied at three configurations of 1.1 m, 1.5 m, and 2.0 m, corresponding to spacing-to-diameter ratios (S/D) of 10, 13, and 16, and the length -to-diameter ratio (L/D), respectively, and the bearing capacity response of the foundation was evaluated under static loading conditions for each configuration.

Table 5.8: Bearing capacity of wall at different S/D and the L/D ratio.

Cantilever Wall Foundation Support Type	Ultimate Bearing Capacity (kPa)	Allowable Bearing Capacity (kPa)	FOS Against Bearing
Without Mps Supported	666.5	222.2	3.7
With Mps Supported (S/D =13)	779.1	259.7	4.4
With Mps Supported (S/D =10)	831.4	277.1	4.7
With Mps Supported (S/D =16)	743.9	248.0	4.2
With Mps Supported (L/D=50)	779.1	259.7	4.4
With Mps Supported (L/D=70)	893.5	297.8	5.0
With Mps Supported (L/D=30)	693.0	231.0	3.9
Maximum pressure at the toe of the wall	178.2		

The factor of safety for calculation of the allowable bearing capacity taken was 3.

All the bearing capacities as per the wall support types, S/D and L/D, were presented in Table 5.8.

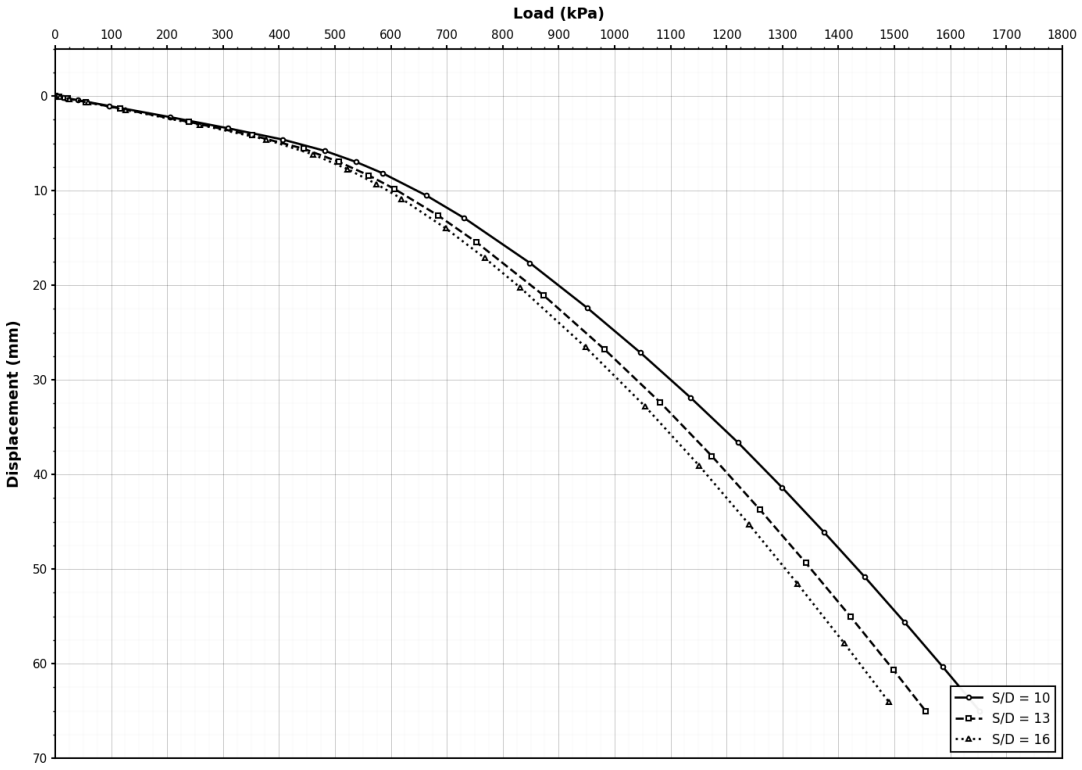

Figure 5.29: Load vs deformation chart at varying S/D ratio.

The Figure 5.29 above indicates that the ultimate bearing capacity vs the spacing to diameter of micropiles (S/D) of 10, 13, and 16. It indicates that an increase in S/D ratio from 10, 13, to 16 decreases the ultimate bearing capacity by an average of 7% in a micropile-supported cantilever wall. The allowable bearing capacity of the S/D ratio 13 is 259 kPa, and the ultimate bearing capacity is 779 kPa.

Overall Trend Across all configurations, decreasing micropile spacing from s/d = 16 to S/D = 10 progressively increases both the ultimate and allowable bearing capacities, confirming that closer micropile spacing enhances load transfer and group efficiency. The S/D = 10 spacing (S = 1.1 m) is identified as the optimal configuration. The factor of safety against bearing increases from 4.37 at S/D 13 to 4.66 at S/D 10, representing a 6.6% improvement as compared with the maximum toe pressure of 178.23 kPa.

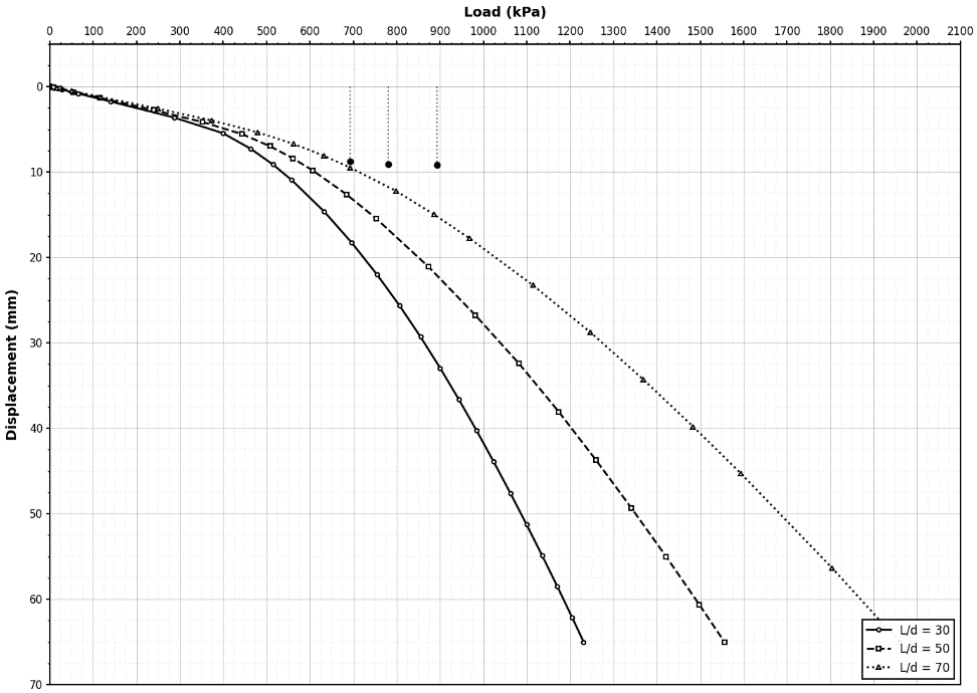

Figure 5.30: Bearing capacity comparison of varying L/D ratio.

According to the FEM results, foundation bearing performance is gradually improved by raising the micropile length-to-diameter ratio (L/D) from 30, 50, and 70. With an overall improvement of 28.9%, the ultimate bearing capacity rises from 692.98 kPa at L/D = 30 to 779.11 kPa at L/D = 50 and achieves a maximum of 893.54 kPa at L/D = 70. The allowable bearing capacities of 230.99 kPa, 259.70 kPa, and 297.85 kPa with FOS =3. All are greater than the maximum toe pressure of 178.23 kPa, and the factor of safety against bearing of the wall increases correspondingly from 3.89 to 4.37 and 5.01. These findings demonstrate that the larger the micropile length, greatly enhances overall foundation stability and load transmission efficiency.

FE analysis also showed that the smaller the spacing to diameter of micropiles (S/D), the greater the reduction in foundation displacement, and provides greater restraint and improved deformation control of the cantilever retaining wall under static loading conditions.

5.9.2 *Load carrying ratio under varying S/D and L/D ratio*

Parametric analysis was carried out to evaluate the load carried proportion by micropile in spacing to diameter ratio (S/D) and the length to diameter ratio (L/D).

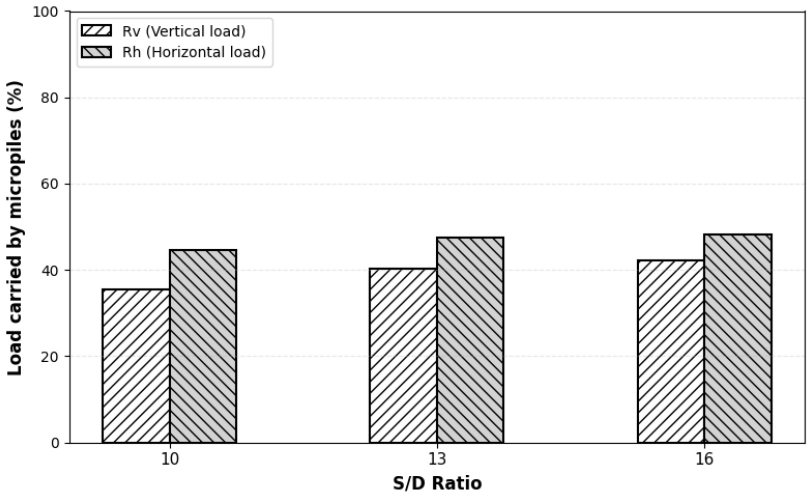

Figure 5.31: Load-carrying ratio by micropile in varying S/D ratio

Lateral and vertical load-carrying proportion of micros with parametric study of spacing-to-diameter ratio (S/D) of micropiles 10, 13, and 16, as shown in the figure. It shows that with an increase in S/D ratio, there is an increase in vertical and lateral load-carrying proportion by micropile, while a mild increase is observed in the lateral load-carrying proportion. In the ratio of S/D 10, the Micropile carried 35.5% and 44.5% in vertical and lateral load, respectively. And increase the average by 8.98% in vertical and 4.3% in horizontal load carried percentage when increasing the S/D ratio from 10 to 16.

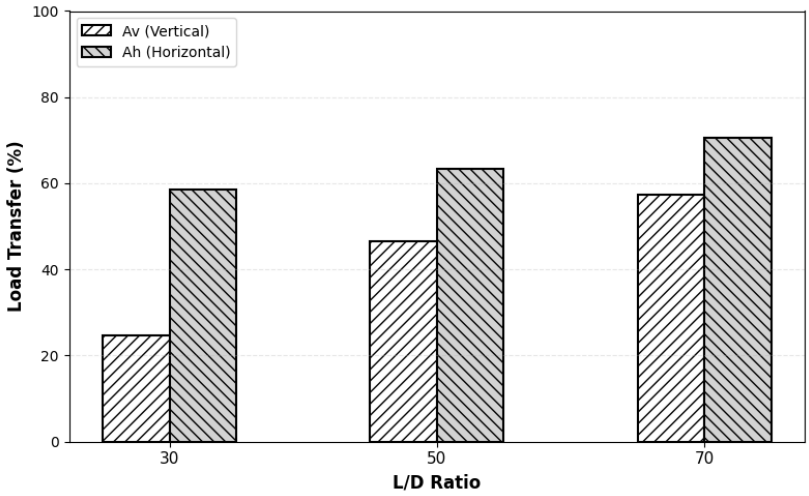

Figure 5.32: Load-carrying ratio by micropile in varying (L/D).

As presented in the figure above, the load carried proportion of the varying ratio of length to diameter (L/D) of the micropile was evaluated. In which L/D ratio 30, the vertical load carried proportion is 21.5% in vertical, and the 43.8% in the horizontal load. When increasing the L/D ratio from 30 to 70, there was an

increase in the load carried percentage average by 40% in vertical load carried, and the 9% in the horizontal load.

5.9.3 *Bending moment, displacement of micropile in varying S/D ratio*

Bending moment and lateral displacement were observed in varying spacing-to-diameter ratios (S/D).

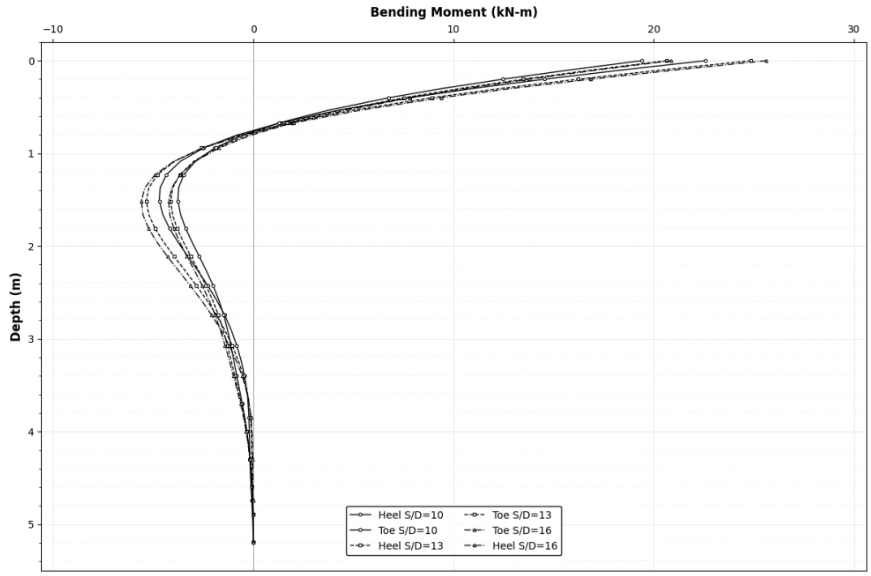

Figure 5.33: Bending moment micropiles in various S/D ratios.

As presented in the figures, both the heel and toe micropiles exhibit a consistent pattern of positive bending moment in the upper depth zone and negative bending moment in the lower depth zone across all three spacing configurations of s/d ratio 10,13,16. For the toe and heel side micropile, the maximum positive bending moment at the surface reaches approximately 19 to 25 kNm in three spacing configurations, while the negative bending moment peak varies slightly from 3kNm to 5 kNm with spacing configurations. It can therefore be concluded that increasing the S/D ratio leads to higher bending moments in individual micropiles. As each pile is required to resist a greater share of the lateral load when the spacing between piles increases, confirming that closer spacing results in better load distribution and reduced individual pile bending demands.

The toe and heel lateral displacements gradually diminish over the entire depth profile as the s/d ratio drops from 16, 13, and 10, demonstrating that closer micropile spacing more successfully limits wall movement and improves overall lateral stability.

5.9.4 *Comparison of the with and without casing in micropile.*

FEM analysis was done without the casing in the micropile and compared with the casing micropile type. The elastic young modulus of the micropile without the steel casing was 27.65 × 10^6 kPa, and the diameter of the micropile is 100mm. Bearing capacity, bending moment, and the lateral displacement were observed.

Comparisons of Bearing Capacity:

Bearing capacity of the wall supported by the micropile without casing was evaluated using FEM modelling and later compared with the cantilever wall supported with both cased micropile-supported wall and the unsupported cantilever wall. The comparison chart is presented below.

Table 5.9: Bearing capacity at micropile with and without steel casing type

Cantilever Wall Foundation Type	Ultimate Bearing Capacity (kPa)	Allowable Bearing Capacity (kPa)	FOS Against Bearing
Without Mps Supported	666.5	222.2	3.7
Micropile Without Casing	705.65	235.22	3.96
With Mps Supported	779.1	259.7	4.4
Maximum pressure at the toe of the wall	178.2		

An ultimate bearing capacity of the uncased micropile-supported wall is 705.65 kPa, and an allowable bearing capacity of 235.22 kPa. And a factor of safety against bearing of the wall 3.96 is obtained for the uncased micropile-supported wall at a spacing of the micropiles of 1.5 m. This is 6% greater than the bearing capacity of the wall foundation without the micropile support, as referenced in Table 13. This concludes that the micropile without casing can also perform better in bearing as compared to the cased micropile.

Pile with uncased type performance depends on the grouting types, method of grouting, bond length, and interaction of the pile and the soil. The steel casing increases the economic cost in the case of the projects if there is sufficient performance provided by the micropiles with uncased types. Proper economic

analysis also needs to consider the during choosen the types of micropile chosen for the economic viability of the project.

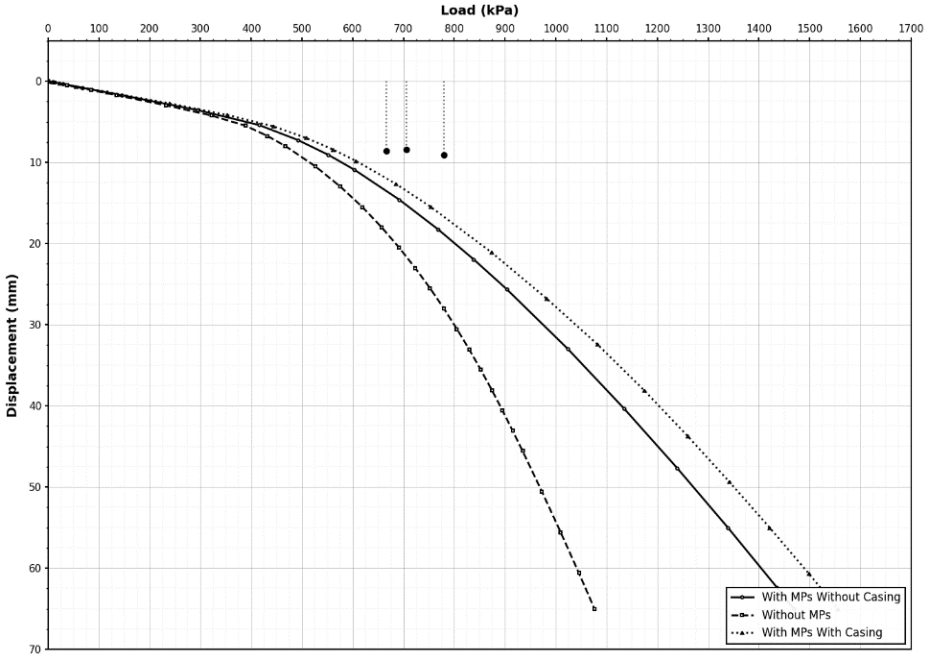

Figure 5.34: Bearing capacity with and without casing type and the wall.

5.9.5 *Use of an alternative solution of secant micropile*

A secant pile wall is a stabilization structure formed by installing piles in an overlapping (interlocking) pattern, where adjacent piles physically intersect each other, creating a continuous wall without gaps between piles. This creates a relatively watertight wall in the high-scouring-prone area. One of the previous case studies of the White Cart Water is a small river that runs through Glasgow. Heavy rainfall has caused numerous floods in the past. Work Section 16 is a 200 m long stretch in the southern part of Glasgow. For this section, a secant pile wall with an in-situ reinforced concrete wall on top has been proposed to form the flood defence wall (Brouwer et al. 2011).

If we used the secant micropile wall in the toe side of the wall of 110 mm diameter, it would reduce the lateral displacement. Almost reduced 24mm lateral displacement by the secant wall pile as compared to the micropile of similar diameter at a spacing of 1.5m. A scant pile wall of micropile could be taken as an alternative solution in roadside stabilization in flood-prone areas or near the riverbank area where maximum scouring occurs.

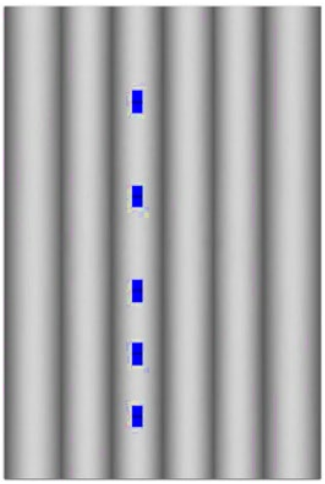

Figure 5.35: Cross-section of secant pile wall

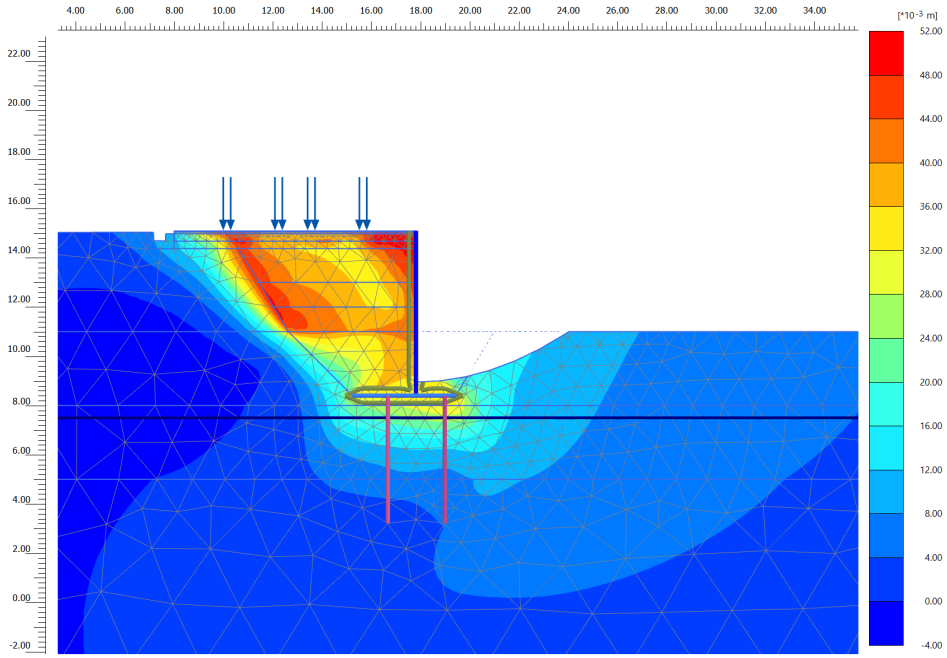

Figure 5.36: Use of secant micropile wall at the toe of the wall.

5.10 Validation of Work:

Validation of the load carried ratio, bending moments of the micropiles of the present FEM, with the previous similar research work conducted by (Elsawwaf et al., 2023).

5.10.1 *Load carried ratio analysis - interpretation & validation*

i. Model parameter context:

Table 5.10:Dimension of micropile used for validation

Model	Length (m)	Diameter (mm)
Paper	13	250
FEM	5.5	110

The two models differ substantially in geometry: the paper used micropile length (L) = 13 m and diameter (D) = 250 mm (L/D range 13–52 in soft clay + dense sand), while the present method (FEM) uses L = 5.5 m and D = 110 mm (L/D range 30–70). This means the models do not share an identical L/D window, but there is enough overlap (L/D = 28–52 vs 30–70) to make a meaningful trend comparison.

ii. Horizontal load carried ratio:

Horizontal load carried ratio of this FEM work was mentioned in Figure 5.32, and the paper's was in Figure 5.37.

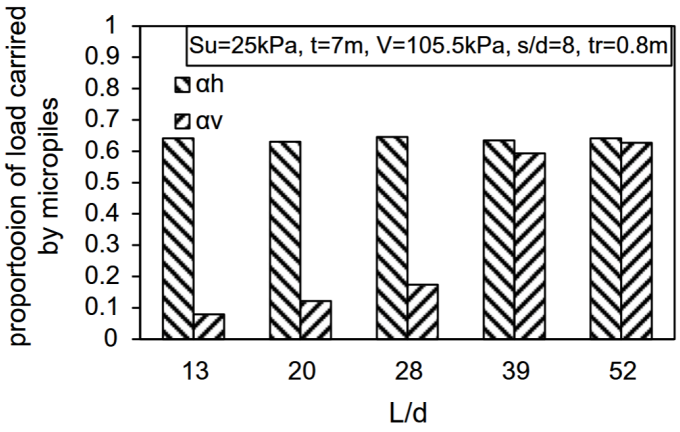

Figure 5.37: Load carried ratio vs L/d ratio(Elsawwaf et al., 2023a)

The paper showed a relatively stable horizontal ratio of 0.58–0.67 across all L/D values studied, meaning micropiles consistently carry 58-67% of total lateral load regardless of length. The present method results show lower values - 0.43 to 0.52 -but with the same upward trend as L/D increases.

Load carried ratio vs L/D: horizontal load:

Comparison of how micropiles share horizontal load as slenderness (L/D) increases, which was presented in Figure 5.38.

Elsawwaf 2023 et al. (Paper) (Blue) and Present FEM - Roshi section (Green)

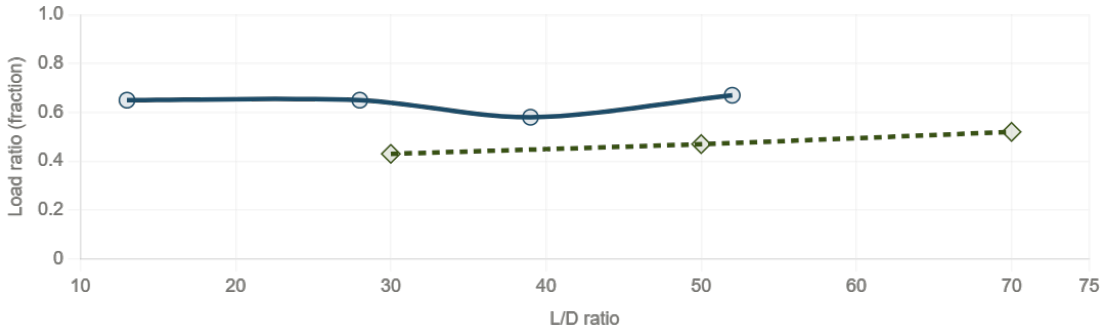

Figure 5.38: Load carried ratio vs L/D: horizontal load.

This consistent offset (~0.18–0.22) is physically well-justified:

- The paper's piles are larger in diameter (250 mm vs 110 mm), giving more lateral stiffness and passive resistance per pile.
- The paper's soil profile includes a deeper soft clay layer, which tends to concentrate lateral load on piles rather than allowing the raft/wall to mobilize friction efficiently.
- The present model uses a wall foundation (not an open raft), which itself contributes significant lateral resistance - so a lower pile ratio is expected by design.

Conclusion: The horizontal trend is validated. The absolute values differ due to legitimate geometric and boundary condition differences, not modelling error.

iii. Vertical load carried ratio:

This is where the most striking validation occurs. At L/D = 28–30, both the paper and the present FEM give a vertical ratio of approximately 0.20–0.21 - an almost exact match. This confirms that at low L/D (shorter, fatter piles), micropiles carry only about 20% of the vertical load, with the foundation element (raft or wall) carrying the majority.

Load carried ratio vs L/D: vertical load:

Comparison of vertical load sharing between micropile and raft/wall foundation was mentioned in Figure 5.39

Elsawwaf 2023 (Paper) (Blue----) and Present FEM - Roshi section (Green ….)

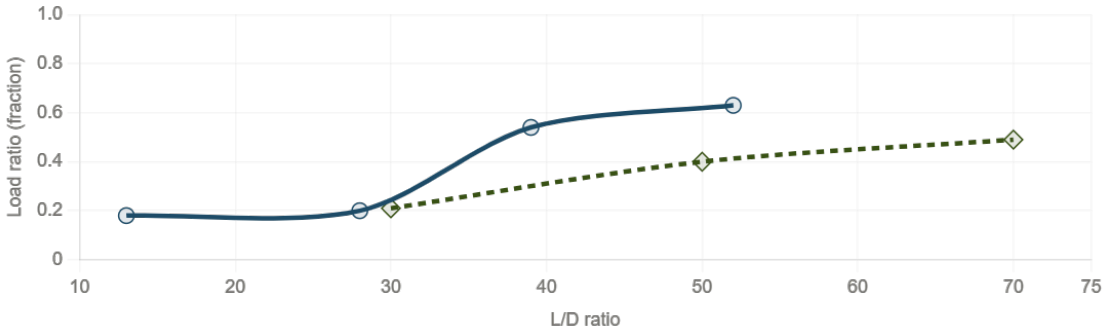

Figure 5.39: Comparison of load carried ratio vs L/D: vertical load

As L/D increases toward 50-52, both show a significant rise: the paper reaches 0.63 and the FEM reaches ~0.40-0.49. The FEM values are lower, again consistent with the wall foundation sharing more load than an open raft would. The trend - increasing vertical load participation with increasing L/D - is fully replicated.

The paper also showed a sharp jump in vertical ratio between L/D = 28 and L/D = 39 (from 0.20 to 0.54), which coincides with piles reaching into the dense sand layer. The present FEM shows a similar but more gradual rise, consistent with site-specific soil stratification at the case study site of the Roshi location.

iv. Overall load split (Present FEM)

The present FEM results, Figure 5.20, showed micropiles carrying 40.3% of the total vertical load and 47.5% of the total horizontal load, with the wall foundation carrying the remainder. This is internally consistent; micropiles were doing real work in both directions without being over-loaded, which is exactly the expected behaviour for a retrofit micropiled foundation under combined loading.

5.10.2 *Bending moment analysis interpretation & validation*

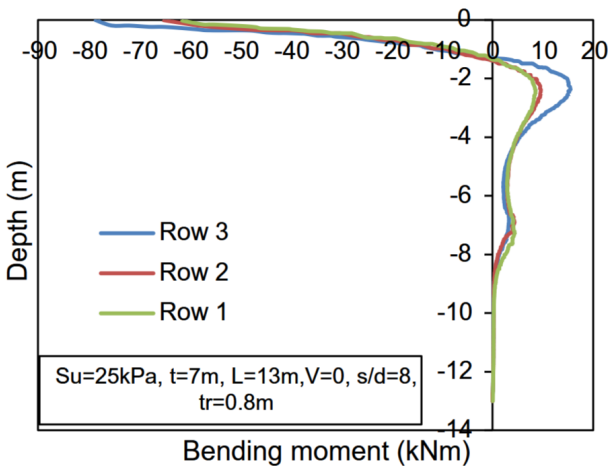

Figure 5.40: Bending moment of micropile, (Elsawwaf et al., 2023a)

Bending moment of the micropile of the paper was mentioned in Figure 5.40. The paper (L = 13 m, S/D = 8) shows the classic long-pile bending moment profile: maximum moment near the pile head, reducing steadily with depth, and approaching near-zero at the pile tip. This is characteristic of flexible pile behaviour where the lower portion of the pile is essentially unloaded.

The present FEM (L = 5.5 m, L/D = 50) shows bending moment as presented Figure 5.15:

- Heel micropile BM = 24.85 kN·m (at top/connection zone)
- Toe micropile BM = 20.64 kN·m (at pile tip)

The fact that significant bending moment is retained at the pile toe (20.64 kN·m ≠ 0) confirms that the present piles are behaving as short/rigid piles rather than long/flexible ones. In short-pile behaviour, the entire pile rotates, and the tip does not have a clear fixity point - so moment is distributed along the full length. This is entirely consistent with the shorter L = 5.5 m and the relatively stiff ground at the Roshi site.

The heel pile carries slightly more bending moment (24.85 vs 20.64 kN·m), which aligns with the paper's finding that under combined vertical + lateral loading, trailing or heel piles redistribute more lateral demand through the vertical load effect. This validates the direction of the asymmetry in the present FEM output.

5.10.3 *Overall validation summary*

Table 5.11:Summary of validation of FEM work

Criterion	Result
Vertical ratio trend with L/D	Validated - same increasing trend, near-exact match at low L/D
Horizontal ratio trend with L/D	Trend validated, absolute values systematically lower (justified by geometry)
Short-pile vs long-pile BM behaviour	Confirmed - present FEM correctly shows rigid pile moment distribution
Heel > Toe bending moment	Consistent with paper's combined-loading redistribution finding
Absolute load ratios (S/D comparison)	Not directly comparable - different foundation type and pile dimensions

The present FEM results were physically coherent and trend-consistent with the paper of (Elsawwaf et al., 2023a). The quantitative differences are explainable and expected given the differences in pile size, length, and foundation configuration. This model was validated in both qualitative behavior and key quantitative benchmarks.

6 CONCLUSIONS AND RECOMMENDATIONS

This thesis report FEM-based numerical evaluated the stability of micropile-supported cantilever retaining wall foundations, taking the case study site of the Roshi Section of the BP Highway. Using a finite element modelling approach via PLAXIS 2D software, the study analyzed performance in static, water level rise, seismic (pseudo-static loading), and scouring conditions. Furthermore, the parametric analysis on the spacing-to-diameter ratio (S/D) and length-to-diameter ratio (L/D) of the micropile was conducted, and the performance was evaluated. Conclusion and the recommendation of this research work was mention followings topics.

6.1 Conclusions

This thesis report presents a numerical evaluation of micropile-supported cantilever retaining wall foundations at the Roshi Section of the BP Highway. Using a finite element modelling approach via PLAXIS 2D software, the study analyzes performance in static, flow rise, seismic (pseudo-static loading), and scouring conditions. The research evaluates parameters such as displacement, bearing capacity of the cantilever wall, load carried proportion, skin friction, bending moments, and lateral displacement of the micropiles. Furthermore, it assesses the load transfer ratio between the foundation base and the piles, alongside overall pile capacity. Also, a parametric study on the spacing-to-diameter (S/D) ratio and length-to-diameter (L/D) ratio to analyze the change in load carrying ratio, bending, bearing, and displacement was conducted.

i. The allowable bearing capacity of a micropile-supported cantilever retaining wall is increased by 16 % in comparison to a conventional cantilever retaining wall, and also increases the FOS against bearing.
ii. Micropiles used in the wall decrease the settlement of the wall with a micropile. Also, the cantilever wall without the micropile supported has safe against bearing, and the micropile enhances the bearing and stability performance.
iii. The micropile beneath the foundation of the retaining wall can make the design uneconomical in the case of a foundation placed below the proposed scour depth, and has a safe bearing failure.
iv. Under water level rise conditions, displacement did not change abruptly with rising water levels; however, bending moments increased progressively with flow intensity, confirming that hydrodynamic effects must be carefully considered in design.

v. Under pseudo-static seismic loading, lateral displacement exceeds vertical displacement in the EW direction. It doubles at the coefficient 0.1g to 0.2g (within permissible limits) and more than doubles above 0.2g

vi. The micropiles carried 40% of the vertical and the 47% of the horizontal load, indicating that micropiles play a more prominent role in resisting lateral forces than vertical loads in a micropiled-supported cantilever wall.

vii. The toe side micropile of the cantilever wall has less flexural demand, carries more compressive load, mobilized greater skin friction than the heel side micropile. The toe-side micropiles are under compression, and the heel side is in tension.

viii. Micropiles are effective in a cantilever wall for decreasing lateral displacement and enhancing overall wall stability during scouring within the proposed scoured depth limit. The lateral extent of scour is crucial for the stability of the wall.

ix. The secant pile wall beneath the wall foundation can increase the stability of retaining structures on a high-scouring riverbank side.

x. The parametric study confirmed that a smaller spacing-to-diameter ratio (S/D) provides an increase in the bearing capacity. The load carried proportion in vertical load is increased by an average of 9% and 4% in horizontal load, with an increase in the S/D ratio by 30%.

xi. Increasing the L/D ratio improves ultimate bearing capacity and safety factor against toe bearing pressure. It also raises micropile load share by an average of 40% (vertical) and 9% (horizontal) per a 1.5 times increase in L/D ratio.

xii. Micropile without casing can also perform better in bearing as compared to the cased micropile of shorter length in the wall foundation. Its performance depends on the grouting types, bond length, and interaction of the pile and the soil.

6.2 Recommendations

Due to time limitations and computational constraints, this research has several limitations that can be addressed in the future. The following are some suggestions for upcoming work:

- 2D finite element model analysis is performed in this study. For further study, a 3D finite element model could be used to improve the accuracy of the work.

- For the validation of the model, previous similar research papers are used in this study. For further study, validation of the model could be conducted with a field test at a similar site.
- The study is limited to one type of cantilever wall, which does not give a variety of parametric analyses. For further study analysis, different types and heights of walls could be used to improve accuracy and achieve better results.
- The water level rise case is performed in this study. For further study, the impact load of floods on the wall could be analyzed with a higher version of the analysis software.
- For an alternative solution for stabilization of a retaining wall near the riverbank, only one type of secant pile wall is used. For further study, a secant pile wall or another type of method could be analyzed for the stabilization of the cantilever retaining wall.
- The numerical results could be validated with results obtained from centrifuge testing, field load test, or shaking table tests to ensure the reliability of the model.

7 REFERENCES

AASHTO. (1993). *Standard specifications for highway bridges* (Vol. 11). American Association of State Highway Officials.

Abdul Karim Elsalfiti. (2011). *Skin Friction of Micropiles Embedded in Gravelly Soils* . Concordia University Montreal, Quebec, CANADA .

Adduce, C., & Sciortino, G. (2006). Scour due to a horizontal turbulent jet: Numerical and experimental investigation. *Journal of Hydraulic Research*, *44*(5), 663–673. https://doi.org/10.1080/00221686.2006.9521715

BRIDGES, S. R. O. F. (n.d.). *Micropile Design and Construction*.

Das, B. M. (2019). *Advanced Soil Mechanics*. CRC Press. https://doi.org/10.1201/9781351215183

Das, B. M., & Sobhan, K. (2006a). *Principles of geotechnical engineering*. Thomson Stamford.

Das, B. M., & Sobhan, K. (2006b). *Principles of geotechnical engineering*. Thomson Stamford.

Duwal, S., Bhattarai, Y., Milapati, R., & Talchabhadel, R. (2023). Charting the Course to Resilience: Hydrodynamic Modeling for Socio-economic Insights for Flood Risk Management in Nepal's Ungauged Roshi River Catchment. *Journal of Hydrology and Meteorology*, *11*(1), 53–66. https://doi.org/10.3126/jhm.v11i1.59666

Ebadi-Jamkhaneh, M., & Kontoni, D.-P. N. (2023). Static analysis of prestressed micropile-raft foundation with varying lengths resting on sandy soil. *Innovative Infrastructure Solutions*, *8*(3), 106.

El Kamash, W., & Han, J. (2017). Numerical Analysis of Existing Foundations Underpinned by Micropiles. *International Journal of Geomechanics*, *17*(6). https://doi.org/10.1061/(ASCE)GM.1943-5622.0000833

Elarabi, H., & Soorkty, A. A. A. (2015). Construction of micropiles using pressure techniques. *Journal of Civil Engineering and Architecture*, *8*(1), 45–50.

Elsalfiti, A. K. (2011). *Skin Friction of Micropiles Embedded in Gravelly Soils*. Concordia University.

Elsawwaf, A., Nazir, A., Azzam, W., & Farouk, A. (2023a). The behavior of micropiled raft foundations subjected to combined vertical and lateral

loading: numerical study. *Arabian Journal of Geosciences*, *16*(3), 187. https://doi.org/10.1007/s12517-023-11246-y

Elsawwaf, A., Nazir, A., Azzam, W., & Farouk, A. (2023b). The behavior of micropiled raft foundations subjected to combined vertical and lateral loading: numerical study. *Arabian Journal of Geosciences*, *16*(3), 187.

FHWA. (2005). *FHWA (2005) Micropile Design and Construction Guidelines. Handbook, 132078.*

Han, J., & Ye, S.-L. (2006). A field study on the behavior of micropiles in clay under compression or tension. *Canadian Geotechnical Journal*, *43*(1), 19–29. https://doi.org/10.1139/t05-089

Hong, V., Zhang, G., Wang, X., & Li, A. (2020). Experimental Investigation on the Shape and Depth of Local Scour Hole Downstream of the Release Structure. *World Journal of Engineering and Technology*, *08*(01), 104–120. https://doi.org/10.4236/wjet.2020.81010

Indian Roads Congress. (2014). *Standard specifications and code of practice for road bridges, Section VII: Foundations and substructure*.

Konstandakopoulou, F., Tsimirika, M., Pnevmatikos, N., & Hatzigeorgiou, G. D. (2020). Optimization of Reinforced Concrete Retaining Walls Designed According to European Provisions. *Infrastructures*, *5*(6), 46. https://doi.org/10.3390/infrastructures5060046

Kshatriya, R., Sathe, P., & Kankarej, P. (2022). Analysis and Behavior of Retaining Wall on Black Cotton Soil by Using Software 'PLAXIS 2D.' *SSRN Electronic Journal*. https://doi.org/10.2139/ssrn.4043255

Kyung, D., Kim, D., Kim, G., & Lee, J. (2017a). Vertical load-carrying behavior and design models for micropiles considering foundation configuration conditions. *Canadian Geotechnical Journal*, *54*(2), 234–247. https://doi.org/10.1139/cgj-2015-0472

Kyung, D., Kim, D., Kim, G., & Lee, J. (2017b). Vertical load-carrying behavior and design models for micropiles considering foundation configuration conditions. *Canadian Geotechnical Journal*, *54*(2), 234–247.

Kyung, D., Kim, D., Kim, G., & Lee, J. (2017c). Vertical load-carrying behavior and design models for micropiles considering foundation configuration conditions. *Canadian Geotechnical Journal*, *54*(2), 234–247. https://doi.org/10.1139/cgj-2015-0472

Kyung, D., & Lee, J. (2018). Interpretative Analysis of Lateral Load–Carrying Behavior and Design Model for Inclined Single and Group Micropiles. *Journal of Geotechnical and Geoenvironmental Engineering*, *144*(1). https://doi.org/10.1061/(ASCE)GT.1943-5606.0001810

Lamichhane, K., Karki, S., Sharma, K., Khadka, B., Acharya, B., Biswakarma, K., Adhikari, S., Kc, R., Danegulu, A., Bhattarai, S., & others. (2025). Unraveling the causes and impacts of increasing flood disasters in the Kathmandu valley: lessons from the unprecedented September 2024 floods. *Natural Hazards Research*.

Laursen, E. M. (1963). An Analysis of Relief Bridge Scour. *Journal of the Hydraulics Division*, *89*(3), 93–118. https://doi.org/10.1061/JYCEAJ.0000896

Liew, S., & Fong, C. (2003). Design and Construction of Micropiles. *Geotechnica*.

Lizzi, F. (1982a). The static restoration of monuments: basic criteria-case histories, strengthening of buildings damaged by earthquakes. *(No Title)*.

Lizzi, F. (1982b). The static restoration of monuments: basic criteria-case histories, strengthening of buildings damaged by earthquakes. *(No Title)*.

Roh, Y., Kim, I., Kim, G., & Lee, J. (2019). Comparative Analysis of Axial Load Capacity for Piled-Raft Foundation with Changes in Groundwater Level. *KSCE Journal of Civil Engineering*, *23*(10), 4250–4258. https://doi.org/10.1007/s12205-019-0239-3

Rollins, K. M., Lane, J. D., & Gerber, T. M. (2005). Measured and computed lateral response of a pile group in sand. *Journal of Geotechnical and Geoenvironmental Engineering*, *131*(1), 103–114.

Shakeel, M., Azam, R., Riaz, M. R., & Shihata, A. (2022). Design Optimization of Reinforced Concrete Cantilever Retaining Walls: A State-of-the-Art Review. *Advances in Civil Engineering*, *2022*(1). https://doi.org/10.1155/2022/4760175

Takai, N., Shigefuji, M., Rajaure, S., Bijukchhen, S., Ichiyanagi, M., Dhital, M. R., & Sasatani, T. (2016). Strong ground motion in the Kathmandu Valley during the 2015 Gorkha, Nepal, earthquake. *Earth, Planets and Space*, *68*(1), 10. https://doi.org/10.1186/s40623-016-0383-7

Terzaghi, K. (1943). *Theoretical Soil Mechanics*. Wiley. https://doi.org/10.1002/9780470172766

Theinat, A. K., & Luna, R. (2019). Load Transfer Mechanism of Micropiles in Weathered Rock. *Geo-Congress 2019*, 55–62. https://doi.org/10.1061/9780784482094.006

Thiyyakkandi, S., McVay, M., Bloomquist, D., & Lai, P. (2014). Experimental study, numerical modeling of and axial prediction approach to base grouted drilled shafts in cohesionless soils. *Acta Geotechnica*, *9*(3), 439–454.

T.P.T. Dao. (2011). *Validation of PLAXIS Embedded Piles For Lateral Loading*.

Vijaykumar, & Prasad, S. K. (2022). Parametric Study of Pile-Raft Foundation System Using PLAXIS-3D. *Journal of Emerging Technologies and Innovative Research (JETIR)*, *9*(5). https://www.jetir.org

Wu, Y., & Prakash, S. (1999). Effect of Submergence on Seismic Displacement of Rigid Walls. *Earthquake Geotechnical Engineering*.

Wulandari, P. S., & Tjandra, D. (2015). Analysis of Piled Raft Foundation on Soft Soil Using PLAXIS 2D. *Procedia Engineering*, *125*, 363–367. https://doi.org/10.1016/j.proeng.2015.11.083

ANNEX-I: FEM MODEL IN DIFFERENT SCOURING

FEM analysis in vertical scour progressive increase in scour depth from the toe of the cantilever wall.

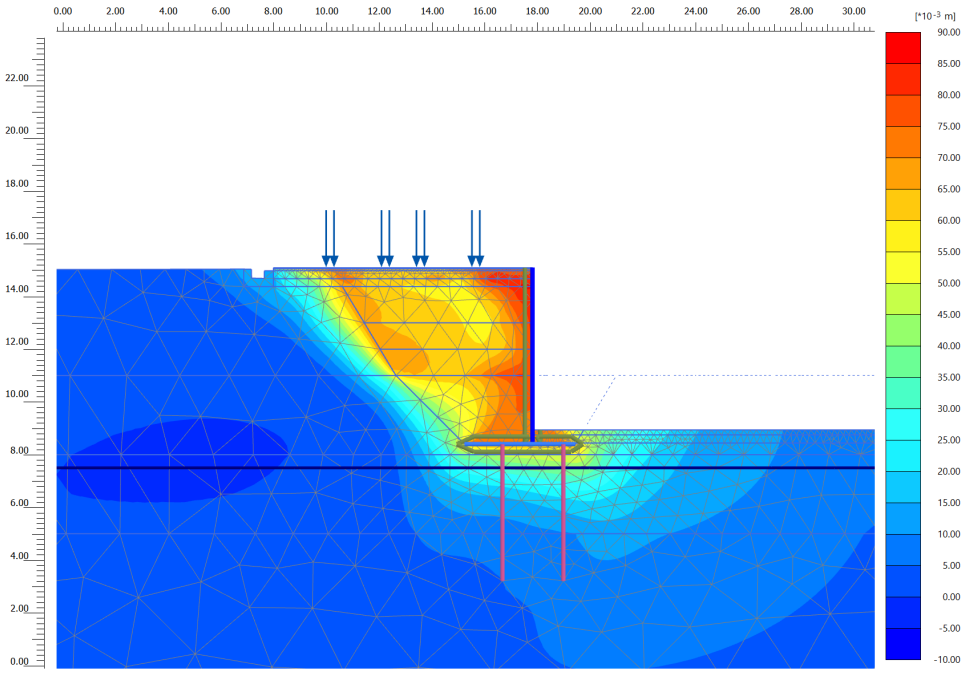

Fig. 1: Scour depth = 2.05 m | u_x = 90 mm

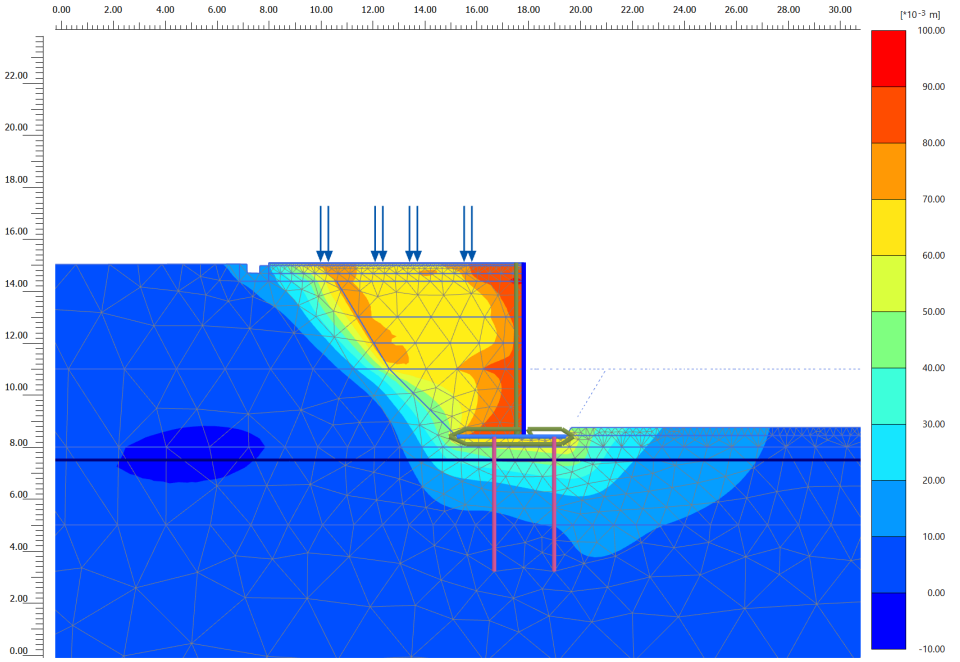

Fig. 2: Scour depth = 2.25 m | u_x = 100 mm

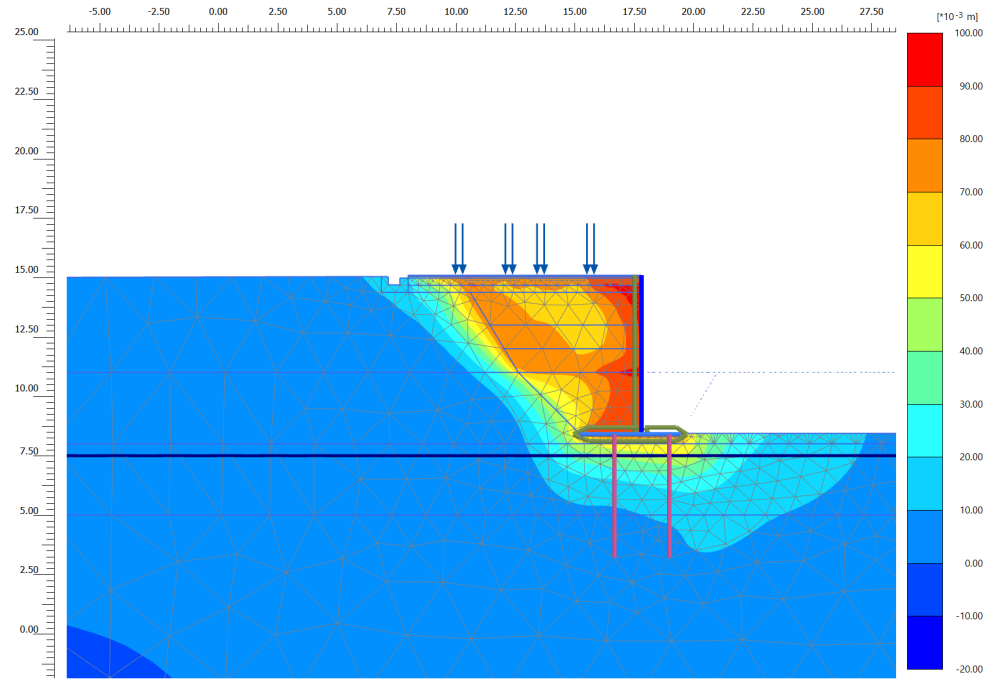

Fig. 3: Scour depth = 2.60 m | u_x = 100 mm

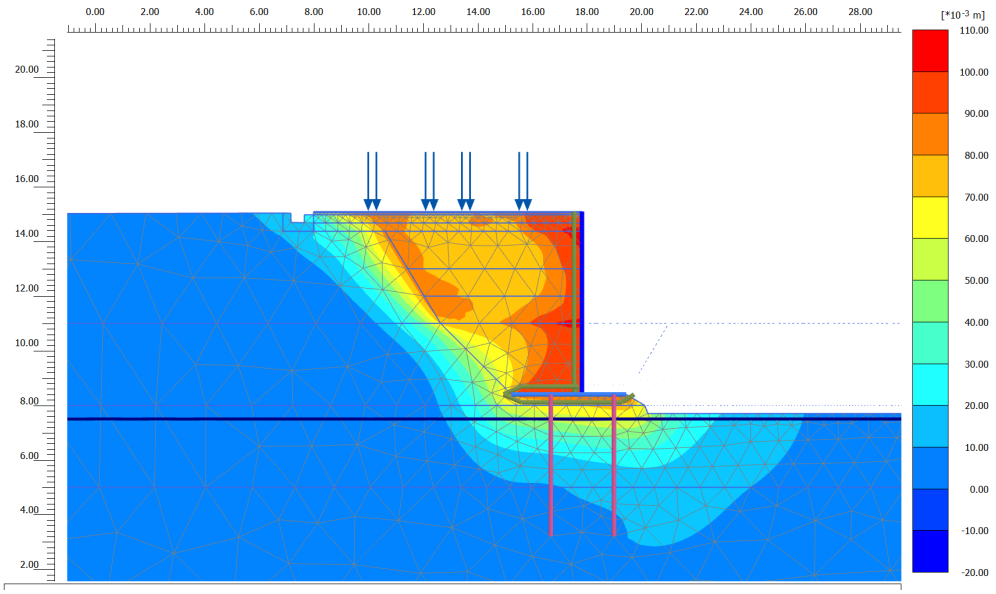

Fig. 4: Scour depth = 3.00 m | u_x = 110 mm

Progressive increase in lateral scour below foundation:

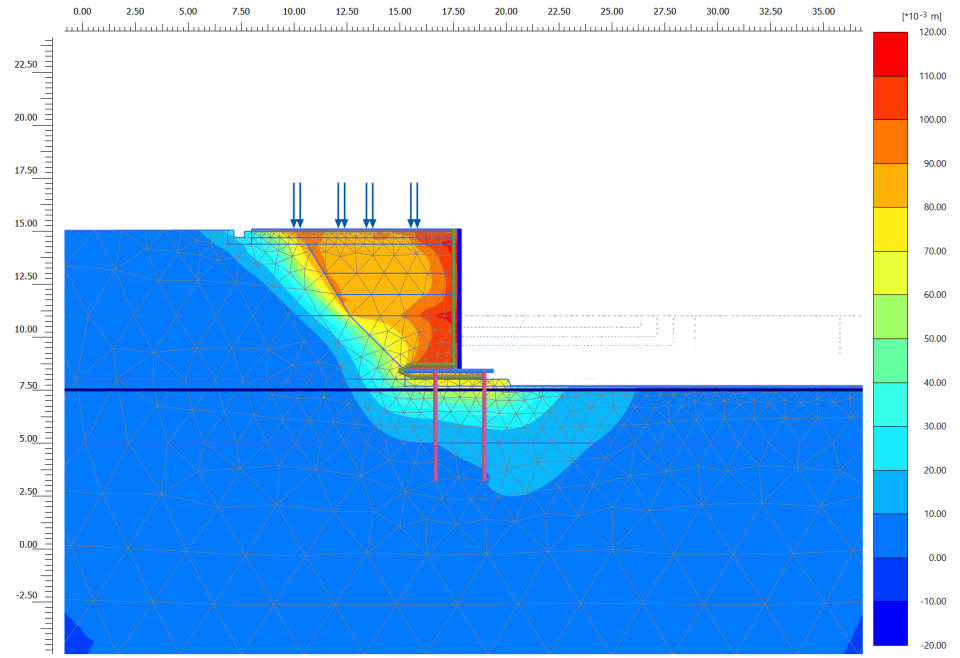

Fig. 5: Scour d = 3.3 m, to micropile toe | u_x = 120 mm

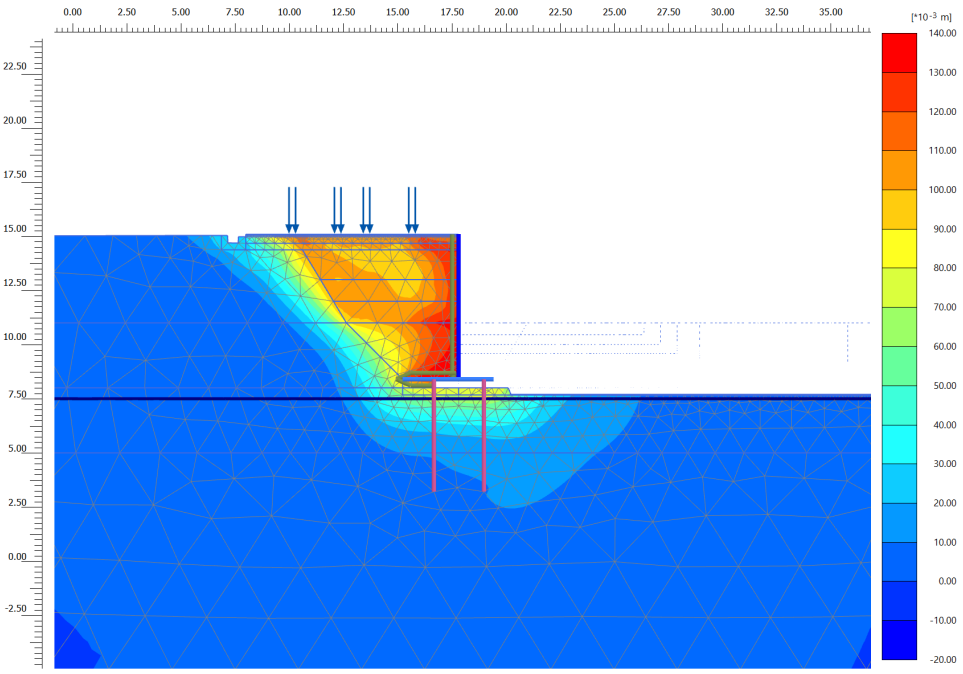

Fig. 6: Scour d = 3.3 m, to micropile heel | u_x = 140 mm

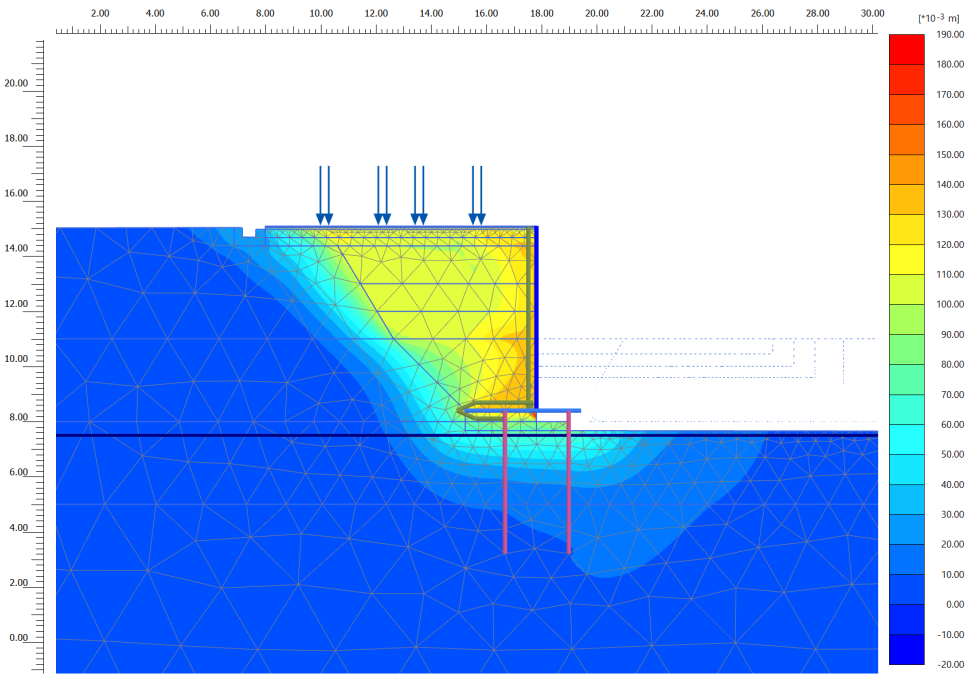

Fig. 7: Scour d = 3.3 m, heel to toe zone | u_x = 170 mm

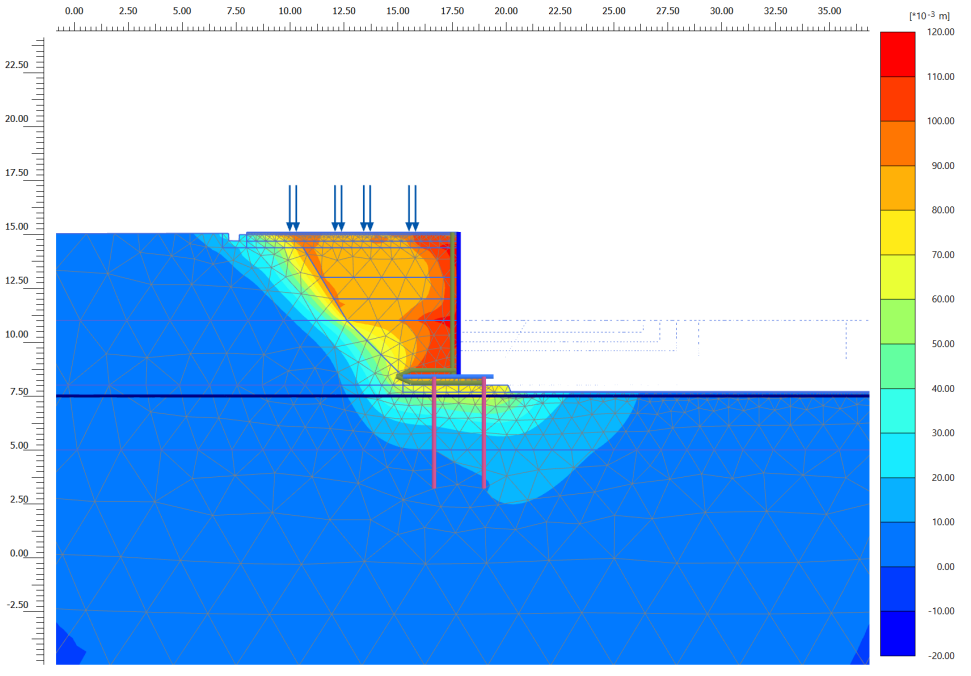

Fig. 8: Scour d = 3.3 m, below full foundation | u_x = 190 mm

ANNEX-II: PHOTOS OF CASE STUDY SITE

Figure: Photos of the case study site of cantiliver wall supported by micropiles.

Photos were taken from the roshi section of the BP Highway, Kavrepalachok. Construction was carried out under the supervision of the Bhaktpur Road Division Office.

ANNEX-III: BOREHOLE LOG OF SITE

Borehole Logs

Soil Description	Symbol	Depth, m	Sample No. &Type	No. of blows 10/15 cm	10/15 cm	10/15 cm	N_c-Value	N-Value
Sand with Gravel and Boulder (SP)		1	DCPT	8	9	14	31	21
		2						
		3	DCPT	9	18	16	43	29
		4	DCPT	10	16	32	58	33
		5						
		6	DCPT	13	19	24	56	32
		7						
		8	DCPT	15	23	27	65	37
		9	DCPT	18	50/4			50
		10	DCPT	17	50/5			50

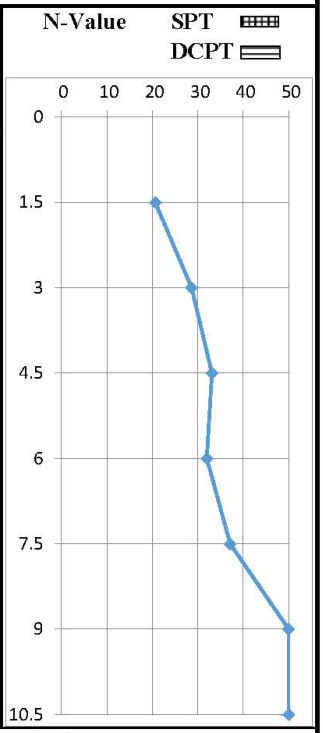

End Depth	* Completed at 10.50m	Ground: Dry

Types of Soil		N Value					
Granular Soil	Compactness	0 to 4	4 to 10	10 to 30	30 to 50	> 50	
		Very Loose	Loose	Med. Dense	Dense	Very Dense	
Cohesive Soil	Consistency	0 to 2	2 to 4	4 to 8	8 to 16	16 to 32	> 32
		Very Soft	Soft	Med. Soft	Stiff	Very Stiff	Hard

Note: N value = 50 is taken for the values that comes greater than 50 for the exploration depth.

Figure: Borehole log of the case study site.

Report provided by the Bhaktpur Road Division Office, Bhaktpur.

ANNEX-IV: LIST OF PUBLICATIONS

Conference Paper:

M.S. Ghimire and R.C. Tiwari, "FEM Based Stability Analysis of Micropiles Supported Cantilever Retaining Wall: A Case Study of the Roshi Section of BP Highway" in *18th IOE Graduate Conference (2026)*, Lalitpur, Nepal